



RESEARCH MEMORANDUM

FLOW AND FORCE CHARACTERISTICS OF 2-PERCENT-THICK
AIRFOILS AT TRANSONIC SPEEDS

By Walter F. Lindsey and Emma Jean Landrum

Langley Aeronautical Laboratory
Langley Field, Va.

NATIONAL ADVISORY COMMITTEE
FOR AERONAUTICS
WASHINGTON

January 18, 1955
Declassified October 8, 1957

NATIONAL ADVISORY COMMITTEE FOR AERONAUTICS

RESEARCH MEMORANDUM

FLOW AND FORCE CHARACTERISTICS OF 2-PERCENT-THICK
AIRFOILS AT TRANSONIC SPEEDS

By Walter F. Lindsey and Emma Jean Landrum

SUMMARY

A two-dimensional investigation utilizing pressure-distribution measurements and schlieren photographs has been made of the flow and force characteristics of slab-sided airfoils of 2-percent thickness at transonic Mach numbers. The airfoils had various combinations of elliptically shaped leading and trailing edges from a fineness ratio of 0 to 10.

The aerodynamic characteristics and an analysis of the flow past the models are presented. The results are compared with previous tests on airfoils of 4-percent thickness and greater, and show at high subsonic Mach numbers that additional improvements in aerodynamic characteristics were obtained with the 2-percent-thick airfoils.

INTRODUCTION

Previous experimental investigations of two-dimensional airfoils at high subsonic Mach numbers from an early investigation (ref. 1) through a more recent investigation (ref. 2) have shown improvements in the aerodynamic characteristics at high subsonic Mach numbers, primarily through the use of reductions in the ratios of thickness to chord. The similarity laws (refs. 3 and 4) also show that decreases in ratios of thickness to chord result in improvements in the aerodynamic characteristics. Although these previous experimental investigations were conducted on airfoils having ratios of thickness to chord of 4 percent and greater, the similarity laws are more nearly applicable as the profiles become thinner (ref. 4). It was therefore considered desirable to determine the aerodynamic characteristics of thinner profiles, and a thickness ratio of 2 percent was chosen for the present investigation.

The investigation of reference 2 showed that changes in the thickness distribution or shape of 9-percent-thick airfoils became of decreasing importance as the Mach number was increased and approached

sonic velocity. Furthermore, it is readily accepted that reductions in thickness of the profile, such as the NACA 6-series airfoils, would of necessity cause a reduction in the aerodynamic significance of the profile-shape changes at high subsonic Mach numbers as the ratio of thickness to chord is decreased and approaches zero. Since the effects of changes in thickness distribution of a 2-percent-thick airfoil could be expected to be small, and in order to provide maximum structural strength for the airfoil, a slab-sided profile was chosen for this investigation.

The investigation was conducted to determine the aerodynamic characteristics at high subsonic Mach numbers of slab-sided profiles of 2-percent thickness which had variations in elliptically shaped leading and trailing edges from a fineness ratio of 0 to 10. Six profiles were investigated at angles of attack between 0° and 10° over a Mach number range from 0.5 to 1.0. The corresponding Reynolds number range was from 1.4×10^6 to 2.1×10^6 .

SYMBOLS

c_d	section drag coefficient
c_{l_i}	design lift coefficient
$c_{m_c/4}$	section pitching-moment coefficient taken about quarter-chord axis
c_n	section normal-force coefficient
M	Mach number of free stream
$M_{l_{max}}$	maximum local Mach number along airfoil surface
n/d	ratio of section normal force to drag
P	pressure coefficient, $\frac{p_l - p}{q}$
p	free-stream static pressure
p_l	local static pressure on model surface
q	free-stream dynamic pressure
t/c	ratio of thickness to chord

α	angle of attack, deg
Δc_m	positive increment in $c_{mC}/4$ due to transonic flow attachment

APPARATUS AND TESTS

Tests were conducted in the Langley 4- by 19-inch semiopen tunnel operating as a direct blowdown tunnel from a supply of dry compressed air (fig. 1). The tunnel test section was open along the top and bottom boundaries, and the chambers extending beyond those two boundaries were connected by a duct. The test region and the calibration of the flow are described in reference 2.

Each model had a 4-inch chord and completely spanned the 4-inch dimension of the tunnel. The models were mounted in circular end plates which maintained the continuity of the tunnel walls. Inasmuch as these models were quite thin, additional stiffness was required. The models extended through the end plates and external tension was applied to the ends of the models. The airfoils were slab-sided with elliptical leading and trailing edges (fig. 2). The fineness ratios of the elliptical edges varied from 0 to 10. The combinations of leading- and trailing-edge shapes of 2-percent-thick airfoils tested and the corresponding airfoil designations are as follows:

Airfoil designation	Leading-edge shape	Trailing-edge shape
1-0	1:1	Square or 0:1
1-4	1:1	4:1
10-4	10:1	4:1
10-10	10:1	10:1
4-10	4:1	10:1
4-1	4:1	1:1

Data were obtained from pressure measurements and schlieren photographs of the flow. Normal-force and moment data were obtained by means of an electrical pressure integrator connected to the 44 static-pressure orifices (fig. 2(a)) installed in the surfaces of the airfoil. The pressure orifices were also connected to a manometer so that the distribution of pressures along the surface could be recorded. Normal-force and moment data were obtained through an angle-of-attack range from 0° to 10° . Drag data were obtained at angles of attack from 0° to 8° .

by the wake-survey method, using a total-pressure survey rake located one chord downstream of the model trailing edge. The Mach number range of the tests extended from 0.5 to 1.0, and the corresponding Reynolds number range was from 1.4×10^6 to 2.1×10^6 .

The models used in obtaining schlieren photographs of the flow also required tensioning to reduce deflections. The portion of the models between the 10- and 90-percent-chord stations extended through the tunnel walls, and the tensioning device was attached to the lower surface. As a consequence, the flow along the central 80 percent of the model for the lower surface was obscured. Along the upper surface the glass-model juncture was sealed with wax. The juncture produced a thin, irregular boundary that obscured, to some extent, the boundary-layer flow along the central part of the upper surface. Neither the juncture of the model and tunnel nor the support system interfered with light passage near the leading and trailing edges. Pictures of the flows were taken over the speed range at a constant angle of attack by using a 35-millimeter motion-picture camera and the technique described in reference 5. Since each picture had an exposure of 4 microseconds, individual frames from the motion pictures were selected as still photographs. Photographs were taken at angles of attack of 0° , 4° , and 8° for all airfoils and at 10° for the 1-4, 10-4, and 4-10 airfoils.

JET BOUNDARY EFFECTS

Aerodynamic data on airfoils tested in this two-dimensional open-throat tunnel (fig. 1) are subject to corrections for jet boundary effects. The simple open-throat correction is subject to modification because of the restraint imposed on jet deflection by the effuser and exit cone located at the end of the test section (ref. 6). The primary correction to which these data are subject is believed to be the jet deflection or angle of attack. For incompressible flow, the correction is $\alpha_{\text{true}} = \alpha_{\text{test}} - 1.85c_n$ (derived from ref. 6). For a compressible flow, reference 7 indicates that the incompressible form is subject to additional corrections in terms of $1 - M^2$. The justification for the application of the compressible form of the correction decreases as the Mach number is increased beyond the attainment of sonic velocity locally within the flow, and a suitable form of correction for application near a Mach number of 1.0 is unknown. As a consequence, data are presented herein without any corrections applied and, as such, can be directly compared with the data of reference 2.

RESULTS AND DISCUSSION

EFFECT OF AIRFOIL SHAPE ON PRESSURE DISTRIBUTION

Pressure distributions for the 1-0, 1-4, and 10-4 airfoils in two-dimensional flow are presented in figures 3, 4, and 5, respectively. The particular airfoils, the Mach numbers, and the angles of attack in these figures were chosen to be representative of the range of this investigation. At zero angle of attack (figs. 3(a), 4(a), and 5(a)), the flow accelerates around the leading edge to a value in excess of the stream velocity and then rapidly decelerates to approximately, or slightly above, stream velocity. The velocities along the flat portion of the airfoils remain approximately constant, and an acceleration occurs around the elliptical trailing edges. These distributions, especially at the lower speeds, indicate that the shape of the leading and trailing edges exerts a local influence on the pressure distribution without any appreciable mutual effect, which may be expected because of the very small chordwise extent of the elliptical portions of the leading and trailing edges. At Mach numbers near 1, the extent of the influence of a leading edge along the chord is increased, and the pressure distributions appear to be primarily a function of the leading-edge shape. The absence of trailing-edge effects on pressure distributions at a Mach number of 1.0 is entirely due to the existence of large regions of supersonic velocities along the surface of the profiles.

At an angle of attack of 4° (figs. 3(b), 4(b), and 5(b)), the shape of the distribution at low speeds is dependent primarily on the leading-edge shape, the trailing edge having no appreciable effect. As the Mach number increases, however, the differences in pressure distribution arising from differences in leading-edge shape become less, although there is still some influence of shape on the distribution at a Mach number of 1.0. With a further increase in angle of attack, the shape effect on the pressure distributions is greatly reduced, except in figure 4(c) at Mach number 0.79 which involves flow separation and attachment and is discussed later.

The pressure distributions for the 1-x airfoils (figs. 3(b) and 4(b)) at 4° angle of attack and at the highest Mach number show evidence of supersonic velocities being obtained on the lower surface. This is a direct result of decreasing circulation with increasing Mach number which, occurring on a blunt leading-edge profile, provides a region on the lower surface conducive to rapid acceleration to velocities exceeding sonic velocities and necessitating shocks for recompression, as shown by the schlieren photographs (figs. 6(b) and 7(b)). Sharpening of the leading edge, however, completely eliminates this lower-surface shock, which is observed at lower angles of attack (not exceeding 4°).

EFFECT OF AIRFOIL SHAPE ON SEPARATION AND OVEREXPANSION

General Result of This Investigation

The schlieren photographs (figs. 6, 7, and 8) show that each of the profiles under lifting conditions encounters flow separation from the leading edge at the low Mach numbers. The occurrence of flow separation is substantiated by the flatness of the pressure distribution along the forward part of the upper surface of the models (figs. 3, 4, and 5). The only exception to this general statement is the sharp-nose profile at moderately low angles of attack. With increasing angle of attack, however, the sharp-nose airfoil (10-4, figs. 5 and 8) encounters the same type of flow as the blunt-edge profiles exhibit.

At any given angle of attack, when the flow is separated from the leading edge and the Mach number is increased in the transonic speed range beyond a value of about 0.8, regions of supersonic flow are formed near the leading edge. The flow around the leading edge expands through a supersonic turn around a corner and eliminates the separated-flow condition. This flow phenomenon or transonic flow attachment is discussed in more detail in references 8 and 9. After flow attachment occurs, the flow undergoes less overexpansion around the sharp-nose profiles than around the blunt-nose profiles, as evidenced by the moderately strong oblique shocks near the leading edge of the blunt l-x airfoils (figs. 6 and 7). These shocks are required for redirection of the flow along the model surface following an overexpansion. Figure 8 indicates that the trend toward overexpansion increases with an increase in the extent of flow separation that exists at the low Mach numbers. Furthermore, the pressure distributions in figures 3, 4, and 5 show that an increase in overexpansion, as exhibited in figures 6, 7, and 8, effects a decrease in the local pressure near the leading edge, which in turn could produce significant force changes at transonic flow attachment.

Examination of Detailed Results of This Investigation

Additional pressure distributions and their corresponding schlieren photographs at Mach numbers near flow attachment are presented to provide more detailed information on the flow changes that occur. Data for the l-x airfoils (figs. 9 and 10) show that the flow attachment occurs at a Mach number that increases with an increasing angle of attack and is in the Mach number range between 0.75 and 0.86. The flow attachment occurs within a Mach number increment of approximately 0.02, as indicated by the pressure distributions corresponding to the highest test Mach number below attachment and the lowest test Mach number above attachment which existed within the data. From an examination of moving pictures of the

flow, the attachment occurred abruptly on the blunt-nose profiles. The pressure distributions in figure 9 show that the flow change is accompanied by a change in load which will have an appreciable effect on some of the aerodynamic characteristics, especially the pitching moment which is subject to an increase in a positive direction. The data indicate further that these flow changes are confined to the upper surface since the pressures on the lower surface are relatively free of any change and therefore of any effect of the transonic flow attachment on the upper surface.

The data presented in figures 9 and 10 for the 1-x airfoils at 8° angle of attack are compared in figures 11 and 12 with similar data from the 4-10 airfoil to show the effects of leading-edge shape on flow attachment. As the Mach number is increased from 0.7 to 0.8 for the 4-10 airfoil, there is a continuous transition in the pressure distribution and, at the Mach number of 0.8 the distribution is quite similar to the distribution observed on the blunt-nose profile at Mach numbers above flow attachment. The transition over the Mach number range of 0.1 for the 4-10 airfoil is quite gradual as compared to the abrupt changes in flow over the blunt-nose profiles. This gradual transition is a direct result of a progressive growth of the velocities over the leading edge, starting at a Mach number of 0.7 with a relatively high velocity, as compared to the velocities on the blunt-nose profiles. While no quantitative measurements were made on the extent of separation at an angle of attack of 8° , an examination of the schlieren photographs at an angle of attack of 4° shows that the extent of separation was greater on the blunt-nose profiles than on the 4-x airfoils, and the 10-x airfoils exhibit no separation.

Examination of Results from Other Investigations

General.- The overexpansion occurring on the blunt, and not on the sharp, airfoil appears to be in direct opposition to the description of this flow phenomenon in reference 8 for 6-percent-thick airfoils, wherein overexpansion was shown to occur on the sharp wedge-type airfoils but not on the round-nose airfoils. Similarly, flow photographs in reference 2 show that at a given angle of attack a decrease in thickness and a consequent decrease in bluntness of the leading edge resulted in overexpansion around the leading edge. Since the results of references 2 and 8 appear to be in direct contradiction with the present investigation, data from reference 2 will be examined for a more careful evaluation of leading-edge effects on transonic flow attachment.

Effect of thickness.- Schlieren photographs from the two-dimensional investigation reported in reference 2 are reproduced in figures 13, 14, and 15 to show the flow past airfoils at Mach numbers and angles of attack beyond those presented in reference 2. Figure 13 illustrates that,

at a Mach number of 0.53 and at a constant angle of attack, an increase in thickness of an airfoil is accompanied by a decrease in separation from a moderately separated flow condition on the 4-percent-thick model to no separation on the 12-percent-thick model. Increasing the Mach number of the flow past the thin airfoil produces a transition from separated to unseparated flow that is accompanied by some overexpansion, as evidenced by the oblique shock near the leading edge. At any given Mach number the amount of overexpansion progressively decreases with increasing thickness, until no evidence of overexpansion is exhibited in the flow past the 12-percent-thick airfoil.

Effect of camber.- Similar occurrences of low-speed separation and high-speed overexpansion are shown in figures 14 and 15 for 6-percent-thick airfoils having various amounts of camber which, expressed in terms of the design-lift coefficient, are 0, 0.2, and 0.5. Since the ratio of thickness to chord and thickness distribution are constant, the bluntness of the leading edge is constant for these profiles. Figure 14 shows the three airfoils at an angle of attack of 6° ; the highest cambered profile is also shown at a reduced angle of attack in order to provide a lift coefficient slightly higher than that for the symmetrical profile. Figure 15 shows the three 6-percent-thick airfoils at angles of attack that increase as the camber increases. The angles of attack were chosen so that at Mach number 0.58 the leading-edge flow separation is approximately the same for the three models. These photographs (figs. 14 and 15) at constant angle of attack show overexpansion at high speeds is always accompanied by leading-edge flow separation at low speeds and is in agreement with the results observed in figure 13.

Effect of leading-edge radius.- An investigation of leading-edge-radius effects on the aerodynamic characteristics of 9-percent-thick airfoils (NACA 0009-64 and -44) is reported in reference 10. An examination of the flow photographs at an angle of attack of 4° in reference 10 indicates that an increase in the leading-edge radius from 0.39 to 0.89 percent chord produces overexpansion around the leading edge and flow separation from the leading edge at low speeds on the NACA 0009-64 airfoil.

Correlation of Data on Flow Attachment

The previous data indicate that, as the degree or extent of flow separation at low speeds decreases, the overexpansion at high speeds decreases and the Mach number for flow attachment decreases. The data also show that, as the angle of attack is decreased for any given profile, the transonic flow attachment gradually fades out at some low-limiting angle of attack, and consequently the Mach number for flow attachment becomes indeterminate at the low angles of attack. The effect of airfoil parameters on the Mach number for transonic flow attachment as obtained

from an examination of present and former investigations (refs. 2 and 8) is presented in figure 16. Data presented in figure 16(a) show the effect of angle of attack and thickness on the Mach number for flow attachment. These data illustrate that, as the angle of attack is increased, the Mach number for flow attachment on the airfoil increases. Furthermore, at any given angle of attack the Mach number for flow attachment decreases as the ratio of thickness to chord is increased. Data for the cambered airfoils (fig. 16(c)) show that the general effects of camber and thickness are similar.

Results from reference 8 for sharp leading-edge airfoils (at an angle of attack of 4° , fig. 16(b)) show a decrease in the Mach number for flow attachment as the included angle of the leading edge increases. Unpublished data on a wedge profile with 0, 25, and 50 percent of the afterbody removed indicate that the Mach number for attachment is dependent upon the forebody shape and the afterbody has no significant effect. An increase in the leading-edge angle, therefore, can be considered to be equivalent to an increase in the ratio of thickness to chord. Thus, at a constant angle of attack, an increase in the leading-edge angle produces a decrease in the Mach number for flow attachment, which is the same effect as an increase in the ratio of thickness to chord.

The data of the present investigation (fig. 16(d)) show that an increase in the angle of attack produces an increase in the Mach number for flow attachment and are in agreement with the preceding results. The data, however, also show that an increase in the fineness ratio of the leading edge results in a decrease in the Mach number for attachment and, as previously stated, a decrease in overexpansion. These results thus appear to be in contradiction to the trend of the data showing the effects of thickness and leading-edge angle. The apparent contradiction, however, is based on the assumption that there is a continuous linear variation of the effects of leading-edge shape throughout the range of leading-edge shapes covered by the present and previous investigations.

The leading-edge shape is to a large extent dependent upon the leading-edge radius. Since the data have indicated that high-speed overexpansion and Mach number for flow attachment correlate with the extent of the flow separation at low speeds, a simple index for flow separation will be examined as a function of the leading-edge radius of symmetrical airfoils expressed in percent of the thickness. The probability of flow separation can be considered a function of the maximum negative pressure coefficient (see also ref. 11). The maximum negative theoretical pressure coefficients for NACA 0009-xx airfoils at an angle of attack of approximately 4° and their variation with the leading-edge radius are presented in figure 17(a). The nonlinear variation is similar to the findings in reference 11 in that a moderately shaped nose, that is, one that is neither blunt nor sharp, produces the

lowest values of the maximum negative pressure coefficient and thus is less likely to encounter flow separation. The Mach number for flow attachment for the airfoils which have been discussed is presented in figure 17(b). These data show a nonlinear variation with the leading-edge radius similar to the variation shown by the theoretical pressure-distribution results. This figure shows that the data from previous investigations (refs. 2 and 8) and the present investigation on the effect of leading-edge shape on Mach number for flow attachment and overexpansion are in agreement. Both results show that an airfoil having a moderately shaped leading edge will alleviate separation and reduce the adverse effects of transonic flow attachment.

EFFECT OF FLOW CHANGES AND AIRFOIL SHAPE ON AERODYNAMIC FORCES

General Effects

The normal-force, drag, and pitching-moment data are presented in coefficient form as a function of Mach number at constant angles of attack for each of the airfoils in figure 18. The most noteworthy characteristic of the normal-force coefficients observed in these basic data is the high Mach number at which the normal-force break occurs, generally around a Mach number of about 0.95. This characteristic was unaffected by changes in leading- and trailing-edge shapes. The high Mach number for normal-force break and the absence of a reversal is in complete agreement with the characteristics of thin airfoils as evidenced by the data on the 4- and 6-percent-thick airfoils in reference 2.

The drag coefficients in the basic data show erratic variations with Mach number. After the usual drag-rise characteristic, most of the profiles undergo a rapid dropoff in drag coefficient at a Mach number between 0.8 and 0.9. At a somewhat higher Mach number, the data indicate a reversal in drag coefficient.

The pitching-moment coefficients for all these 2-percent-thick profiles exhibit an abrupt change at a Mach number between 0.75 and 0.85. The abruptness of this change and the Mach number at which it occurs appear to increase with angle of attack. An examination of these data indicates that the Mach number at which the moment pitch-up occurs M_a coincides with the Mach number at which the rapid rise in normal-force coefficient begins and is near the Mach number for the usual drag rise. At a somewhat higher Mach number M_b , a minimum value of negative moment occurs and is followed by a rapid increase in negative pitching moment. The Mach number M_c at which a second inflection in the pitching moment occurs coincides with the Mach number for the normal-force break.

Effect of Flow Changes on Pitching Moment

The initial moment pitch-up or break occurs at M_a as a result of the elimination of flow separation by the transonic flow attachment. The flow change produces an increase in the maximum local Mach number $M_{l_{max}}$ and in the chordwise extent of low pressures. The compression shock for this flow condition generally occurs at a station ahead of the 25-percent-chord station. The pressure changes produce a positive increment in the pitching moment Δc_m , and the flow conditions represent the beginning of the range in which the normal force increases rapidly with the Mach number. The normal-force increases are due to rapid rearward-chordwise movement of the shock.

The Mach number M_b for minimum negative pitching moment was caused by the compression shock moving past the quarter-chord station and thus starting to contribute toward negative pitching moments. This Mach number is in the speed range in which the load at the leading edge is dropping off rapidly thereby producing a decrease in the maximum local Mach numbers (fig. 19) and a decrease in the shock intensity with increasing stream Mach number (fig. 20). The fact that the shock moves rearward more rapidly than the loading over the forward part of the profile decreases is proved by the fact that the total normal force continues to increase rapidly.

The Mach number M_c is attained when the shock on the upper surface reaches the trailing edge. With the shock at the trailing edge, further expansion of the low-pressure field along the upper surface is impossible; consequently, further increases in normal force and negative moment are halted.

Examination of Drag Distribution Across Wakes

In an attempt to evaluate the factors that contributed to the erratic behavior of the drag coefficients, an analysis was made, not only of the variation in the maximum local Mach number with the stream Mach number, but also of the changes that occurred in the distribution of drag across the wake of the models. Typical examples are shown in figures 19 and 20. In this analysis it was found that the lower surface did not contribute to any aerodynamic fluctuations of the drag coefficient. It did, however, contribute toward an increase in drag coefficient at a Mach number above a value somewhere between 0.9 and 0.95. The drag from the central part of the wake varied for some airfoils in a manner similar to the variation in the total drag coefficients. In other cases this drag in the central region of the wake was essentially constant, and the fluctuations occurred only in the upper-surface drag.

The explanation of these fluctuations in drag coefficients was not discernible in either the pressure distributions or the schlieren photographs. The fluctuations are probably due to a combination of small effects which are not detectible in this investigation. Similar variations of drag coefficient with Mach number have been observed in tests of rocket-powered models in free flight (ref. 12).

Effect of Airfoil Shape on Pitching Moment

A quantitative evaluation of the effects of leading- and trailing-edge shapes and the normal-force coefficient on the pitching-moment break which accompanies flow attachment at the leading edge of the profile is shown in figure 21. The Mach number at which the pitching-moment break occurs generally increases with normal-force coefficient and is further increased by increasing the bluntness of the leading edge (fig. 21(a)). The trailing-edge shape has only a minor effect, except when in combination with a blunt leading edge at c_n between 0.6 and 0.7. For this combination, increasing the bluntness of the trailing edge to values less than four results in increased Mach number for the moment break.

The increment in pitching moment at transonic flow attachment Δc_m increases with the normal-force coefficient (fig. 21(b)), as was also observed in the basic data (fig. 18). It was also seen in figure 21(b) that the increment increases as the leading edge becomes progressively more blunt, and a similar effect is observed for trailing-edge shape. The effect is rather significant for trailing-edge shapes having fineness ratios less than 4.

AERODYNAMIC CHARACTERISTICS

The data from figure 18 are cross-plotted to show changes in aerodynamic characteristics of these 2-percent-thick airfoils over the range of variables investigated. These data, as previously described, are uncorrected for jet-boundary effects because no suitable means of correction exists.

Normal-Force Coefficients

The variation in normal-force coefficient with angle of attack at selected Mach numbers from 0.7 to 1.0 is shown in figure 22. The data indicate that the maximum normal-force coefficient can be expected to increase from 0.8 at a Mach number of 0.70 to a value in excess of 1.00

at Mach numbers between 0.95 and 1.00. The figure also illustrates some effects of leading- and trailing-edge changes. At a Mach number of 0.70, the effects of the leading- and trailing-edge shape on the normal-force-curve slope are relatively large, and the airfoil having the most blunt leading edge combined with the most blunt trailing edge has the largest normal-force-curve slope. While the blunt leading edge retains its ability to improve the normal-force-curve slopes at high Mach numbers, the improvement contributed by the blunt trailing edge progressively decreases as Mach number increases. Furthermore, increases in the fineness ratio of the leading or trailing edge from 4 to 10 have little effect on the normal force throughout the range.

Drag Coefficients

The variation in the section drag coefficient with section normal-force coefficient is presented in figure 23 at Mach numbers from 0.70 to 1.00. An examination of the data indicates that shape has quite a large effect on drag, particularly at low normal-force coefficients. As the section normal-force coefficient is increased beyond 0.6, the effects of shape on drag appear to become small. These effects, however, are illustrated more clearly in figure 24, which shows the variation in the section drag coefficient with Mach number at constant normal-force coefficient as affected by profile shape. The data at a normal-force coefficient of zero indicate, in general, that blunting of the leading or the trailing edge, or both, causes a marked increase in the section drag coefficient. At a normal-force coefficient of 0.4 and Mach numbers less than 0.95, the profiles having blunt noses and blunt trailing edges (1-4 and 1-0) have the highest section drag coefficients. Increasing the fineness ratio of the leading and trailing edges produces a decrease in drag. The profiles having the least drag were the 10-10 airfoil at Mach numbers from 0.50 to 0.95 and the 4-10 airfoil at Mach numbers from 0.96 to 1.0. At a normal-force coefficient of 0.8 the effects of shape are of decreased importance and somewhat erratic in nature. The 10-4 profile, however, had the lowest drag coefficient over the high Mach number range.

The variations in the ratio of normal force to drag with section normal-force coefficient for the various airfoils, as affected by Mach number, are shown in figure 25. The maximum ratio of normal force to drag increases with an increase in Mach number to a maximum value at a Mach number between 0.9 and 0.95. Further increases in the Mach number result in a reduction in the maximum ratio of normal force to drag. The highest value of the ratio of normal force to drag for each of the airfoils occurs at a normal-force coefficient of 0.5 or greater. The effect of profile shape on the ratio of normal force to drag is illustrated in figure 26. The data show, in general, a decided effect of shape at Mach numbers of 0.95 and below, while at a Mach number of 1.00,

shape has little effect. At these lower Mach numbers, profiles with leading- and trailing-edge combinations of fineness ratios of 4 and 10 have the highest ratios of normal force to drag, whereas the profiles with the blunt shapes have the lowest values. These effects are maintained throughout the speed range even though, as previously stated, the magnitude of the changes in the ratio of normal force to drag at a Mach number of 1.0 is small.

Pitching-Moment Coefficients

The variations of pitching-moment coefficient with section normal-force coefficient are shown in figure 27. The data illustrate, as did the normal-force data, that the largest effect of shape on the pitching moment occurs at the lowest test Mach numbers where blunting of either the leading edge or the trailing edge, or both, produces a negative shift in pitching moment at a lower normal-force coefficient. With an increase in Mach number, the effect of shape on variations in the pitching-moment coefficient rapidly decreases, and at Mach number of 1.0 there is little effect due to shape.

Summary of Aerodynamic Characteristics

The data show that improvements in the normal-force-curve slope are attained throughout the speed range by using blunt leading edges. Some improvement, especially at Mach numbers around 0.7, is produced also by blunting the trailing edge of the airfoil. These beneficial effects on normal-force coefficient, however, are accompanied by increases in the drag coefficient. Airfoils having leading- and trailing-edge combinations of fineness ratios of 4 and 10 not only produce the highest ratios of normal force to drag, but also have the smallest abrupt change in pitching moment at the transonic flow attachment.

The general effect of changes in leading- and trailing-edge shapes from fineness ratios of 4 to 10 is small. Sufficient variations occur through the ranges of Mach number and normal-force coefficient to make the choice of a particular combination dependent on the requirements for a specific application.

Effects of Thickness

Data for the 4-10 airfoil of 2-percent thickness are compared with similar data obtained from reference 2 on the NACA 64A004 and 64A006 airfoils in order to evaluate the effect of thickness on the aerodynamic characteristics. Figure 28 shows that at a Mach number of 0.7, there is

little effect of thickness on the section normal-force coefficient; however, an increase in Mach number to values in excess of 0.9 results in an appreciable increase in the section normal-force coefficient at any given angle of attack as a result of a decrease in the ratio of thickness to chord. The maximum benefit is observed at the highest test Mach number of 1.0. The ratios of normal force to drag (fig. 29) illustrate that reductions in thickness to 2 percent produce additional improvements in the ratio of normal force to drag. At a Mach number of 0.7, the thinnest airfoil has the lowest ratio of normal force to drag. Increase in the Mach number causes a progressive shift in the effect of thickness on this ratio, and at Mach number of 0.95 to 1.0, the thinnest profile has the highest ratio of normal force to drag.

The previously observed effects of thickness are also retained in the variation of the center-of-pressure location with Mach number (fig. 30) for normal-force coefficients of 0.2 and 0.4. A reduction in thickness results in an increase in the Mach number at which the center of pressure starts moving rearward. In general, this comparison at high subsonic Mach numbers illustrates that the beneficial effects of reductions in thickness to 4 percent, shown by previous investigations to increase the normal-force curve slope and ratio of normal force to drag, as well as to increase the Mach number at which the center of pressure started moving rearward, are also observed in the present investigation of 2-percent-thick airfoils.

CONCLUDING REMARKS

A two-dimensional investigation at transonic Mach numbers has been made of the flow and force characteristics of slab-sided airfoils of 2-percent thickness. The airfoils had various combinations of elliptically shaped leading and trailing edges from a fineness ratio of 0 to 10.

The results indicate that with an increase in Mach number an abrupt break in pitching moment occurred as a consequence of an abrupt transition from separated to unseparated flow at transonic flow attachment. The abruptness of the flow change was reduced by increasing the fineness ratio of the elliptical leading edge, a result which is in agreement with the data of NACA Technical Note 1211. Both investigations show that a properly shaped leading edge alleviates flow separation and thereby reduces overexpansion at transonic flow attachment.

The data illustrate that airfoils having leading- and trailing-edge combinations of fineness ratios of 4 and 10 not only produce the highest ratios of normal force to drag, but also have the smallest abrupt change in pitching moment at transonic flow attachment. Although the general

effect of changes in leading- and trailing-edge shapes from fineness ratios of 4 to 10 was small, sufficient variations occur through the range of Mach number and normal-force coefficient to make the choice of a particular combination dependent on the requirements for a specific application.

A comparison of the aerodynamic characteristics of the 2-percent-thick profiles was made with the characteristics of 4- and 6-percent-thick profiles obtained under the same test conditions. The comparison at high subsonic Mach numbers indicates that the beneficial effects of reductions in thickness to 4 percent, shown by previous investigations to increase the normal-force-curve slope and ratio of normal force to drag, as well as to increase the Mach number at which the center of pressure started moving rearward, are also observed in the present investigation of 2-percent-thick airfoils.

Langley Aeronautical Laboratory,
National Advisory Committee for Aeronautics,
Langley Field, Va., September 17, 1954.

REFERENCES

1. Stack, John: The N.A.C.A. High-Speed Wind Tunnel and Tests of Six Propeller Sections. NACA Rep. 463, 1933.
2. Daley, Bernard N., and Dick, Richard S.: Effect of Thickness, Camber, and Thickness Distribution on Airfoil Characteristics at Mach Numbers Up to 1.0. NACA RM L52G31a, 1952.
3. Busemann, Adolf: Application of Transonic Similarity. NACA TN 2687, 1952.
4. Kaplan, Carl: On Similarity Rules for Transonic Flows. NACA Rep. 894, 1948. (Supersedes NACA TN 1527.)
5. Lindsey, Walter F., and Burlock, Joseph: A Variable-Frequency Light Synchronized With a High-Speed Motion-Picture Camera To Provide Very Short Exposure Times. NACA TN 2949, 1953.
6. Katzoff, S., Gardner, Clifford S., Diesendruck, Leo, and Eisenstadt, Bertram J.: Linear Theory of Boundary Effects in Open Wind Tunnels With Finite Jet Lengths. NACA Rep. 976, 1950. (Supersedes NACA TN 1826.)
7. Goldstein, S., and Young, A. D.: The Linear Perturbation Theory of Compressible Flow, With Applications to Wind-Tunnel Interference. R. & M. No. 1909, British A.R.C., 1943.
8. Lindsey, W. F., Daley, Bernard N., and Humphreys, Milton D.: The Flow and Force Characteristics of Supersonic Airfoils at High Subsonic Speeds. NACA TN 1211, 1947.
9. Lindsey, Walter F., and Dick, Richard S.: Two-Dimensional Chordwise Load Distributions at Transonic Speeds. NACA RM L51I07, 1952.
10. Humphreys, Milton D., and Robinson, Raymond A.: The Effect of Changes in the Leading-Edge Radius on the Aerodynamic Characteristics of a Symmetrical, 9-Percent-Thick Airfoil at High-Subsonic Mach Numbers. NACA RM L9L09, 1950.
11. Loftin, Laurence K. Jr., and von Doenhoff, Albert E.: Exploratory Investigation at High and Low Subsonic Mach Numbers of Two Experimental 6-Percent-Thick Airfoil Sections Designed To Have High Maximum Lift Coefficients. NACA RM L51F06, 1951.
12. Morrow, John D., and Nelson, Robert L.: Large-Scale Flight Measurements of Zero-Lift Drag of 10 Wing-Body Configurations at Mach Numbers From 0.8 to 1.6. NACA RM L52D18a, 1953.

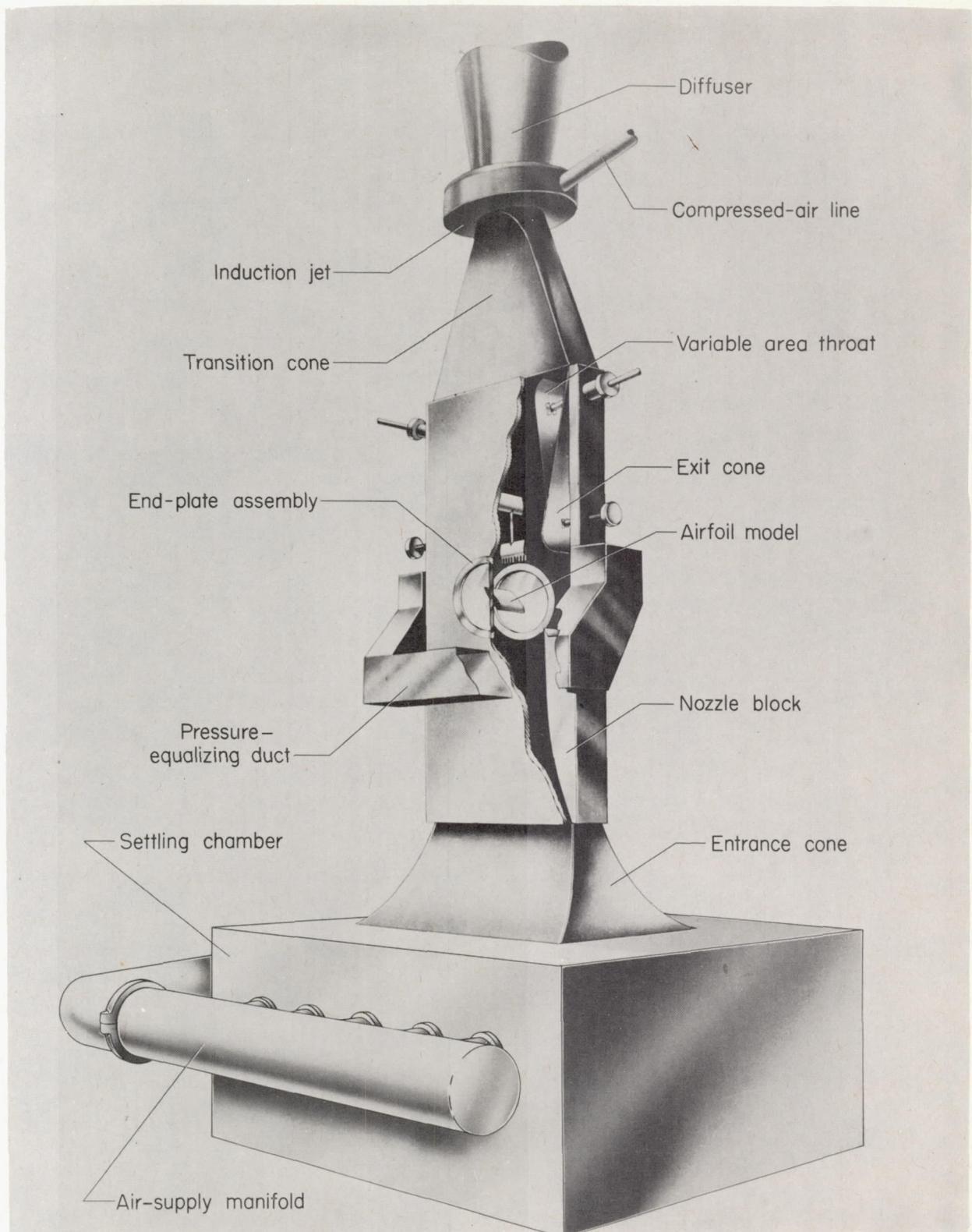
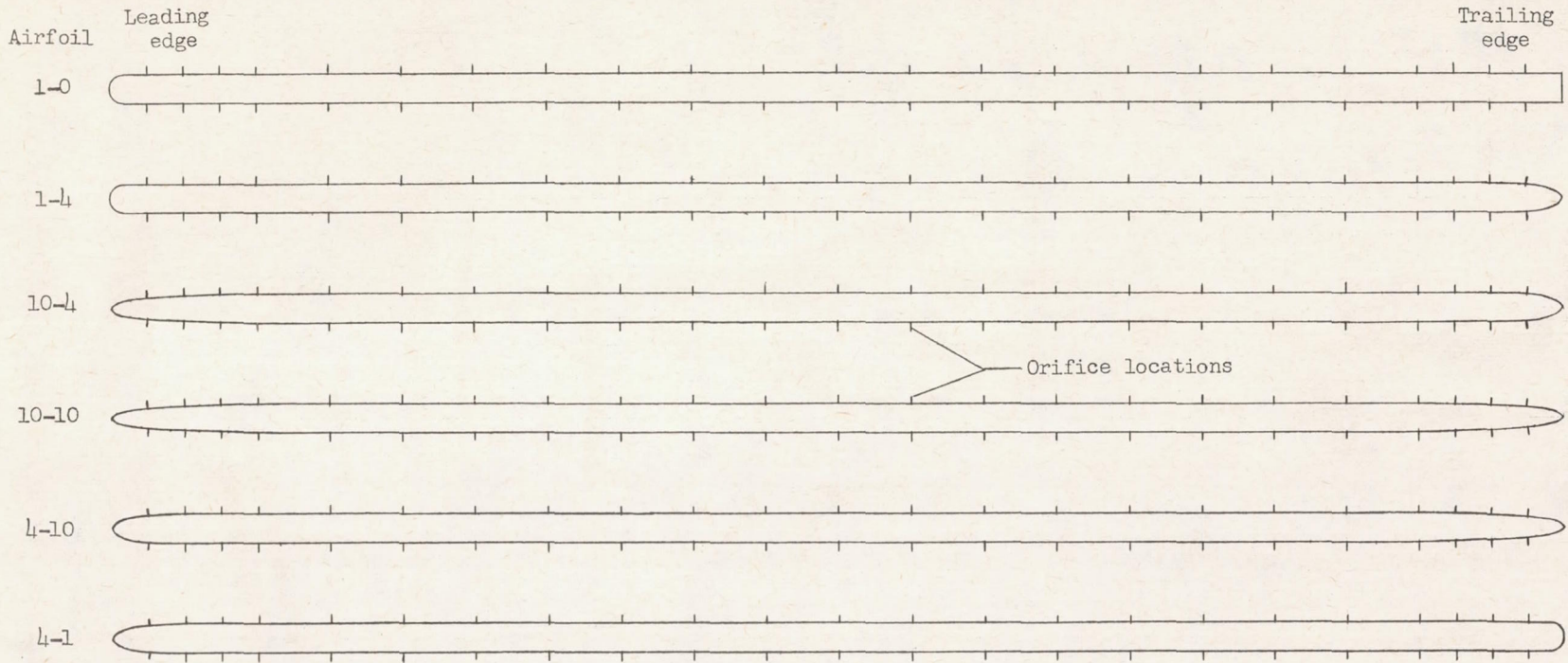


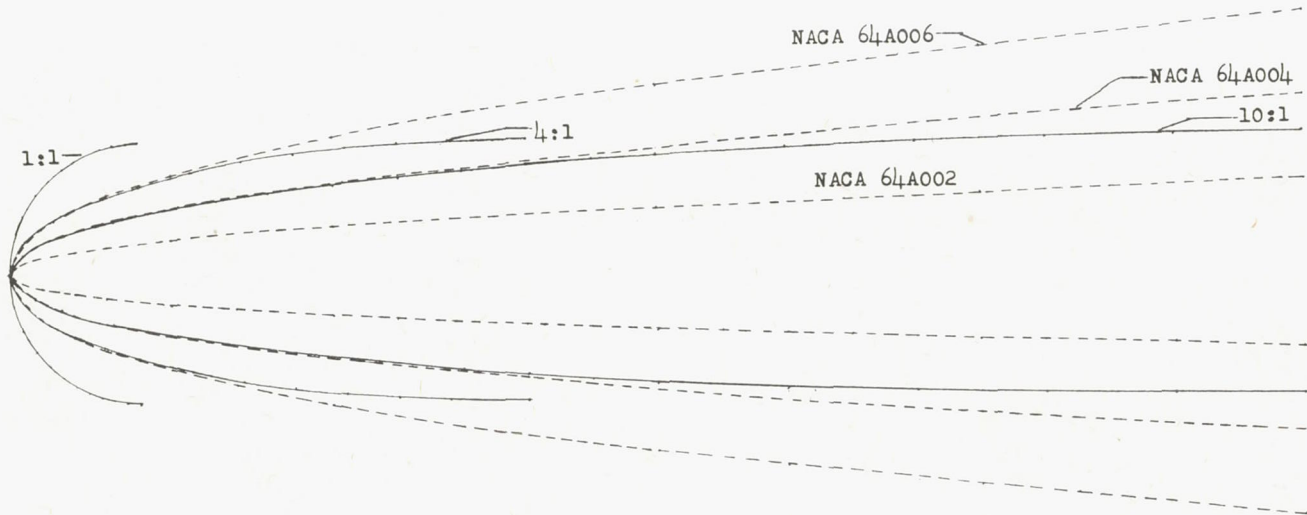
Figure 1.- Langley 4- by 19-inch semiopen tunnel.

L-83293.1

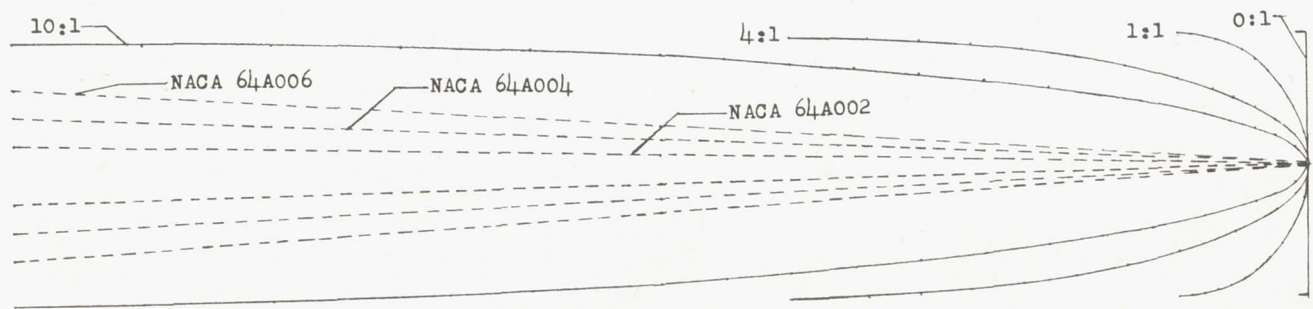


(a) Airfoil profiles and orifice locations.

Figure 2.- Models.



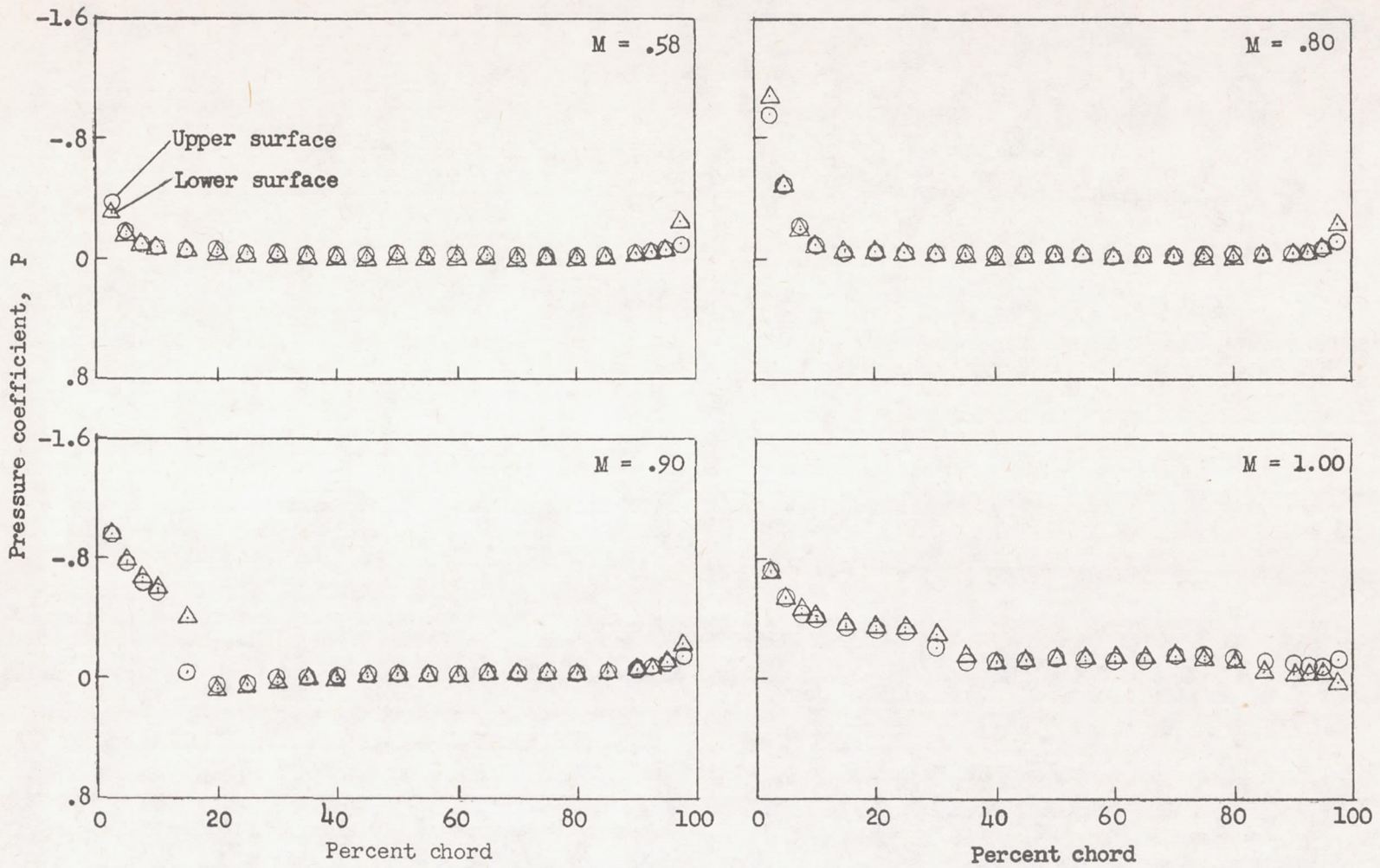
Leading-edge shape



Trailing-edge shape

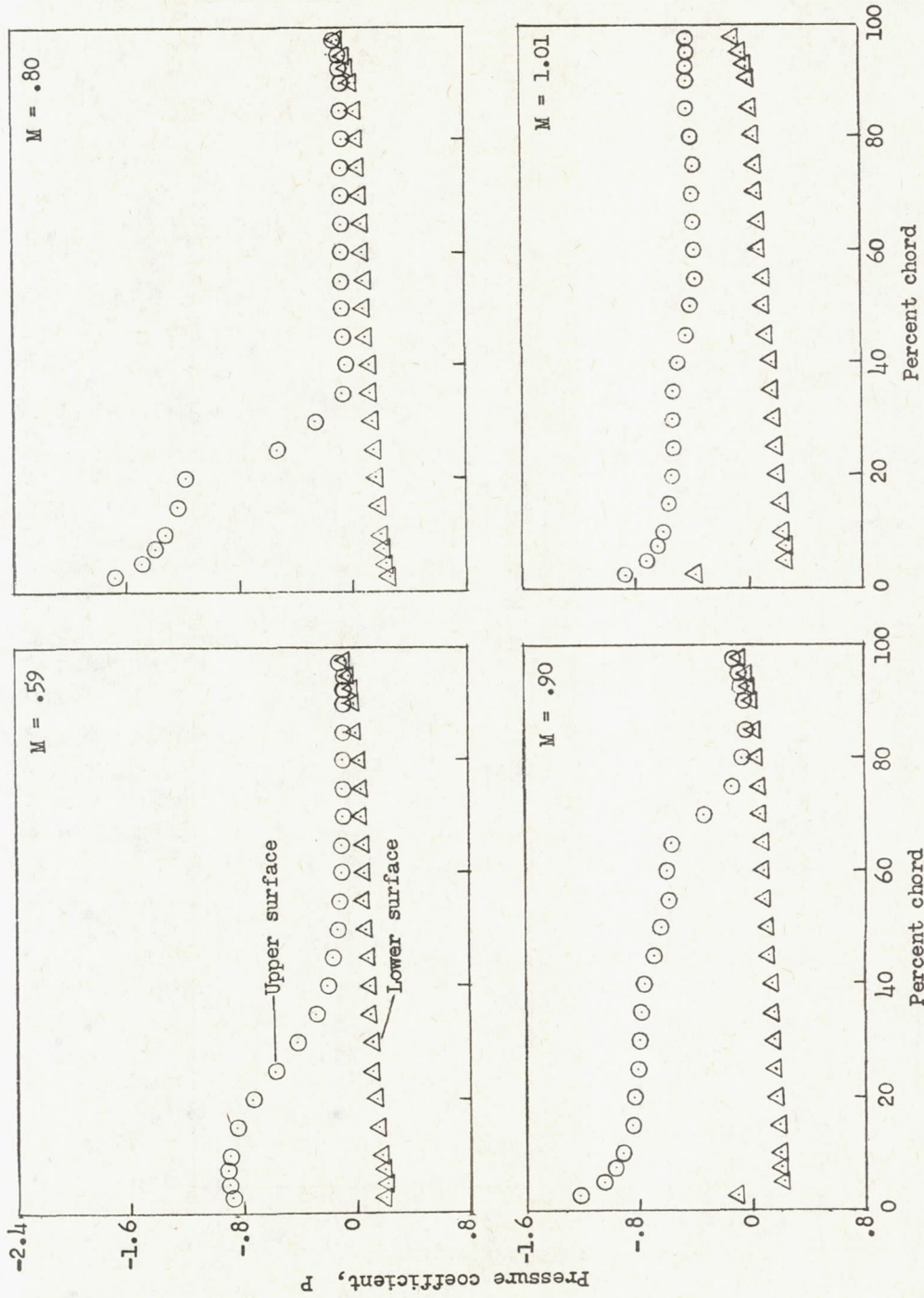
(b) Comparison of leading- and trailing-edge shapes.

Figure 2.- Concluded.



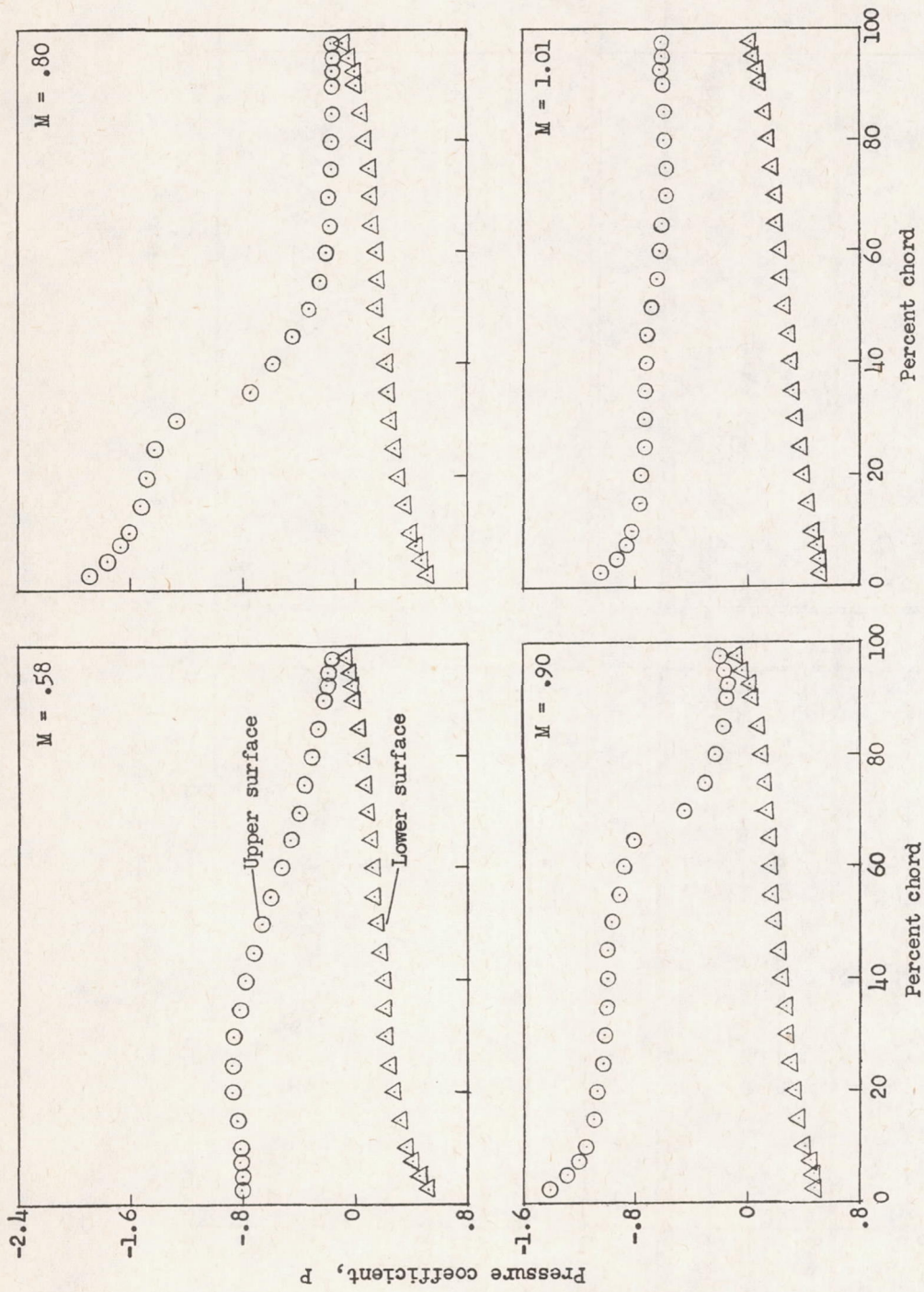
(a) $\alpha = 0^\circ$.

Figure 3.- Pressure distributions for the 1-0 airfoil.



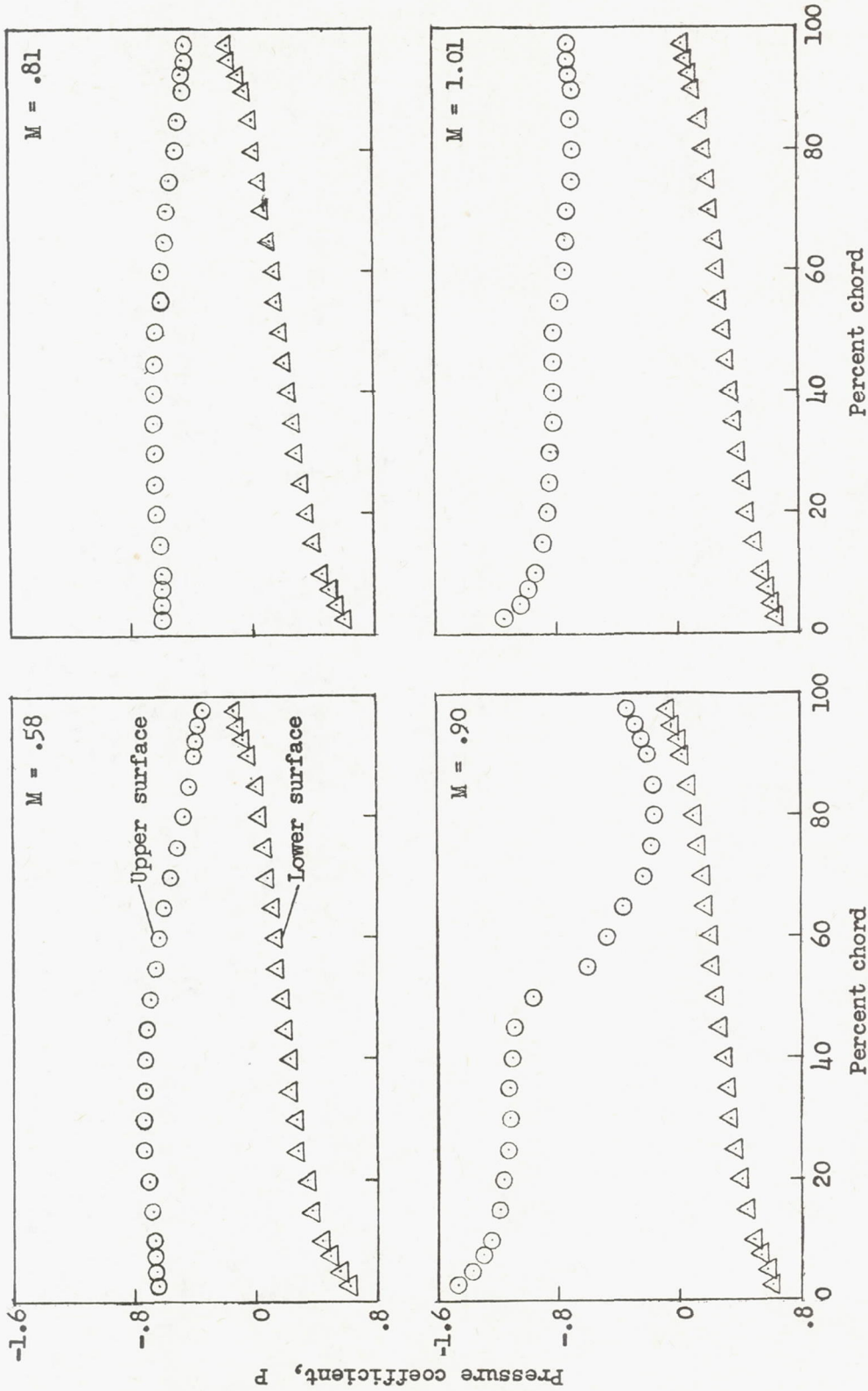
(b) $\alpha = 4^\circ$.

Figure 3.-- Continued.

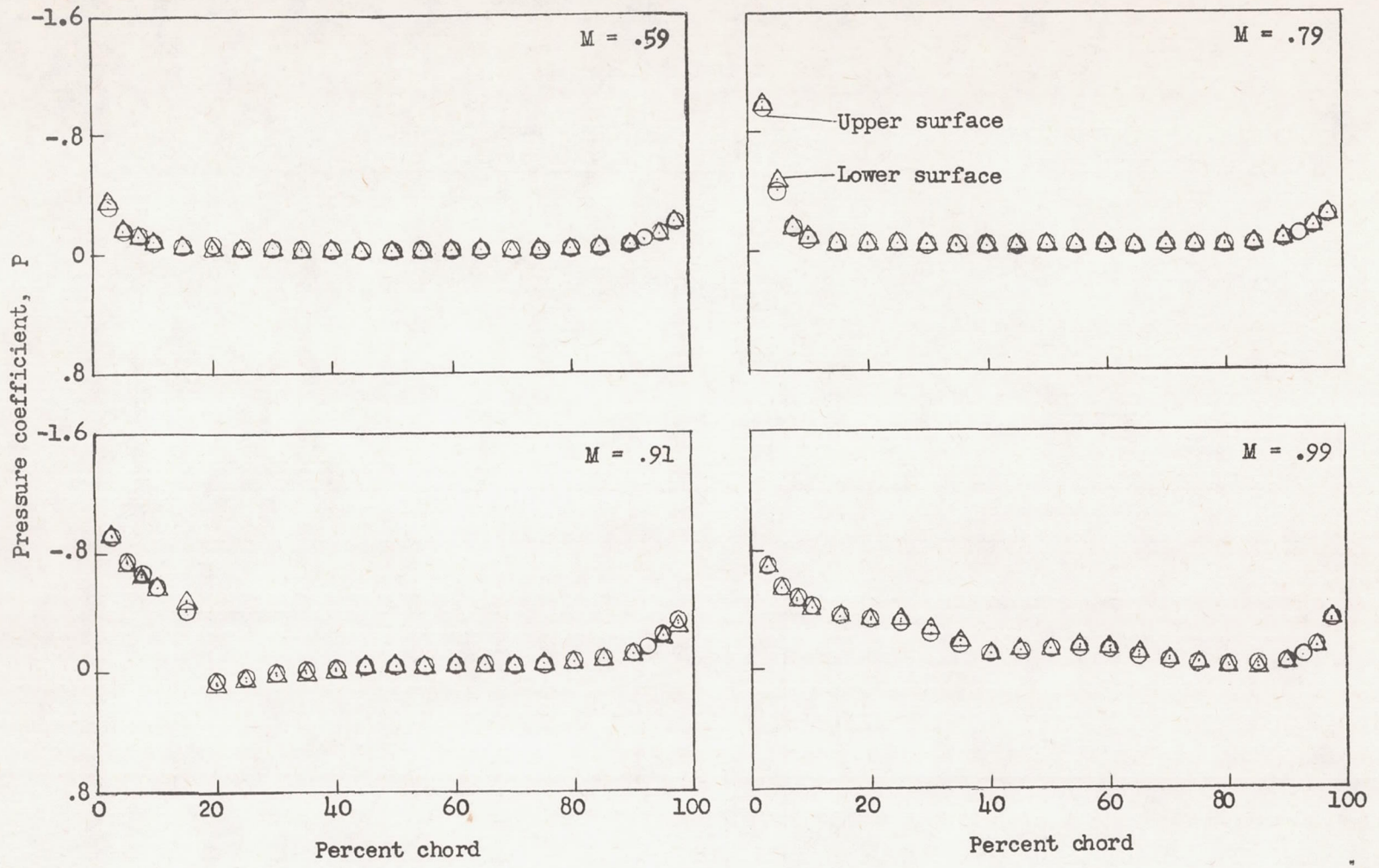


(c) $\alpha = 8^\circ$.

Figure 3.- Continued.

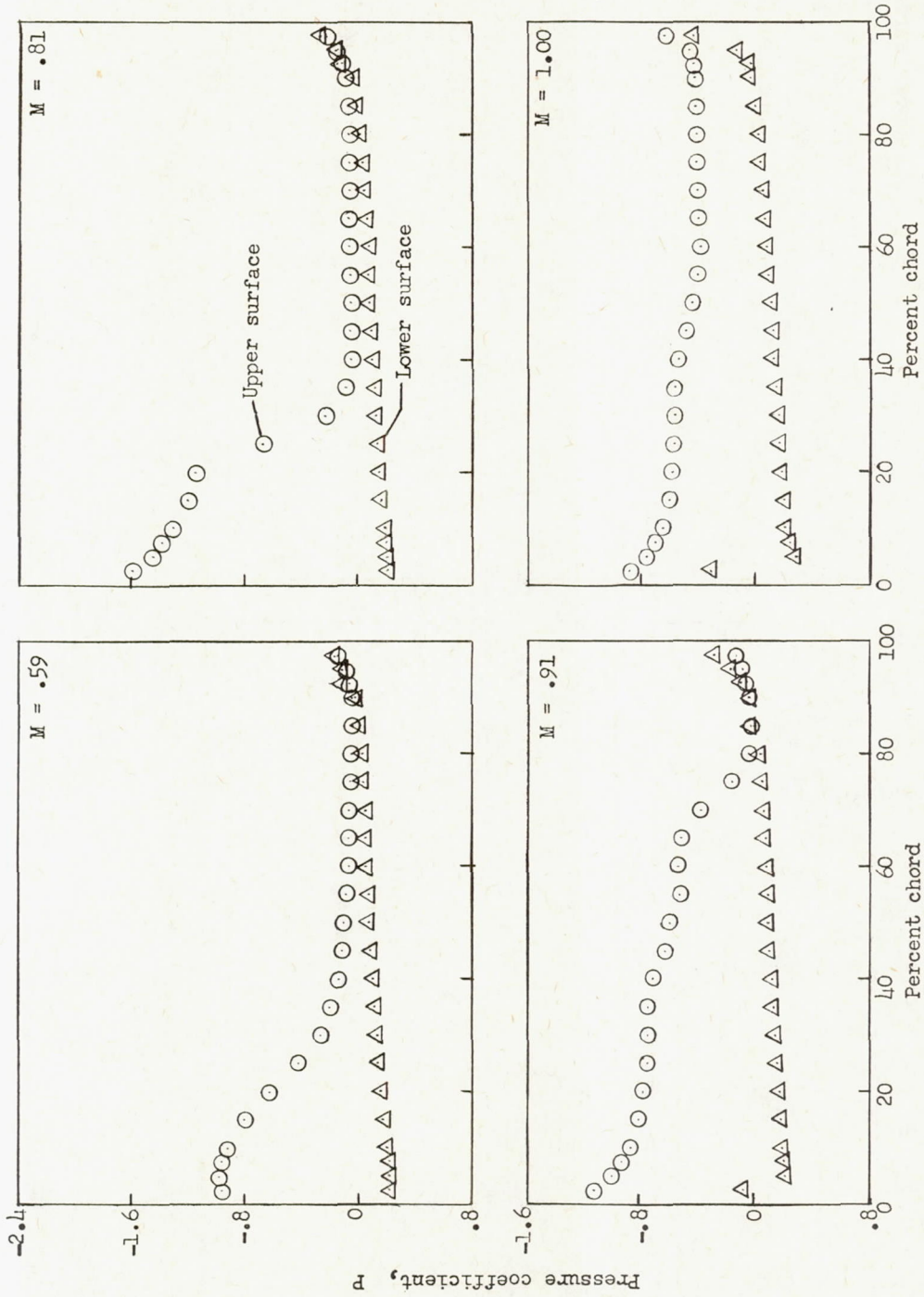


(d) $\alpha = 10^\circ$.
Figure 3.- Concluded.



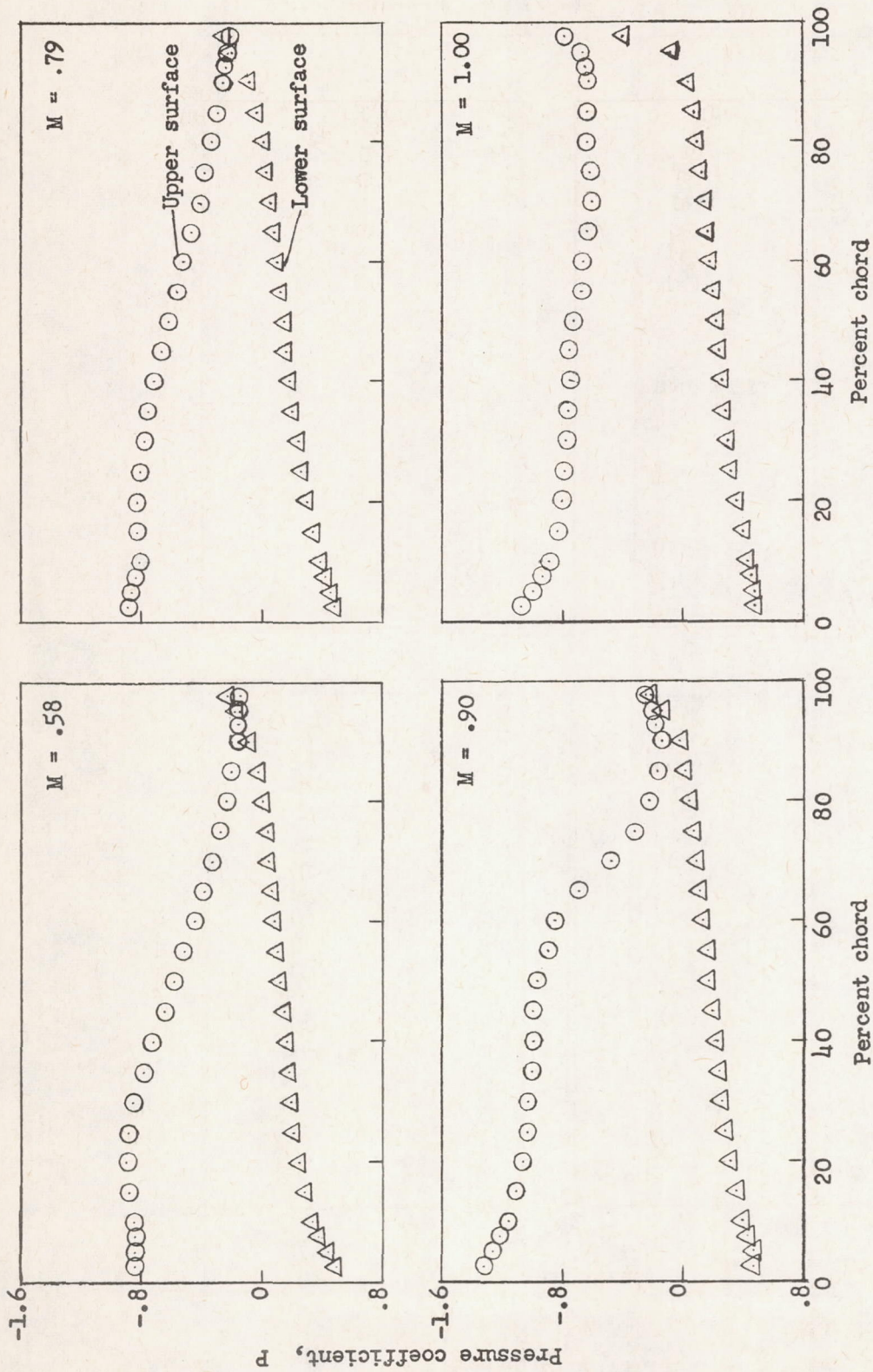
(a) $\alpha = 0^\circ$.

Figure 4.- Pressure distributions for the 1-4 airfoil.

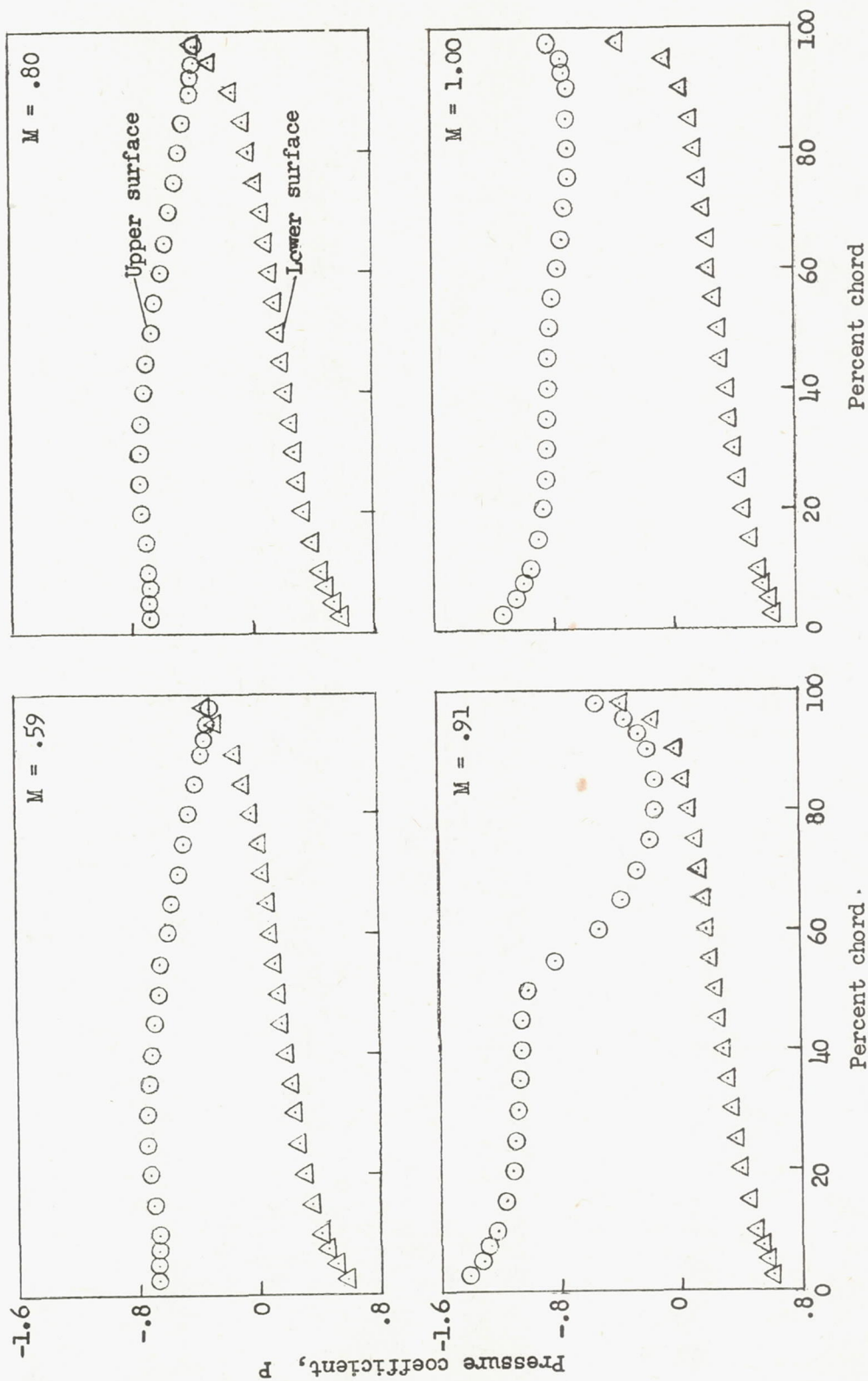


(b) $\alpha = 4^\circ$.

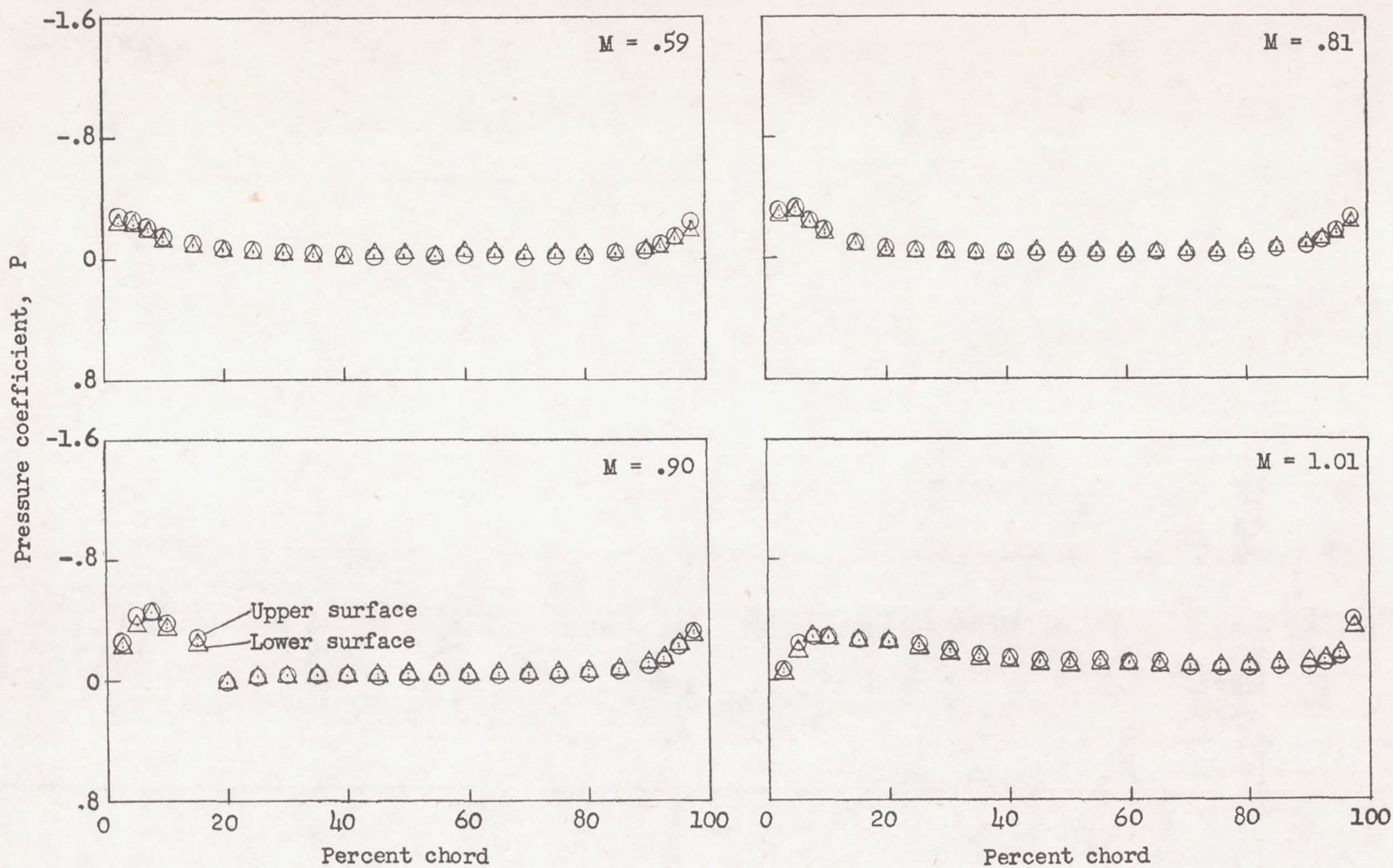
Figure 4.- Continued.



(c) $\alpha = 8^\circ$.
Figure 4.- Continued.

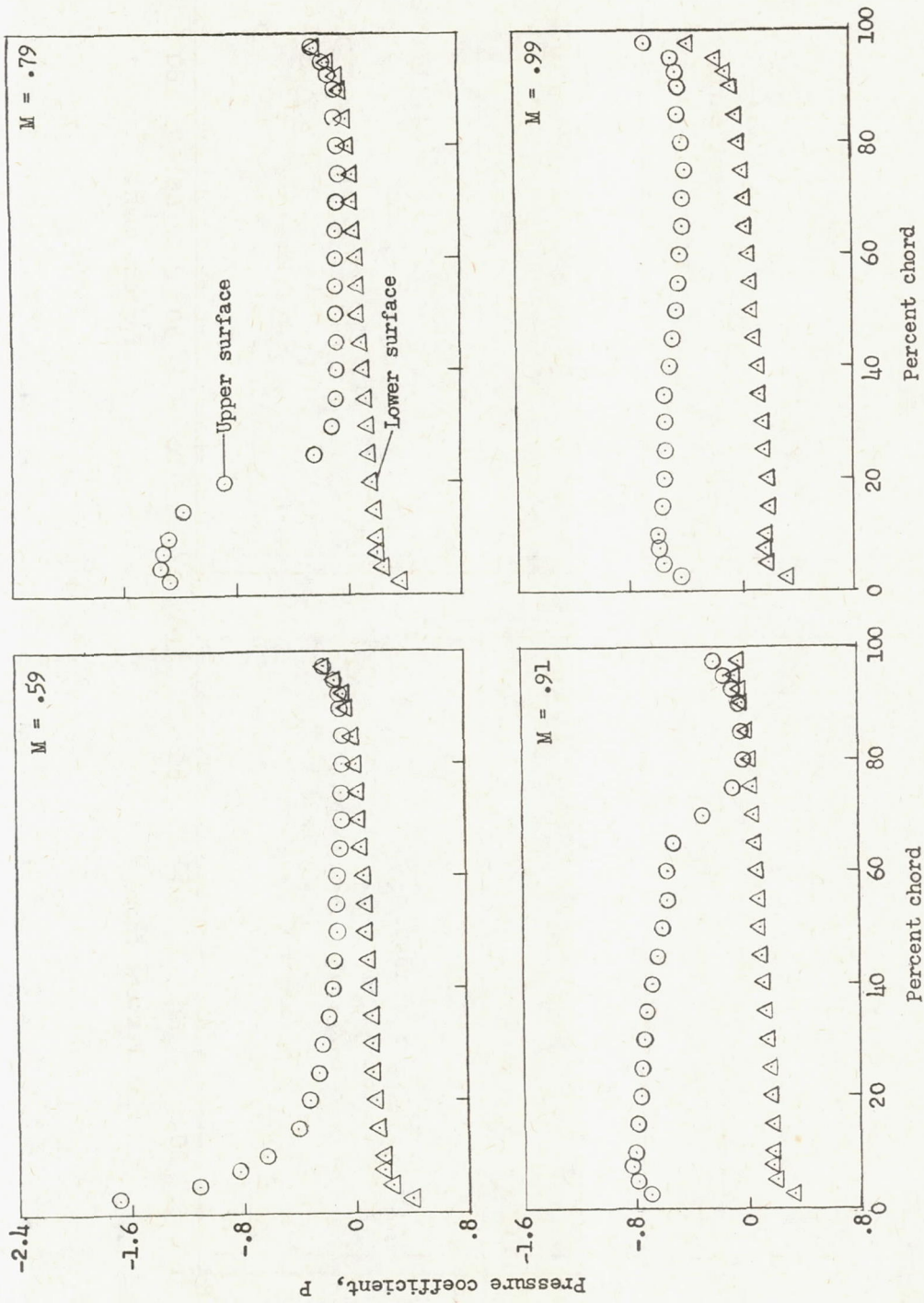


(d) $\alpha = 10^\circ$.
Figure 4.- Concluded.



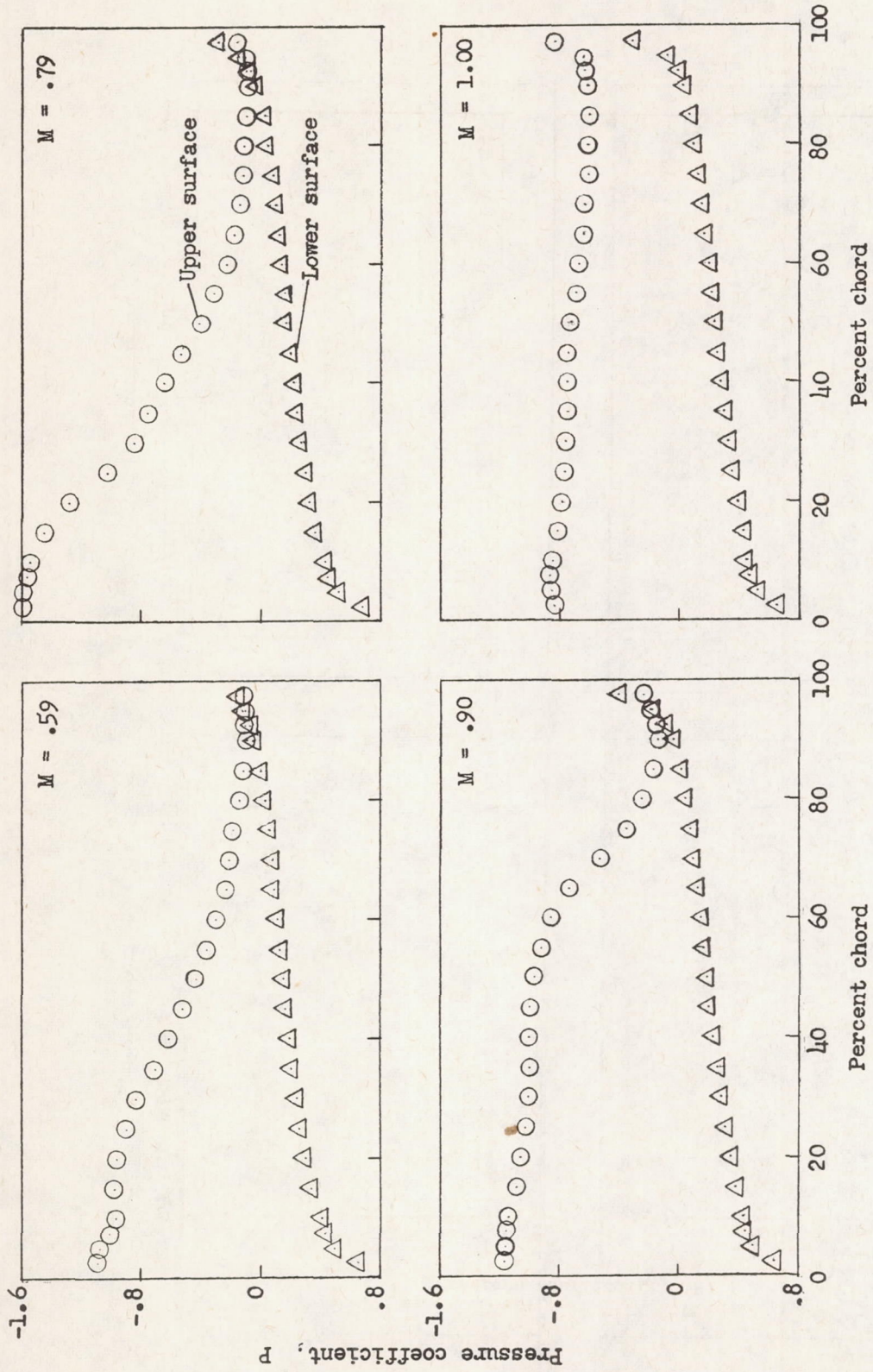
(a) $\alpha = 0^\circ$.

Figure 5.- Pressure distributions for the 10-4 airfoil.

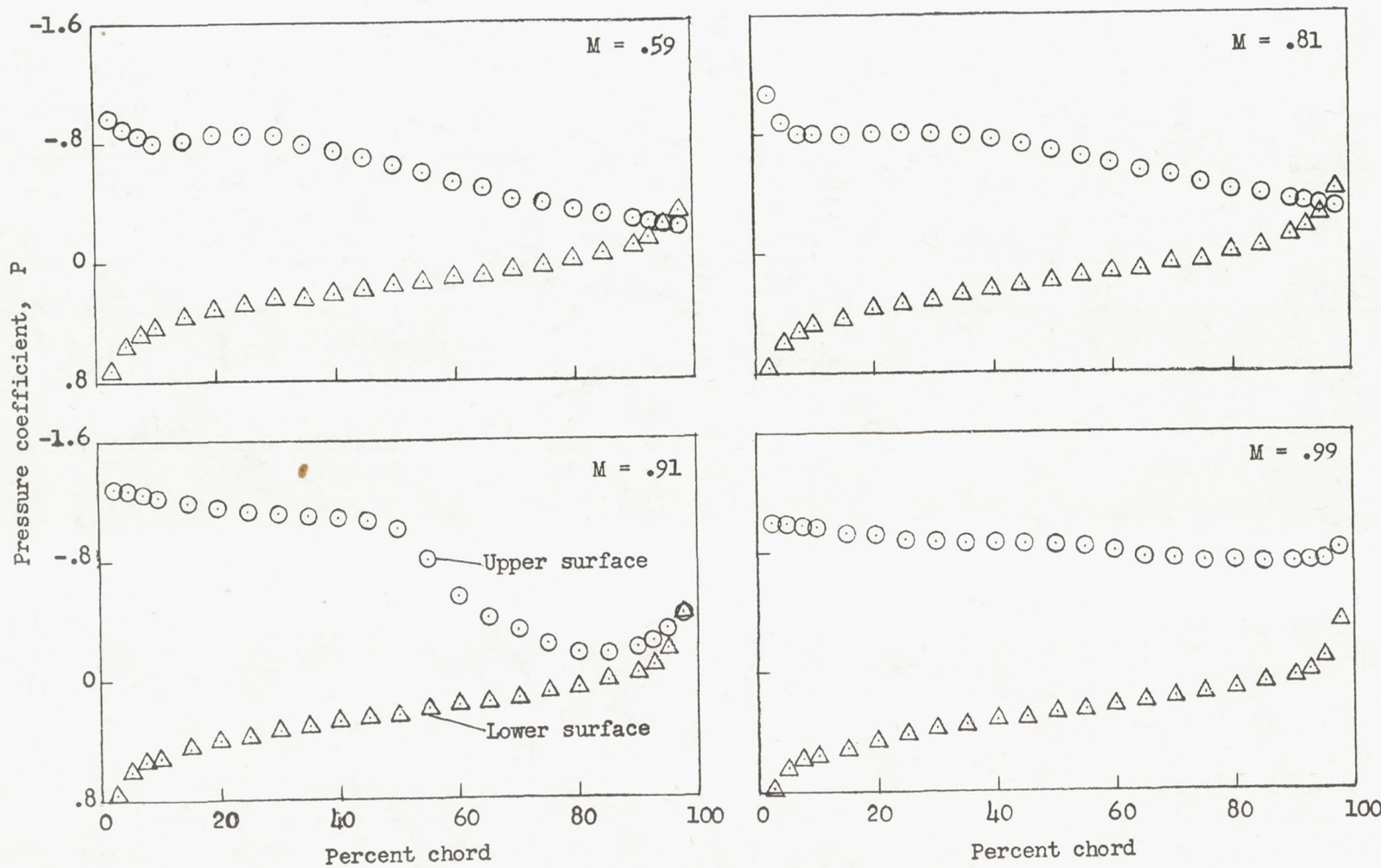


(b) $\alpha = 4^\circ$.

Figure 5.- Continued.

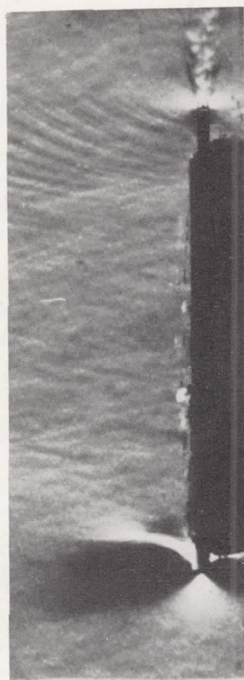


(c) $\alpha = 8^\circ$.
Figure 5.- Continued.



(d) $\alpha = 10^\circ$.

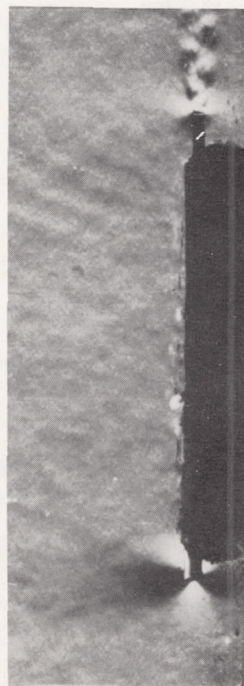
Figure 5.- Concluded.



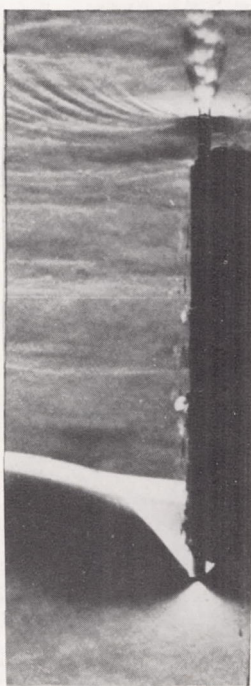
M = .80



M = 1.00



M = .58



M = .90

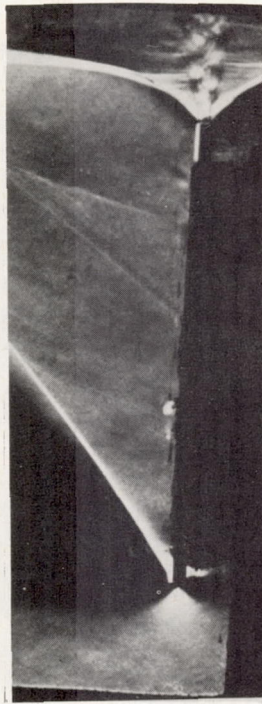
L-86423

(a) $\alpha = 0^\circ$.

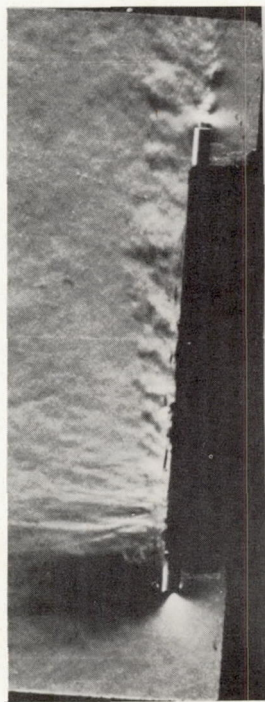
Figure 6.- Flow past 1-0 airfoil.



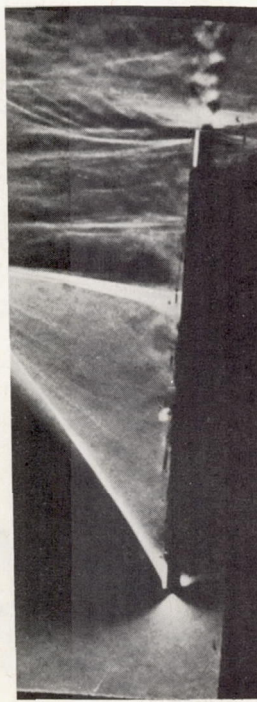
M = .80



M = 1.01



M = .59



M = .90

(b) $\alpha = 4^\circ$.

L-86424

Figure 6.- Continued.



M = .80



M = 1.01



M = .58

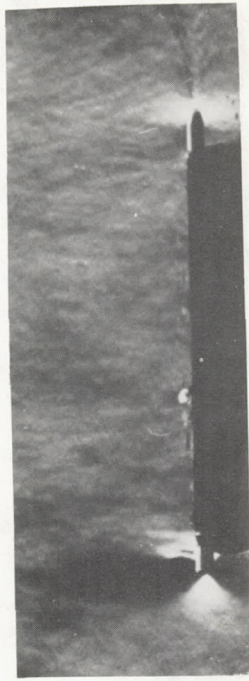


M = .90

(c) $\alpha = 8^\circ$.

I-86425

Figure 6.- Concluded.



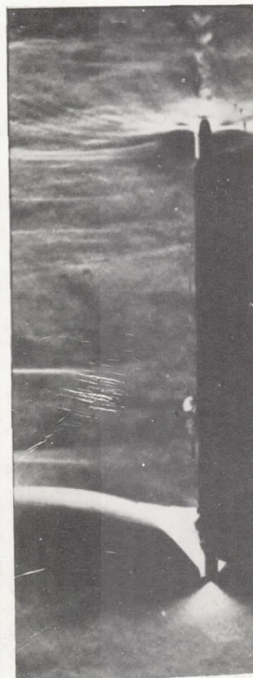
M = .79



M = .99



M = .59



M = .91

L-86426

(a) $\alpha = 0^\circ$.

Figure 7.- Flow past l-4 airfoil.



M = .81



M = 1.00



M = .59

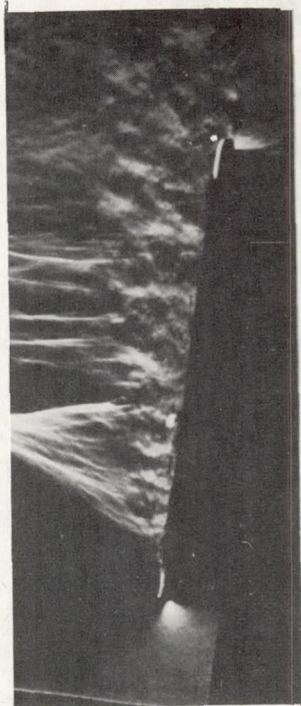


M = .91

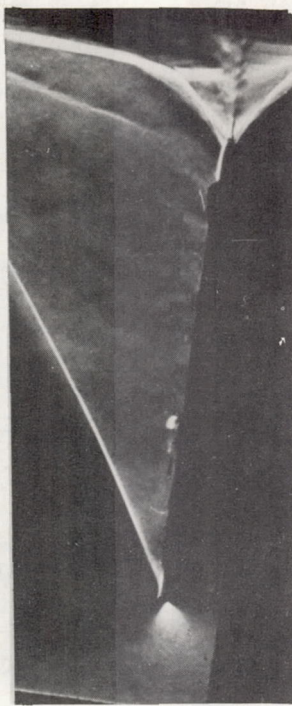
L-86427

(b) $\alpha = 4^\circ$.

Figure 7.- Continued.

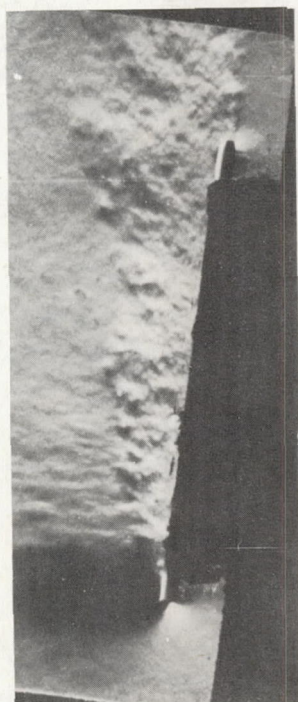


M = .79



M = 1.00

L-86428



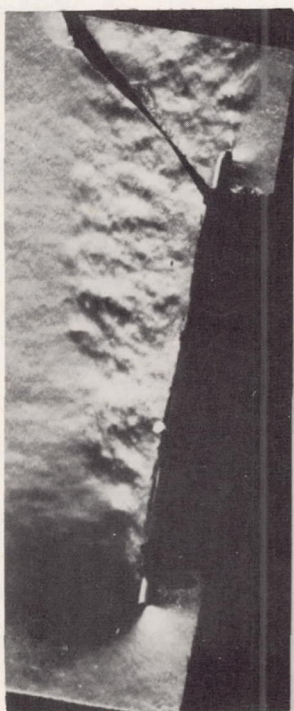
M = .58



M = .90

(c) $\alpha = 8^\circ$.

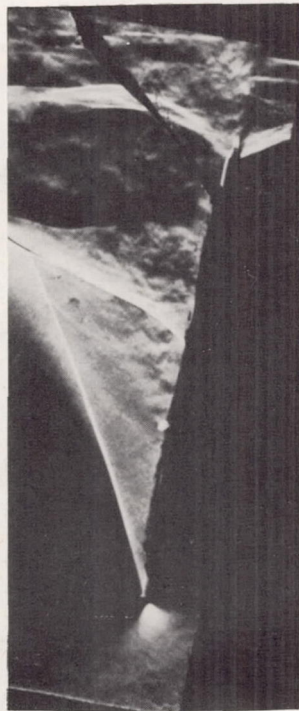
Figure 7.- Continued.



M = .59



M = .80



M = .91

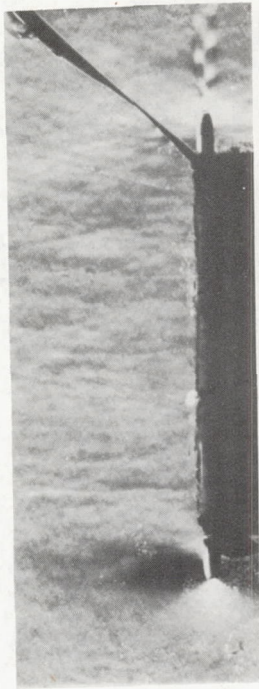


M = 1.00

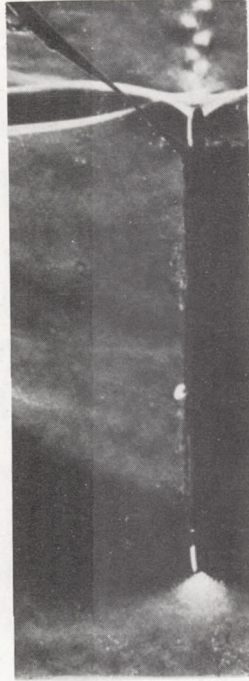
(d) $\alpha = 10^\circ$.

L-86429

Figure 7.- Concluded.



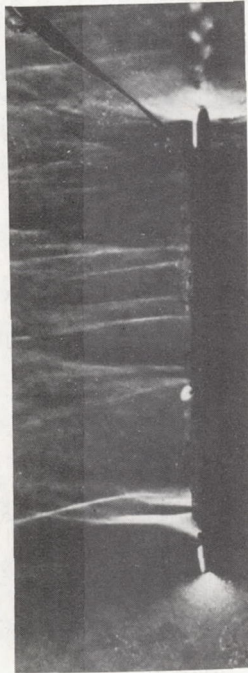
M = .81



M = 1.01



M = .59

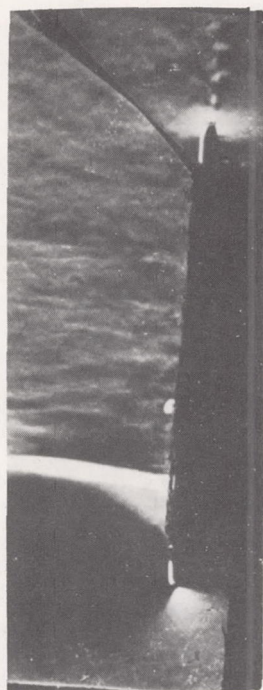


M = .90

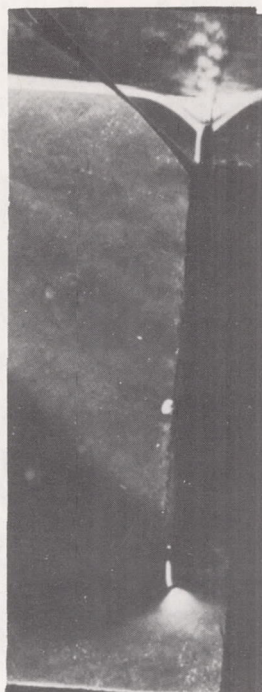
L-86430

(a) $\alpha = 0^\circ$.

Figure 8.- Flow past 10-4 airfoil.



M = .79



M = .99



M = .59

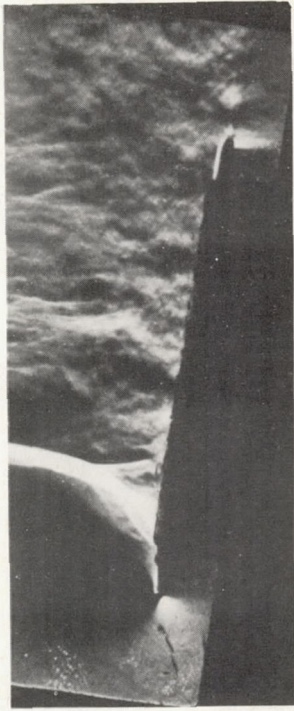


M = .91

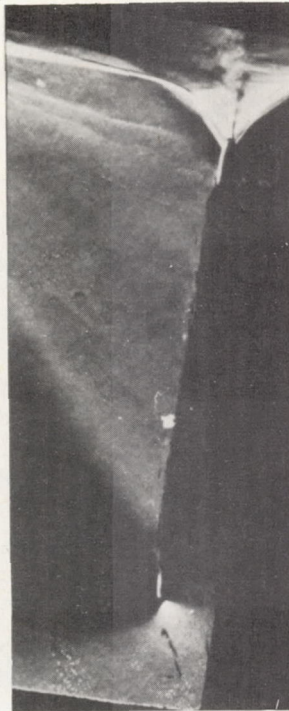
L-86431

(b) $\alpha = 4^\circ$.

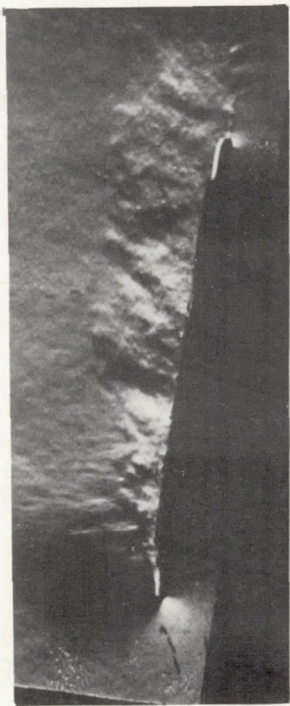
Figure 8.- Continued.



M = .79



M = 1.00



M = .59

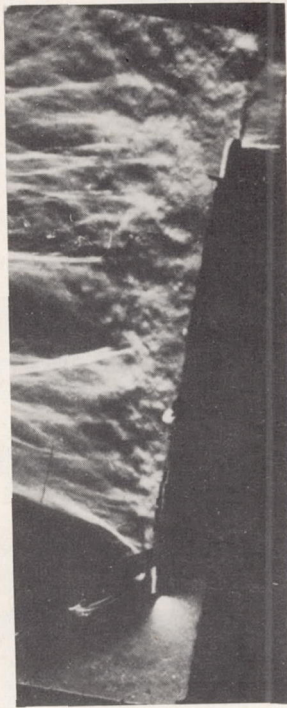


M = .90

L-86432

(c) $\alpha = 8^\circ$.

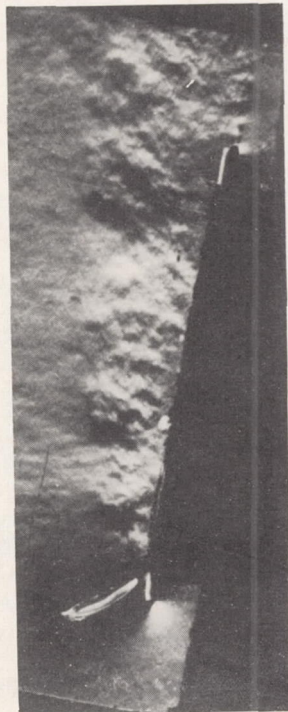
Figure 8.- Continued.



$M = .81$



$M = .99$



$M = .59$

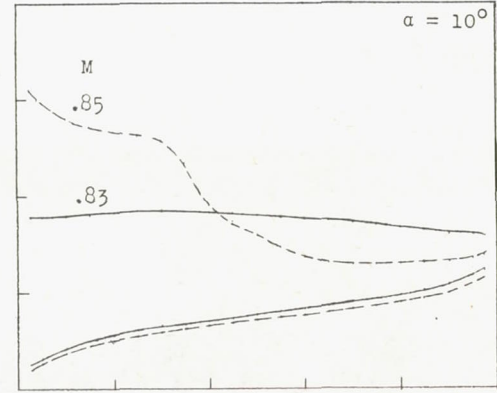
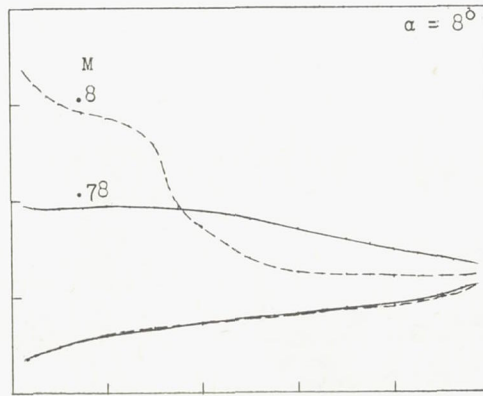
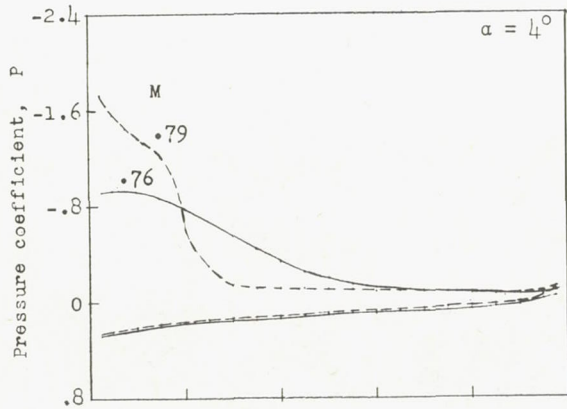


$M = .91$

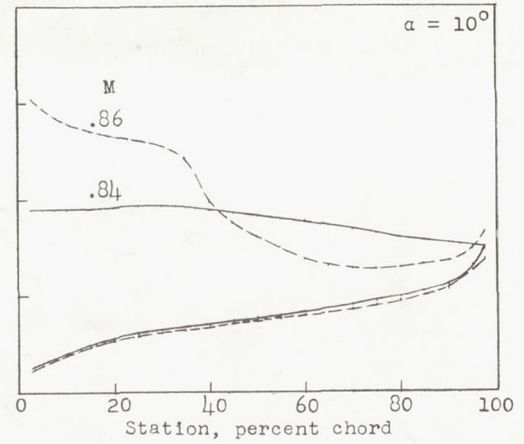
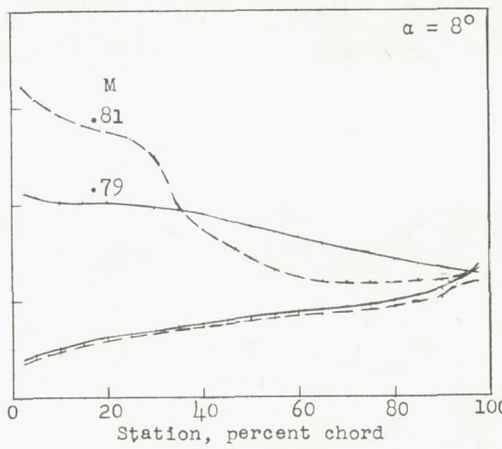
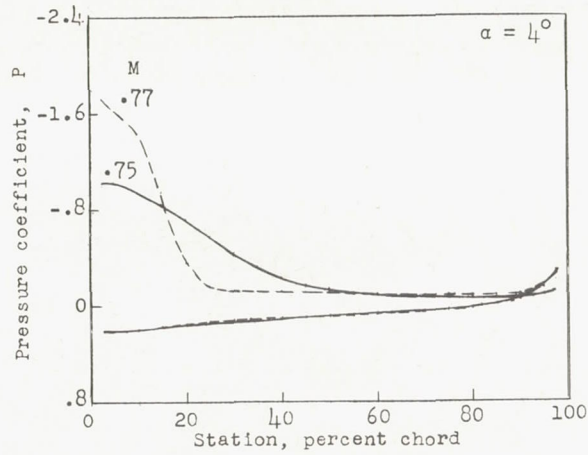
L-86433

(d) $\alpha = 10^\circ$.

Figure 8.- Concluded.

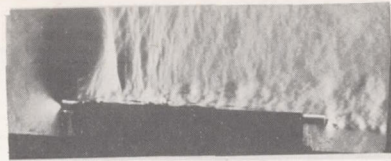


(a) 1-0 airfoil.



(b) 1-4 airfoil.

Figure 9.- Pressure distributions at transonic flow attachment. 1-x airfoils.



M = .76



M = .78



M = .79



M = .80

(a) 1-0 airfoil.



M = .75



M = .79



M = .84



M = .77

$\alpha = 4^\circ$



M = .81

$\alpha = 8^\circ$



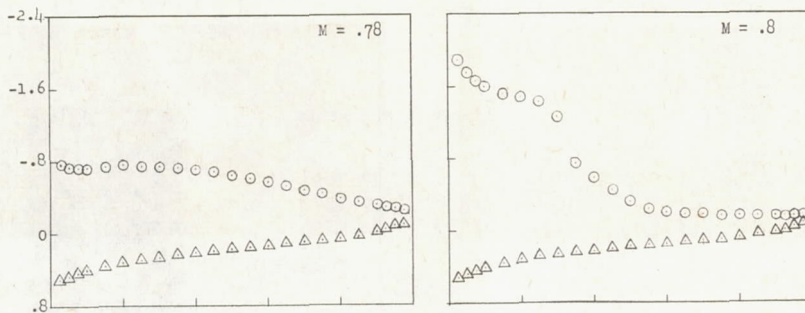
M = .86

$\alpha = 10^\circ$

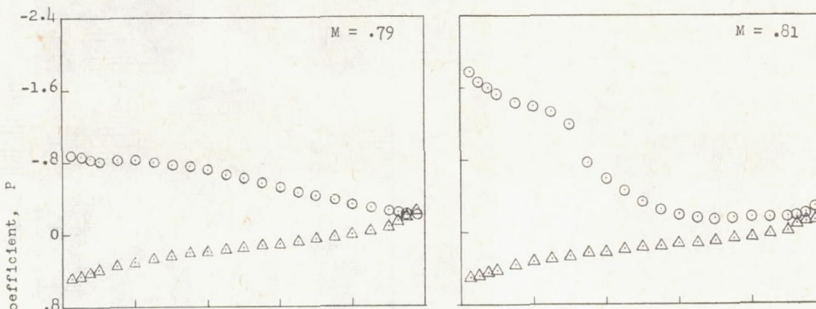
(b) 1-4 airfoil.

L-86434

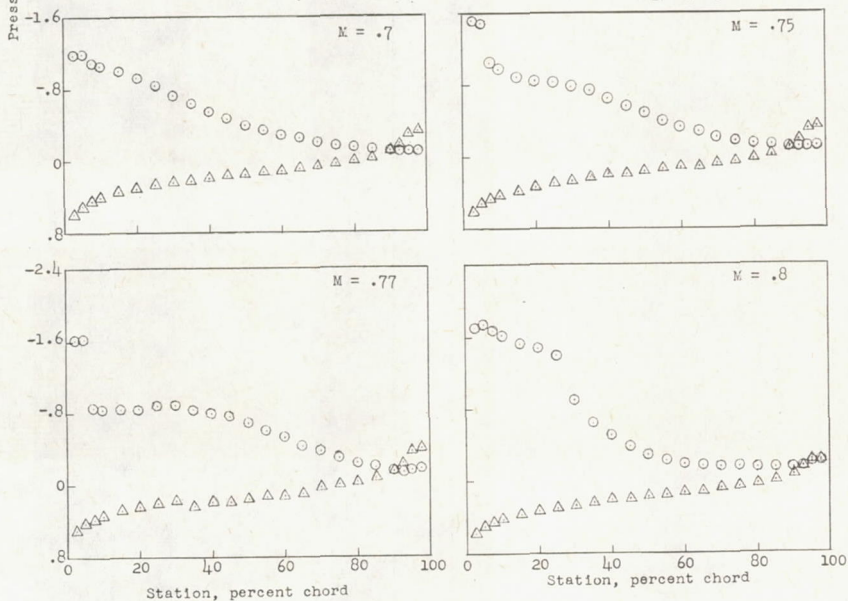
Figure 10.- Flow photographs at transonic flow attachment. 1-x airfoils.



(a) 1-0 airfoil.



(b) 1-4 airfoil.



(c) 4-10 airfoil.

Figure 11.- Effects of profile shape on pressures at transonic flow attachment. $\alpha = 8^\circ$.

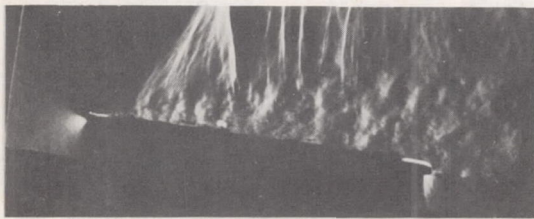


M = .78

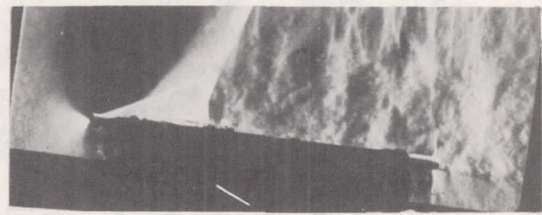


M = .80

(a) 1-0 airfoil.



M = .79

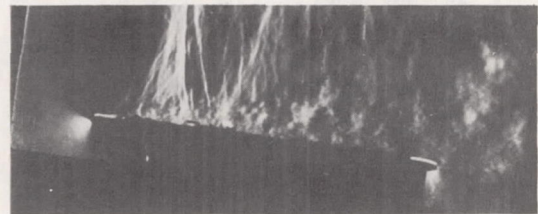


M = .80

(b) 1-4 airfoil.



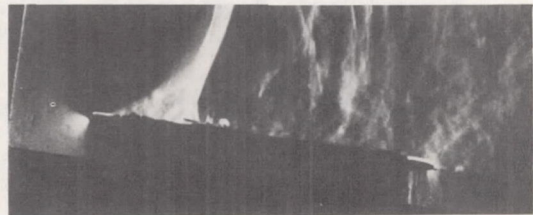
M = .70



M = .75



M = .77

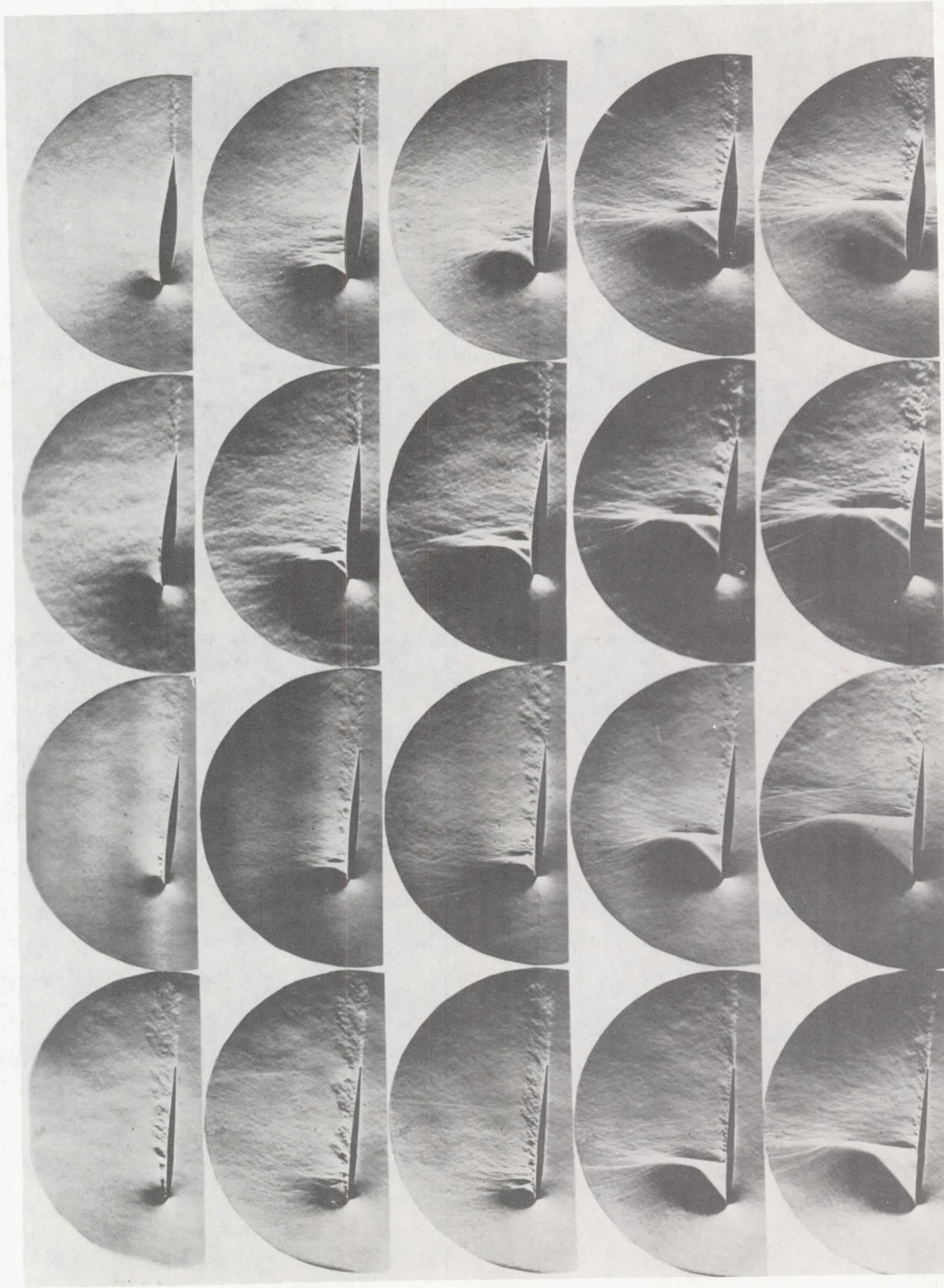


M = .80

(c) 4-10 airfoil.

L-86435

Figure 12.- Effects of profile shape on flow at transonic flow attachment.
 $\alpha = 8^\circ$.



M = .53

M = .67

M = .70

M = .74

M = .80

NACA 64A004

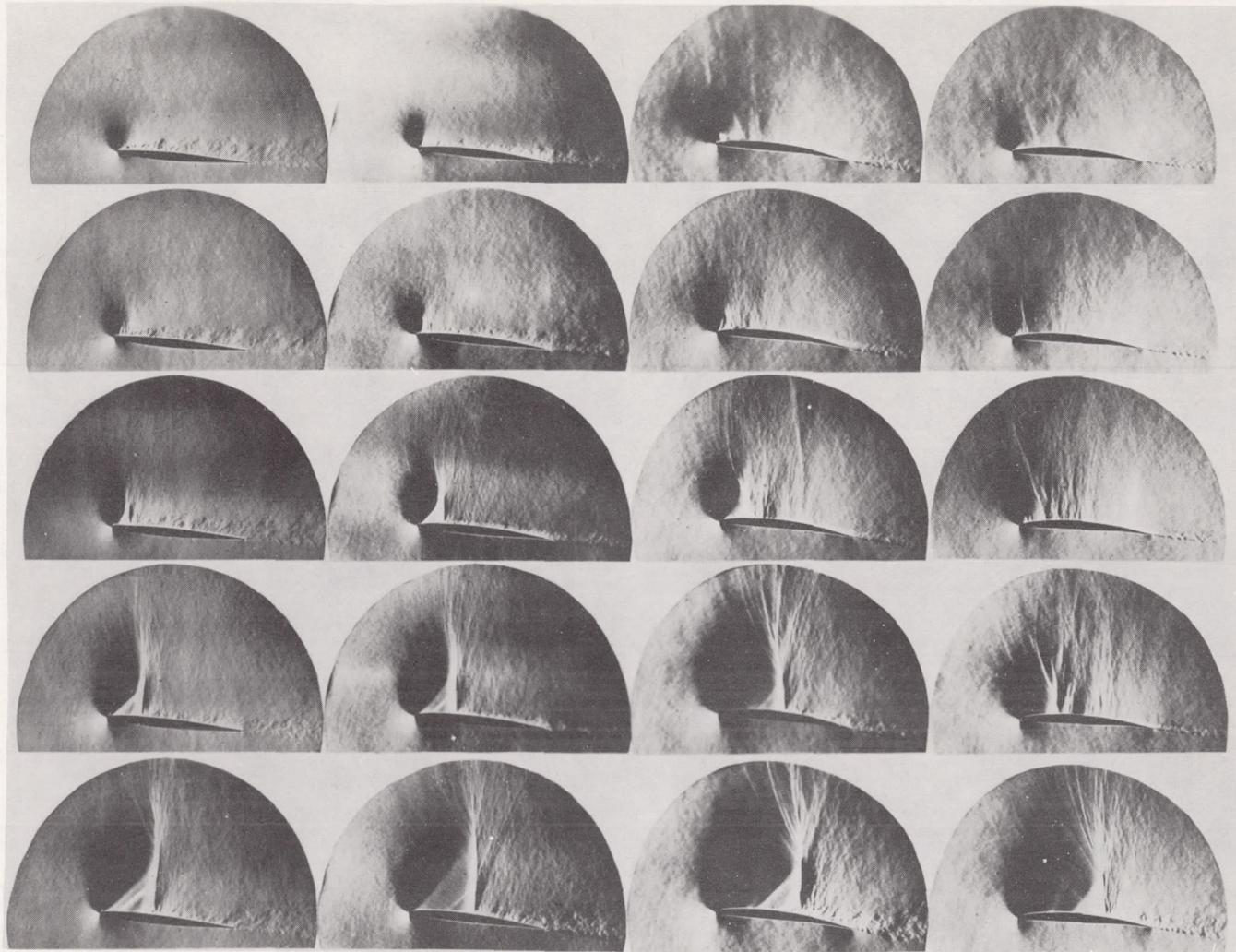
NACA 64A006

NACA 64A009

NACA 64A012

L-86436

Figure 13.- Effects of thickness on flow. $\alpha = 6^\circ$.



NACA 64A006 $\alpha = 6^\circ$

NACA 64A206 $\alpha = 6^\circ$

NACA 64A506 $\alpha = 6^\circ$

NACA 64A506 $\alpha = 4^\circ$

Figure 14.- Effects of camber on flow α or $c_n \approx$ constant.

L-86437

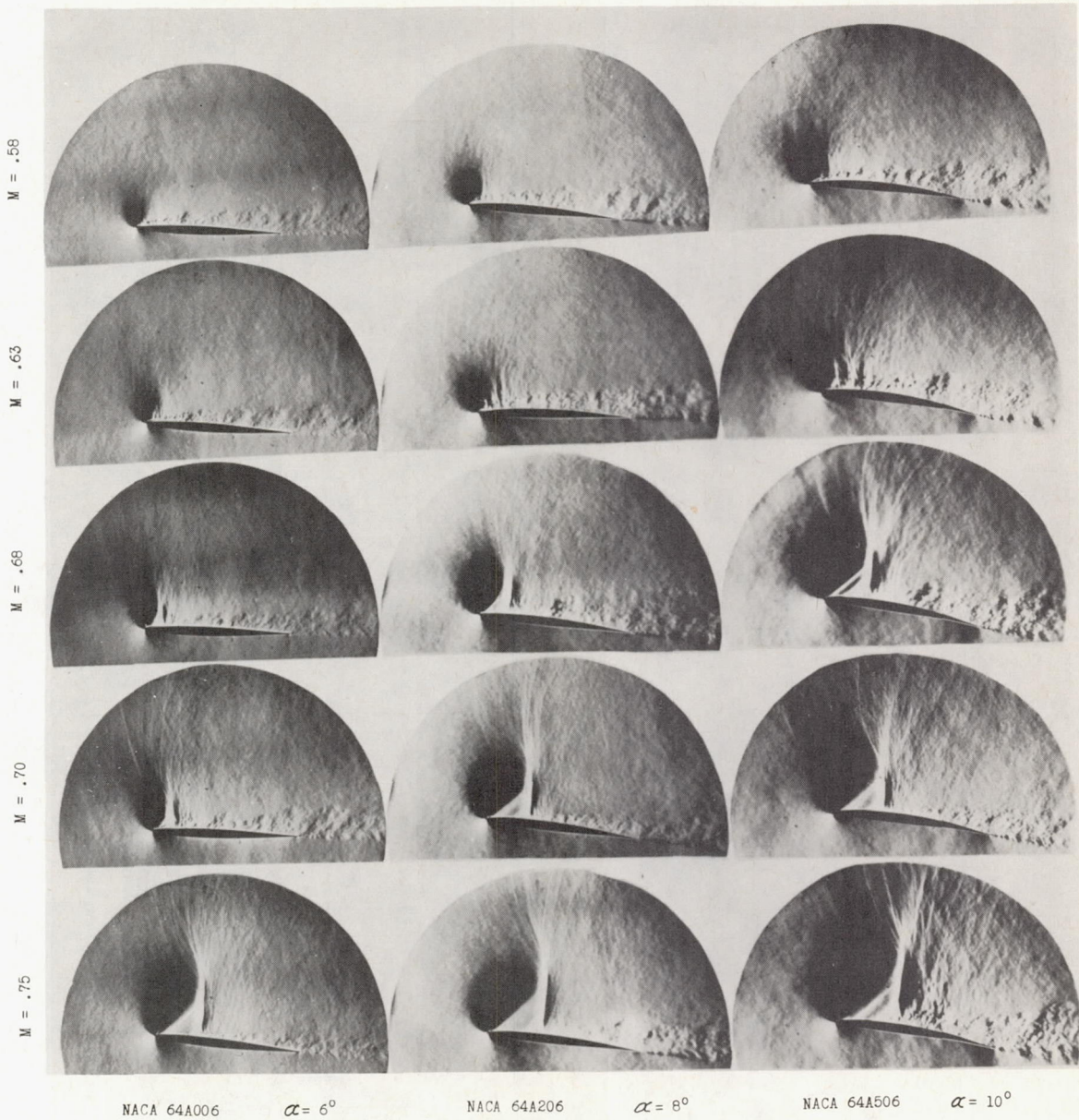
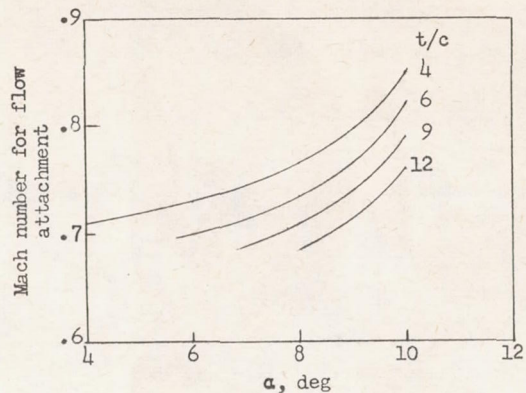
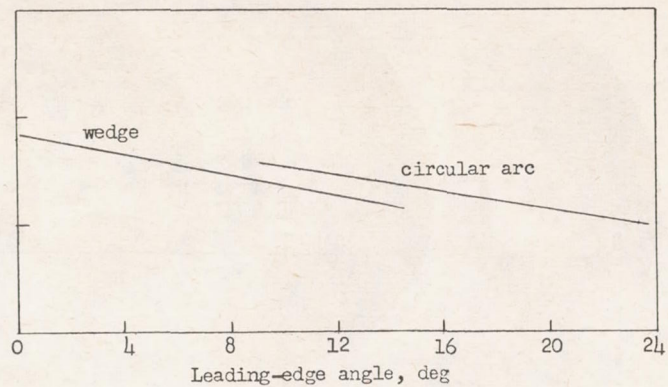


Figure 15.- Effects of camber on flow with low-speed separation.

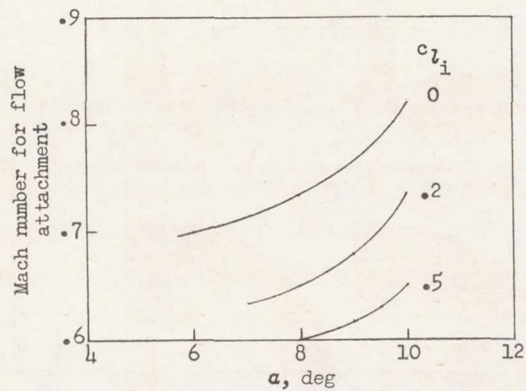
L-86431



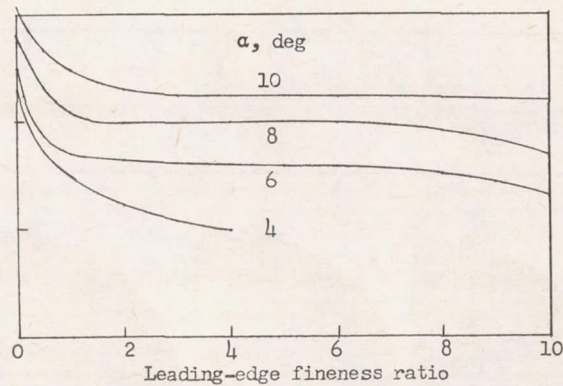
(a) Effect of thickness for NACA 64AOXX airfoils.



(b) Effect of leading-edge angle. $\alpha = 4^\circ$.

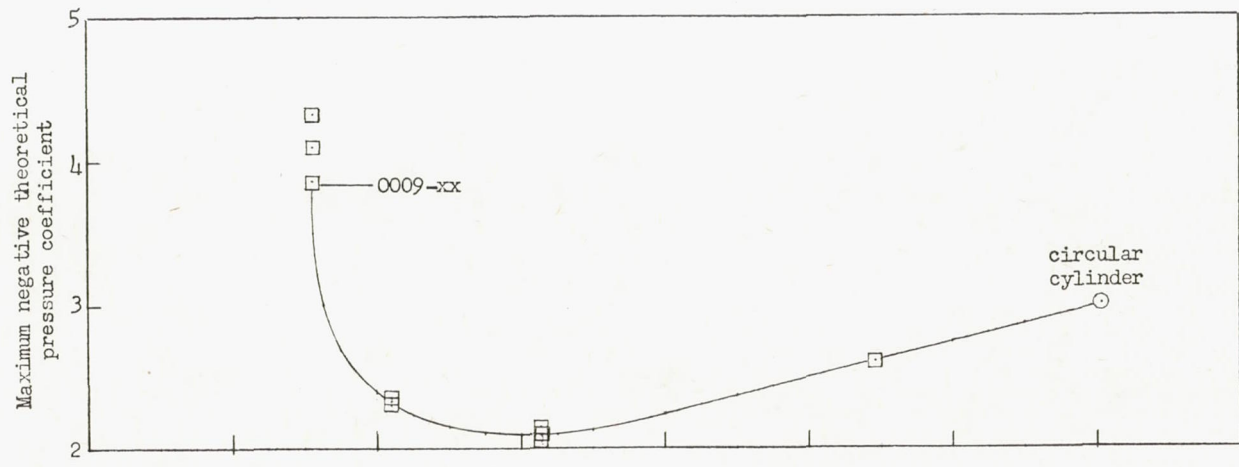


(c) Effect of camber for NACA 64AX06 airfoils.

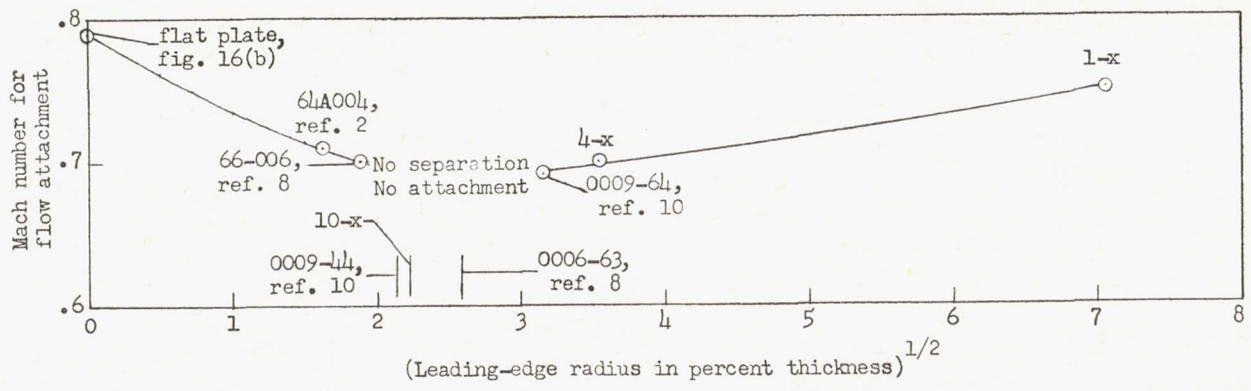


(d) Effect of leading-edge fineness ratio. $t/c = 0.02$.

Figure 16.- Factors affecting transonic flow attachment.

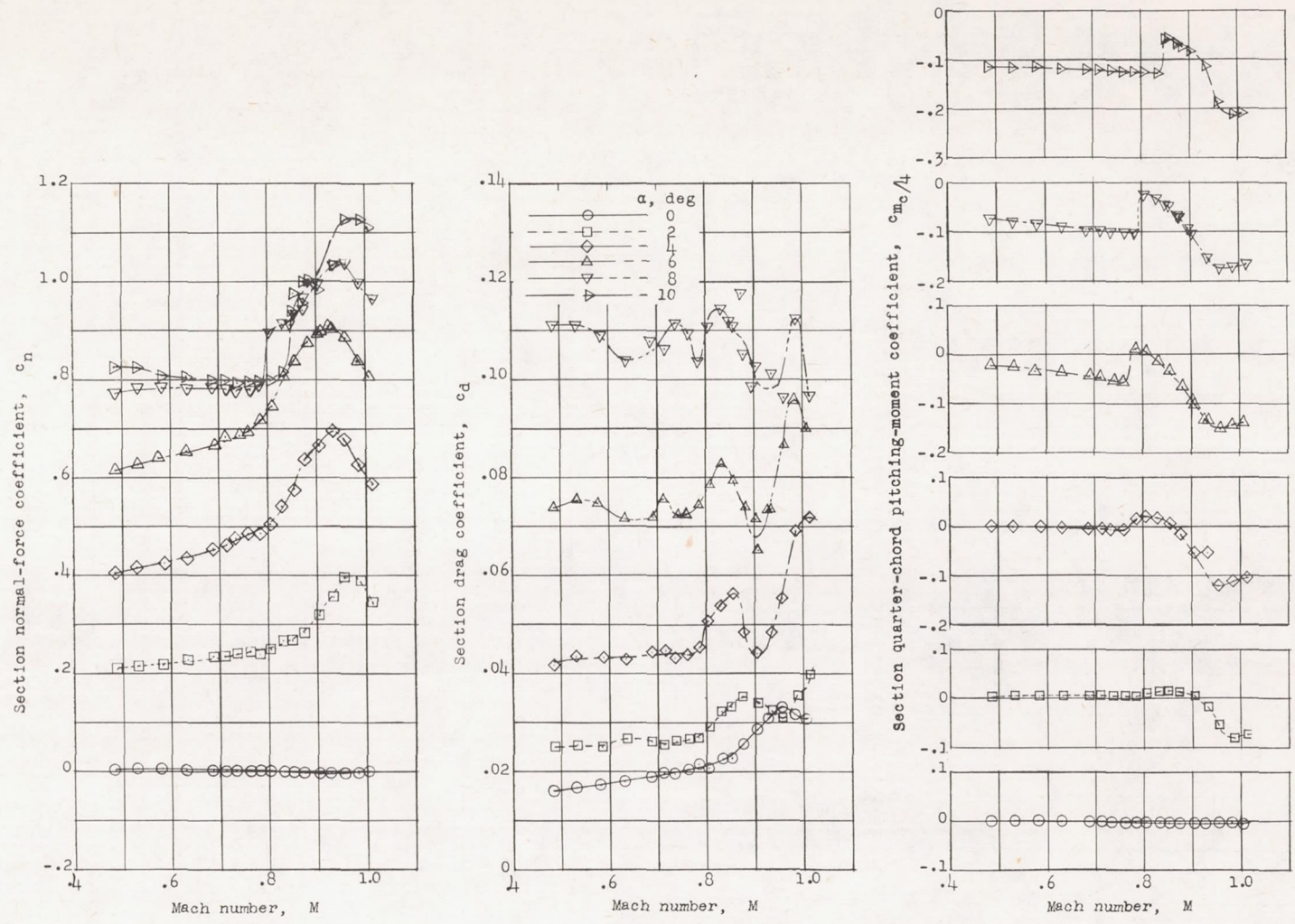


(a) Maximum negative theoretical pressure coefficient. $c_n = 0.5$; $\alpha = 4^\circ$.



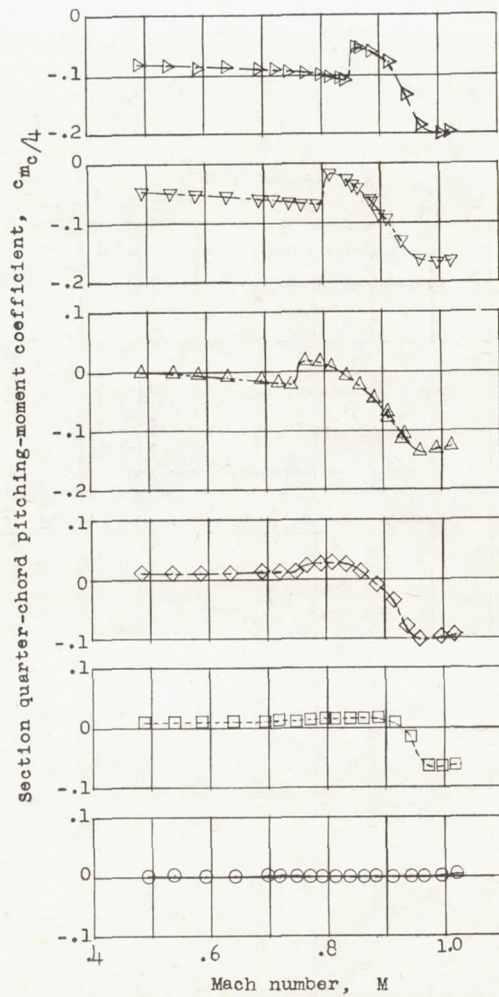
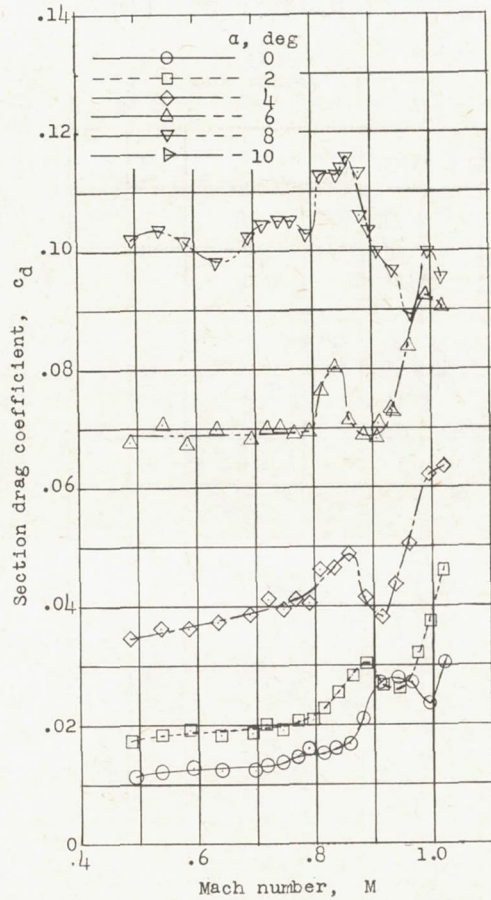
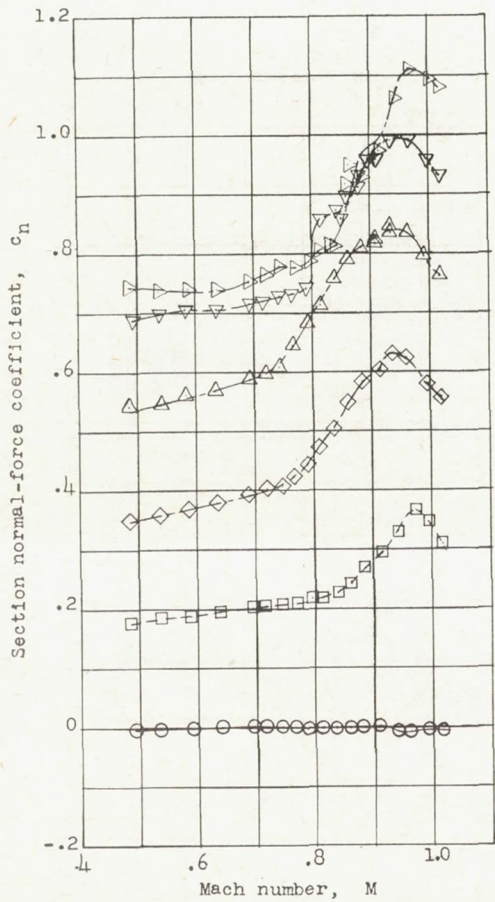
(b) Mach number for transonic flow attachment. $\alpha = 4^\circ$.

Figure 17.- Correlation of leading-edge shape effects on transonic flow attachment.



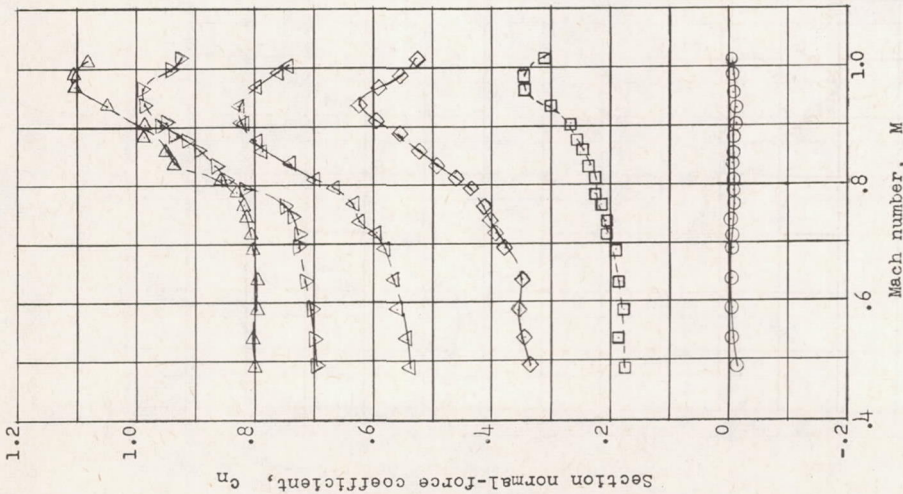
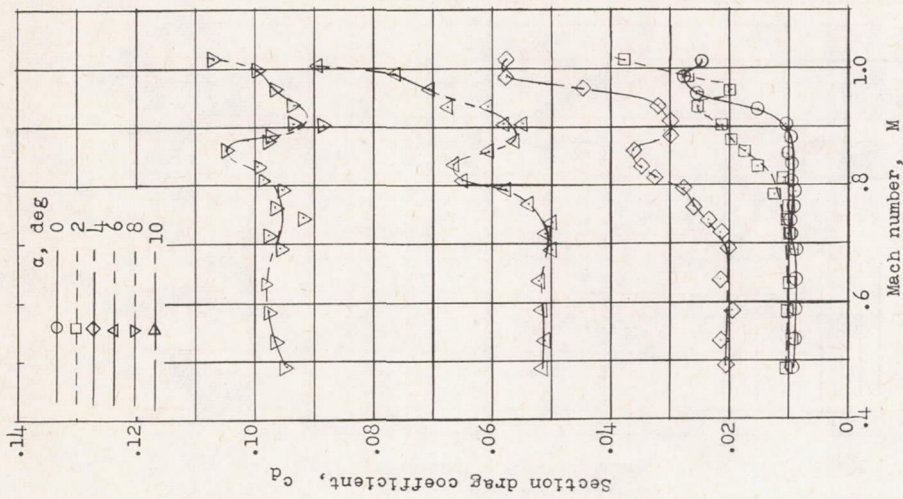
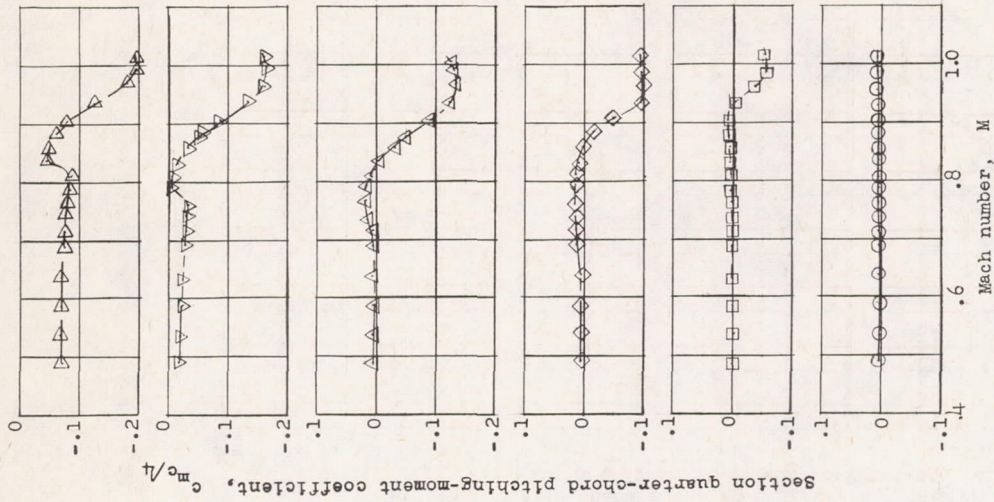
(a) 1-0 airfoil.

Figure 18.- Basic aerodynamic characteristics of 2-percent-thick airfoils.

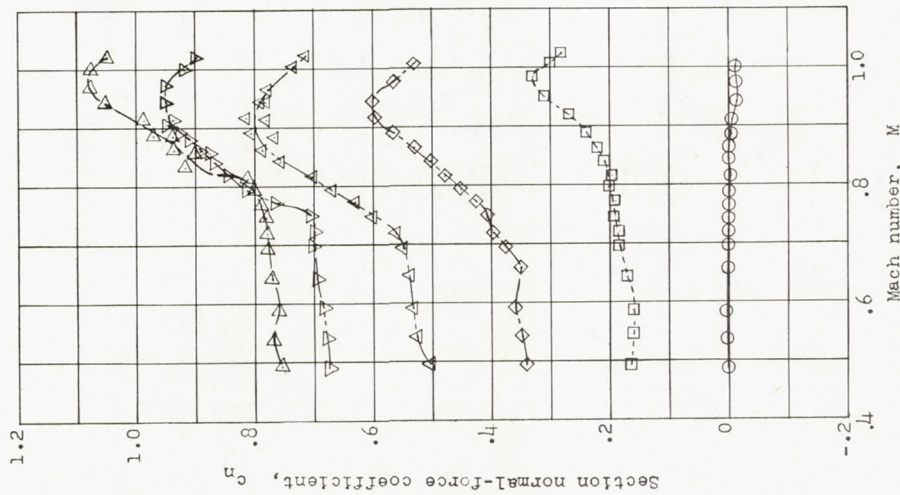
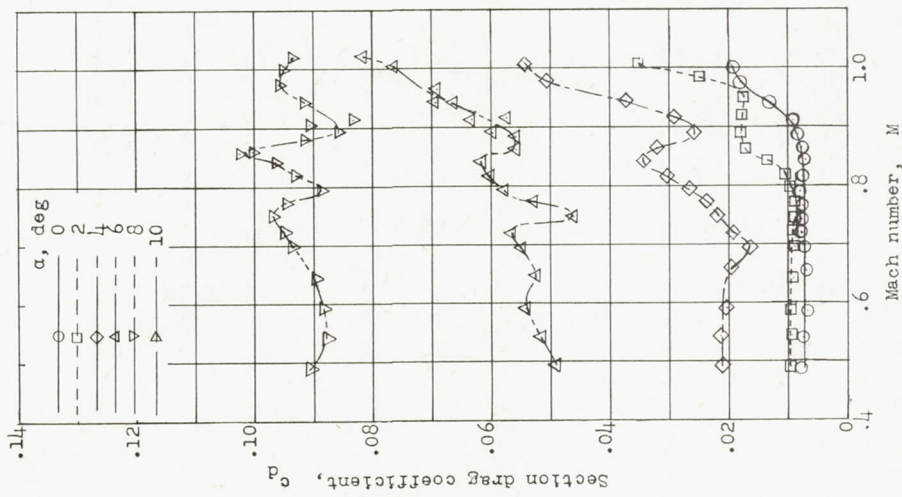
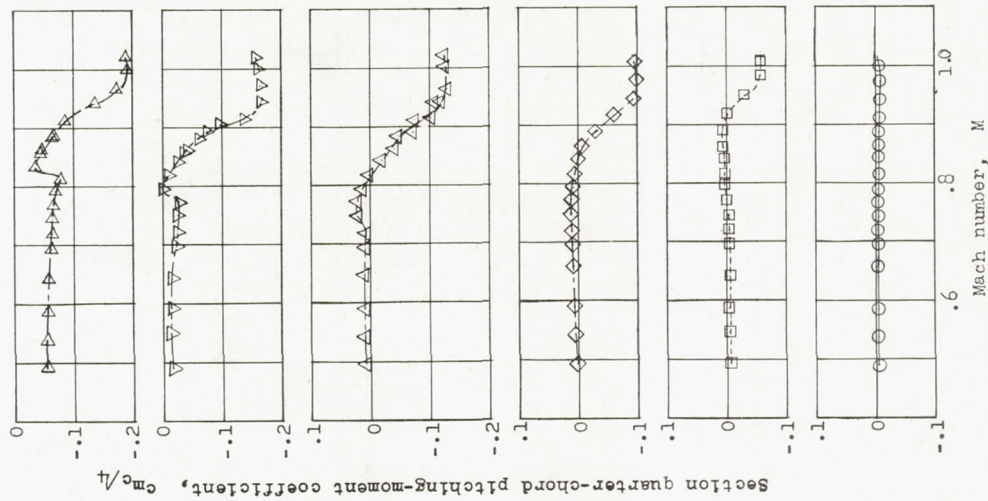


(b) 1-4 airfoil.

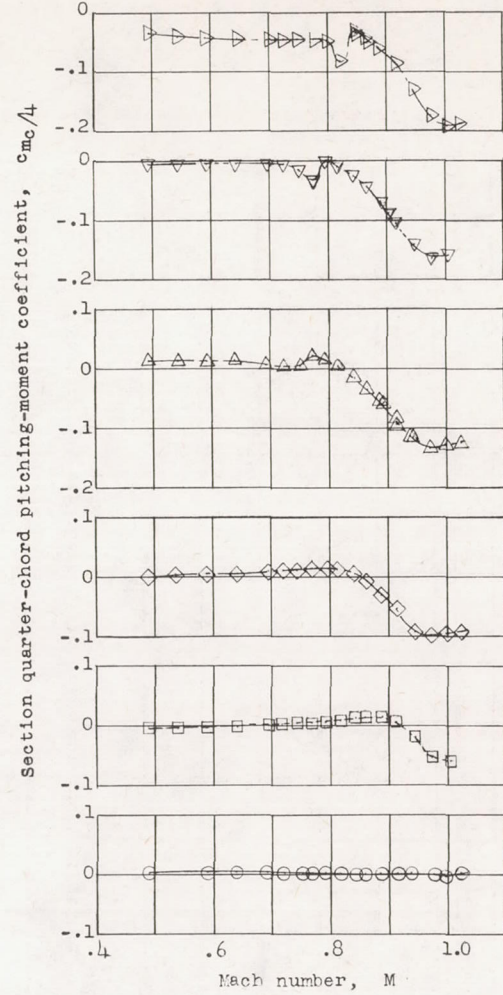
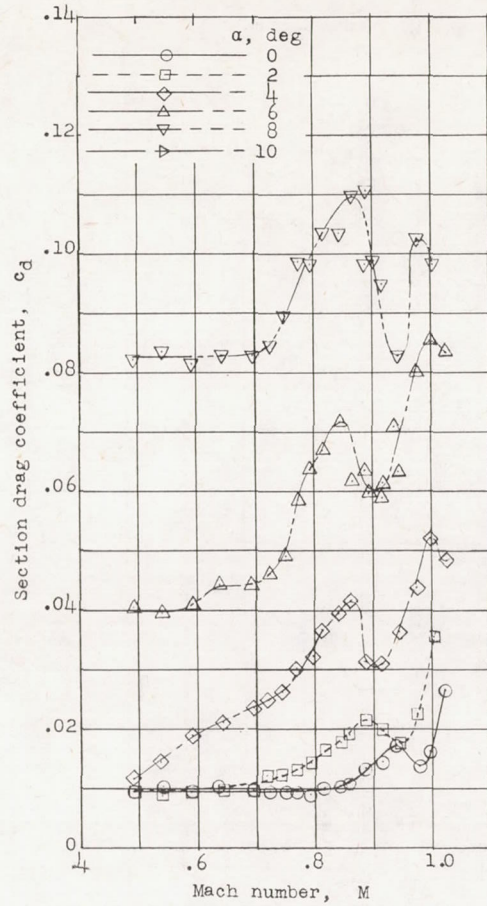
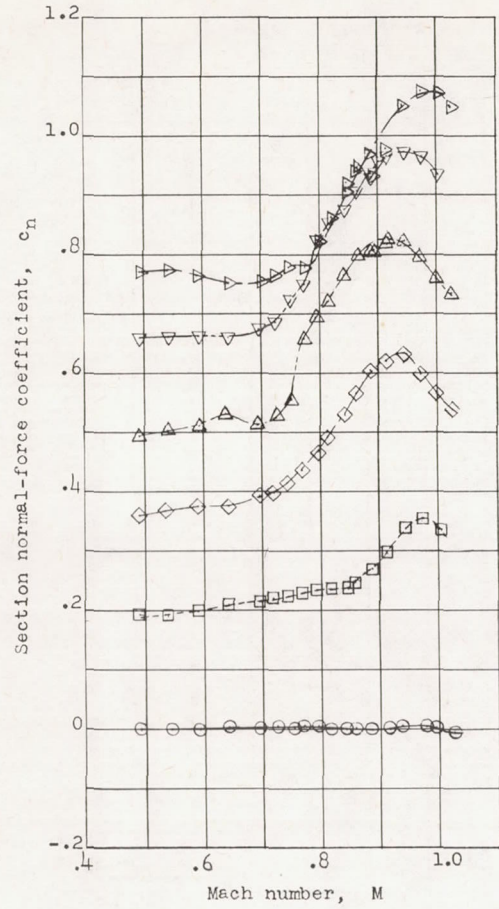
Figure 18.- Continued.



(c) 10-4 airfoil.
Figure 18.- Continued.

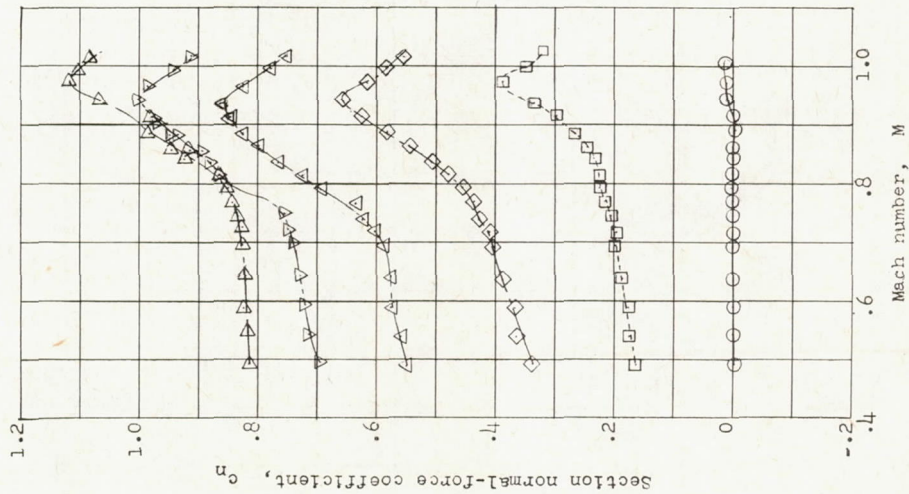
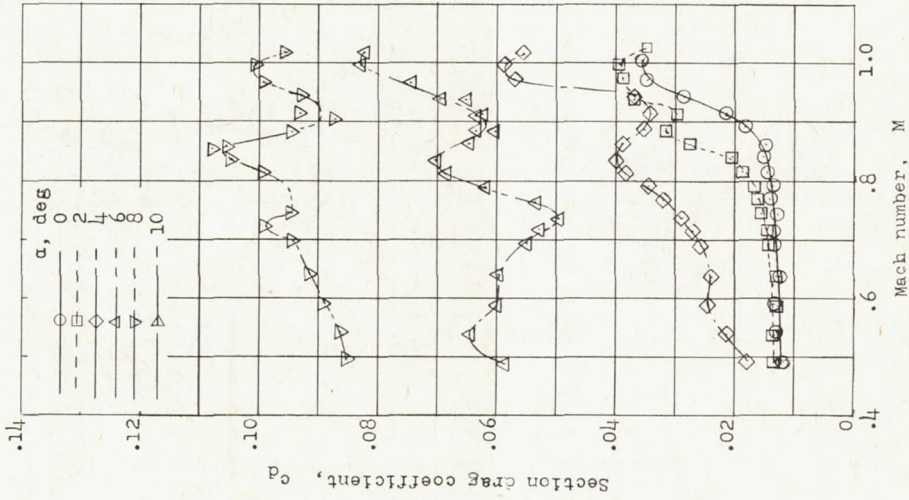
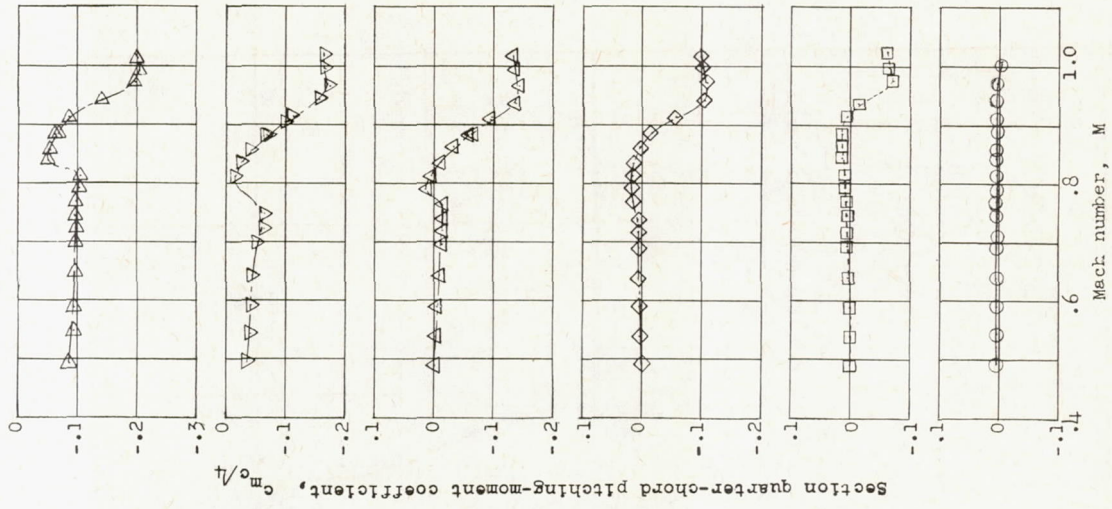


(d) 10-10 airfoil.
Figure 18.- Continued.



(e) 4-10 airfoil.

Figure 18.- Continued.



(f) 4-1 airfoil.

Figure 18.- Concluded.

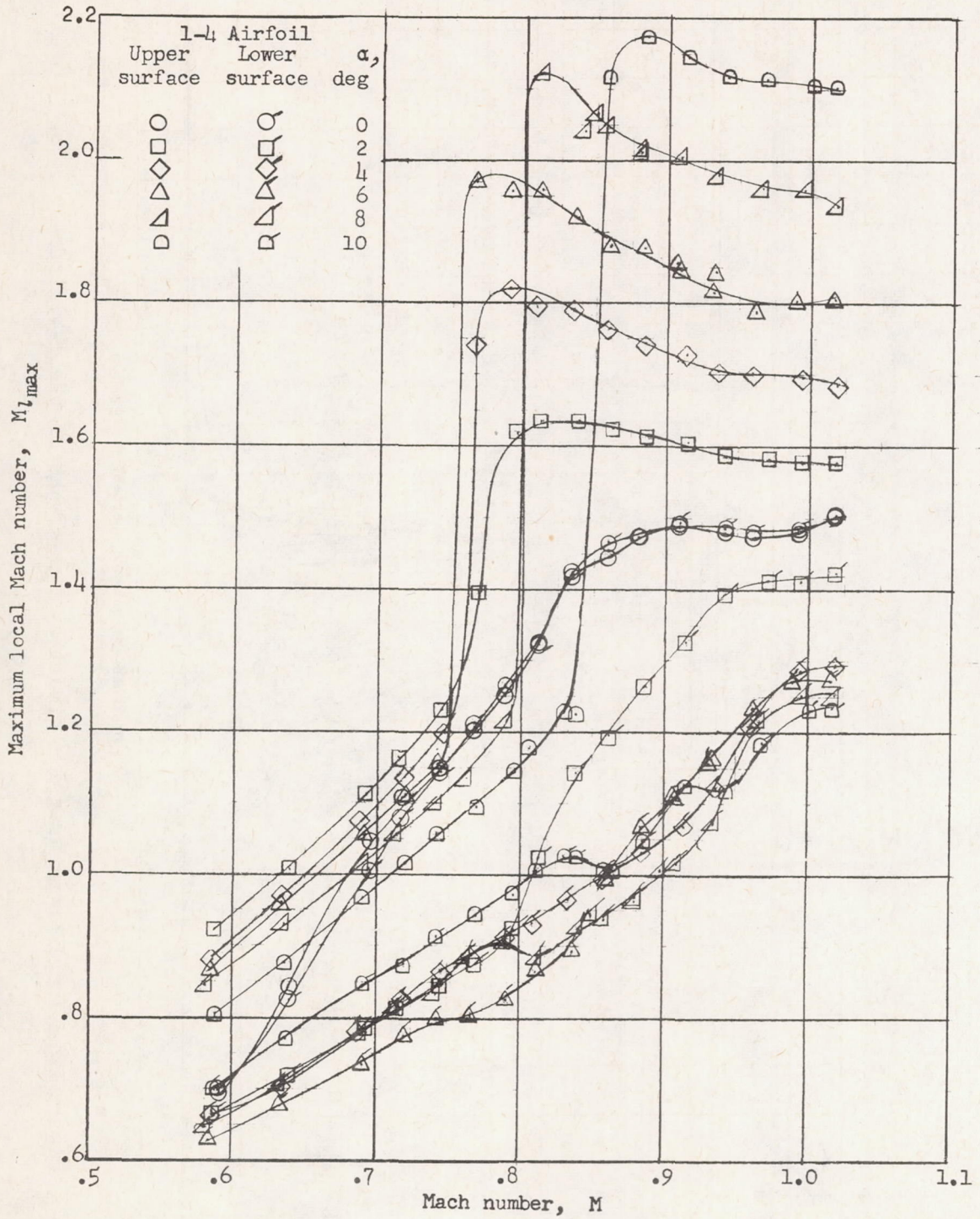


Figure 19.- Representative variation in maximum local Mach numbers.

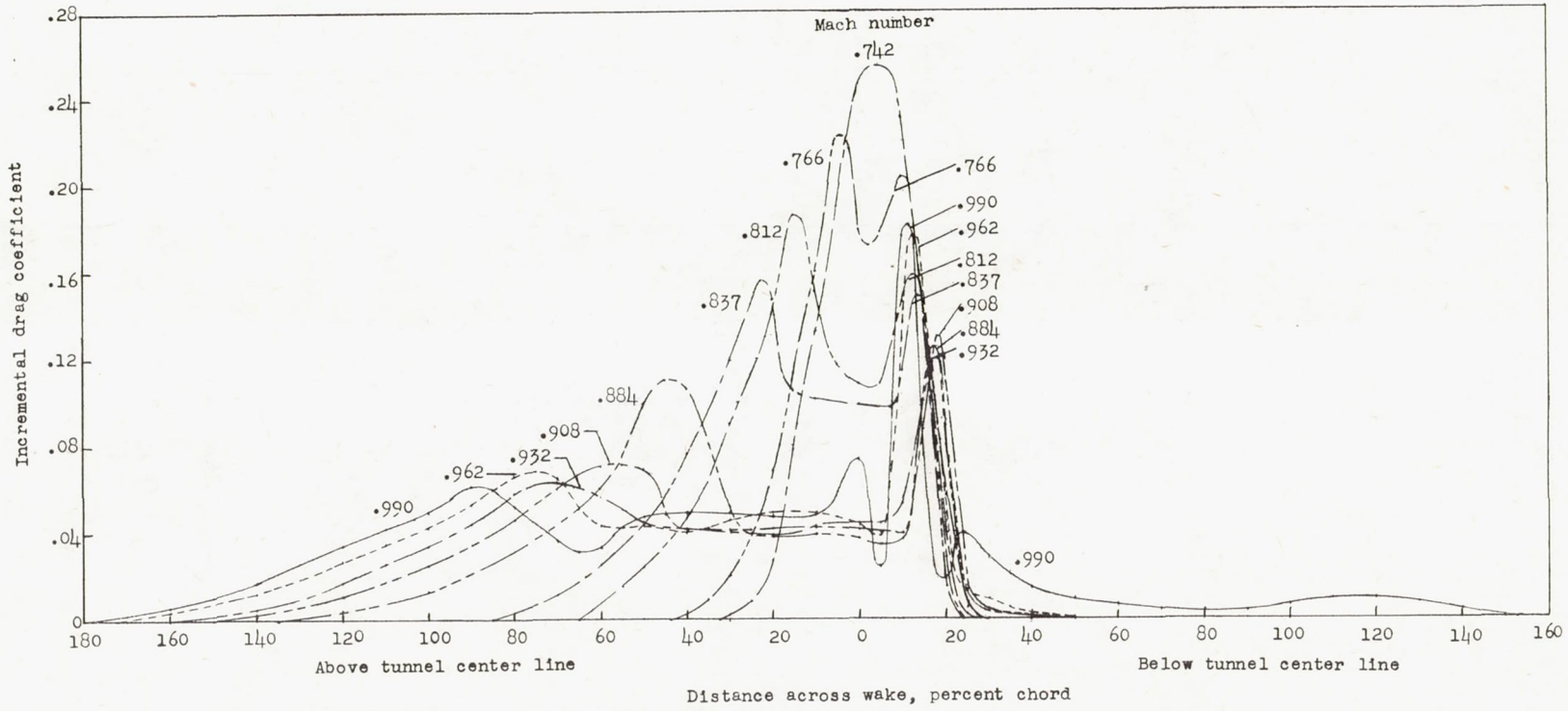
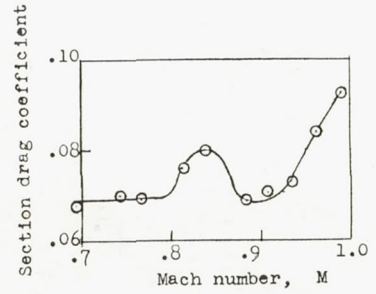
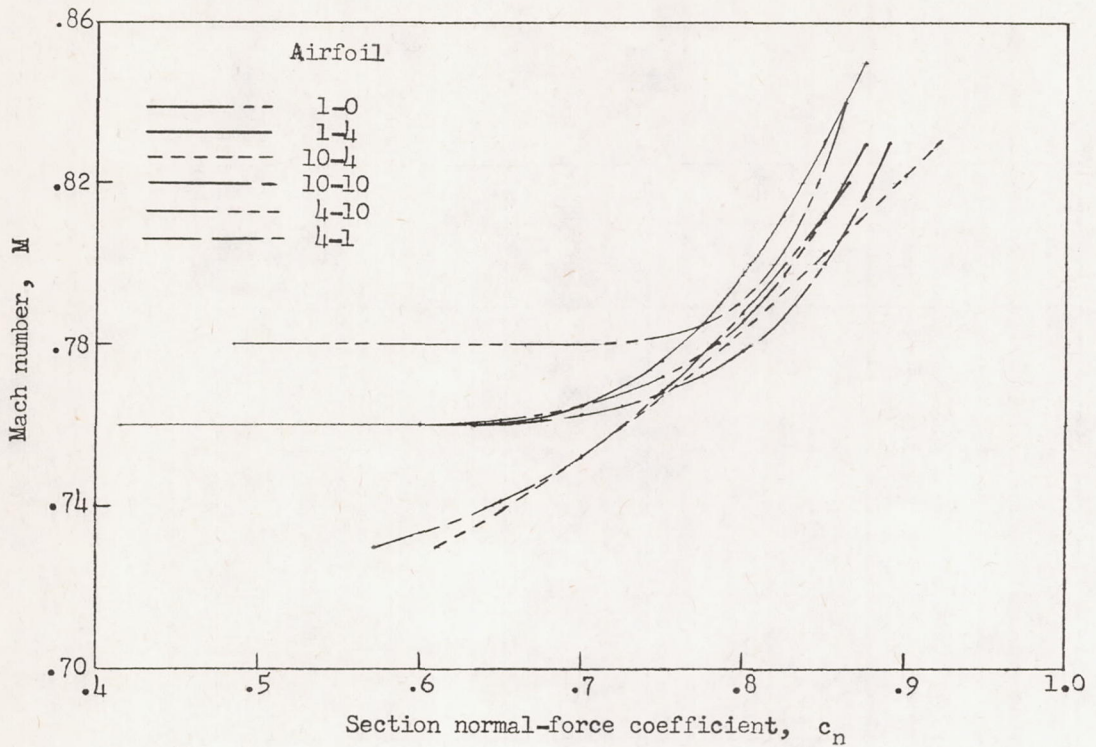
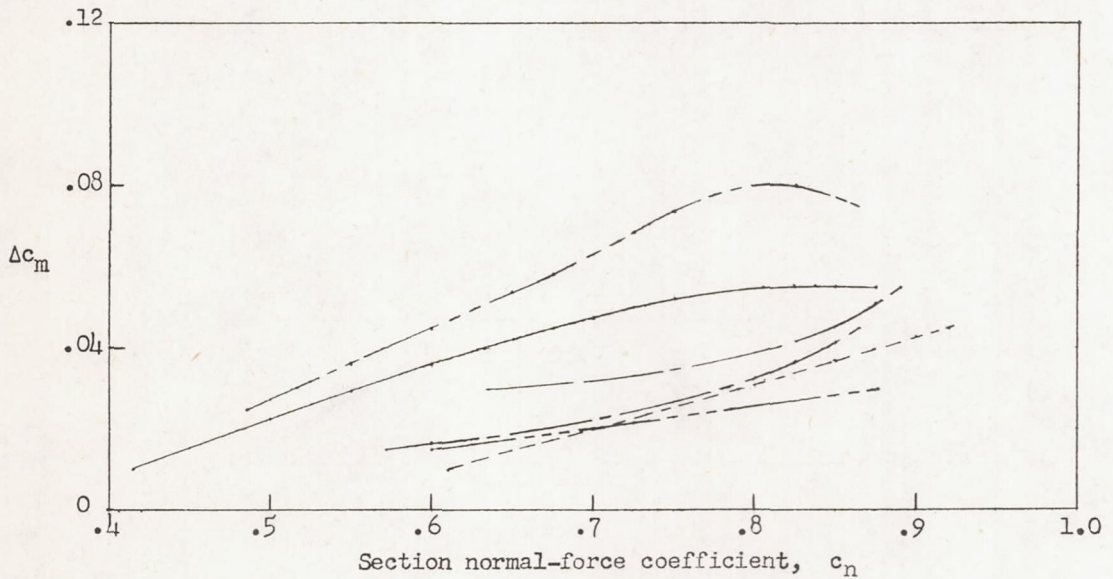


Figure 20.- Incremental drag distribution across wake of the 1-4 airfoil.
 $\alpha = 6^\circ$.

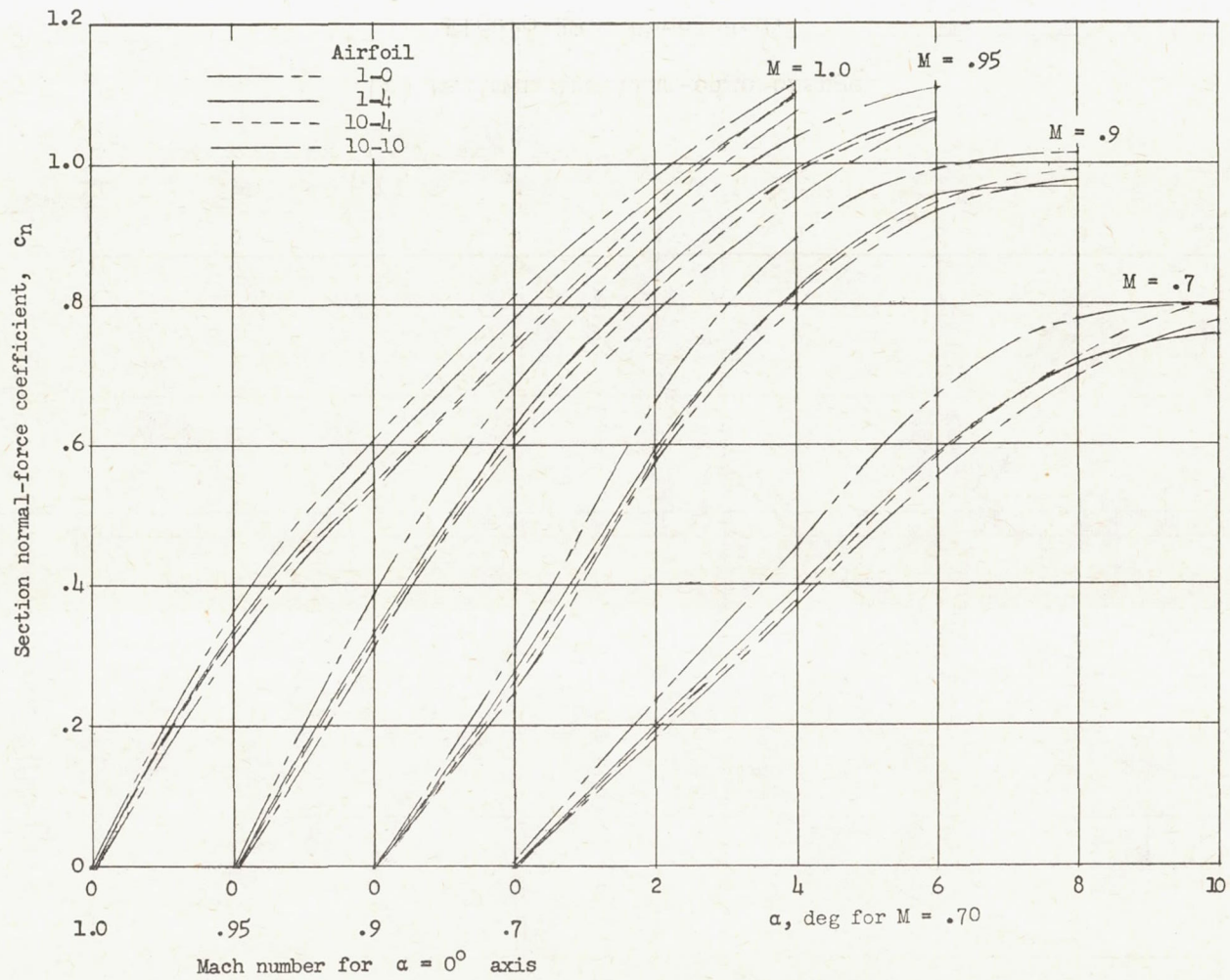


(a) Mach number for pitching-moment break.



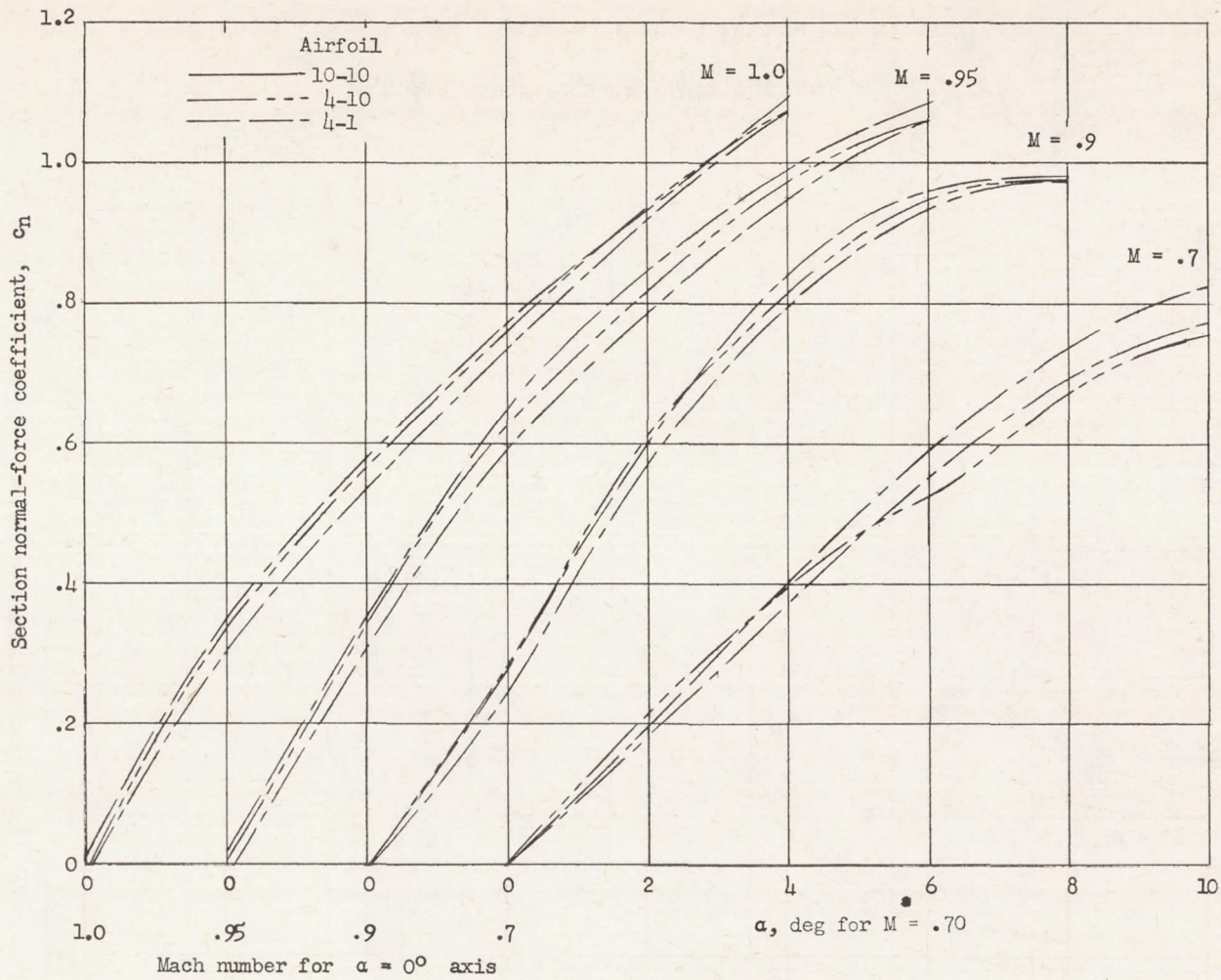
(b) Magnitude of pitching-moment break.

Figure 21.- Factors affecting pitching-moment break at transonic flow attachment.



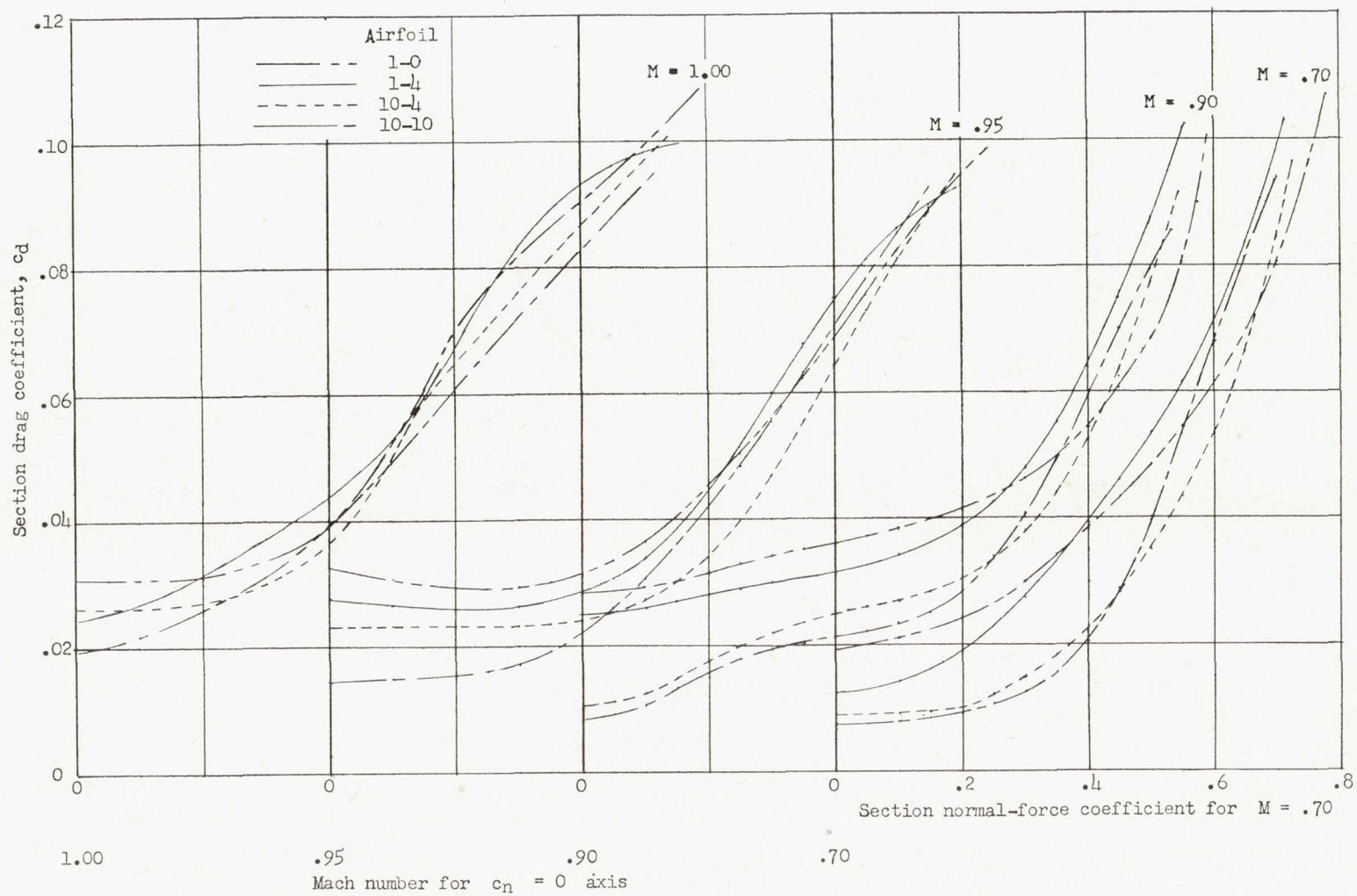
(a) Maximum leading-edge change.

Figure 22.- Normal-force characteristics of airfoils.



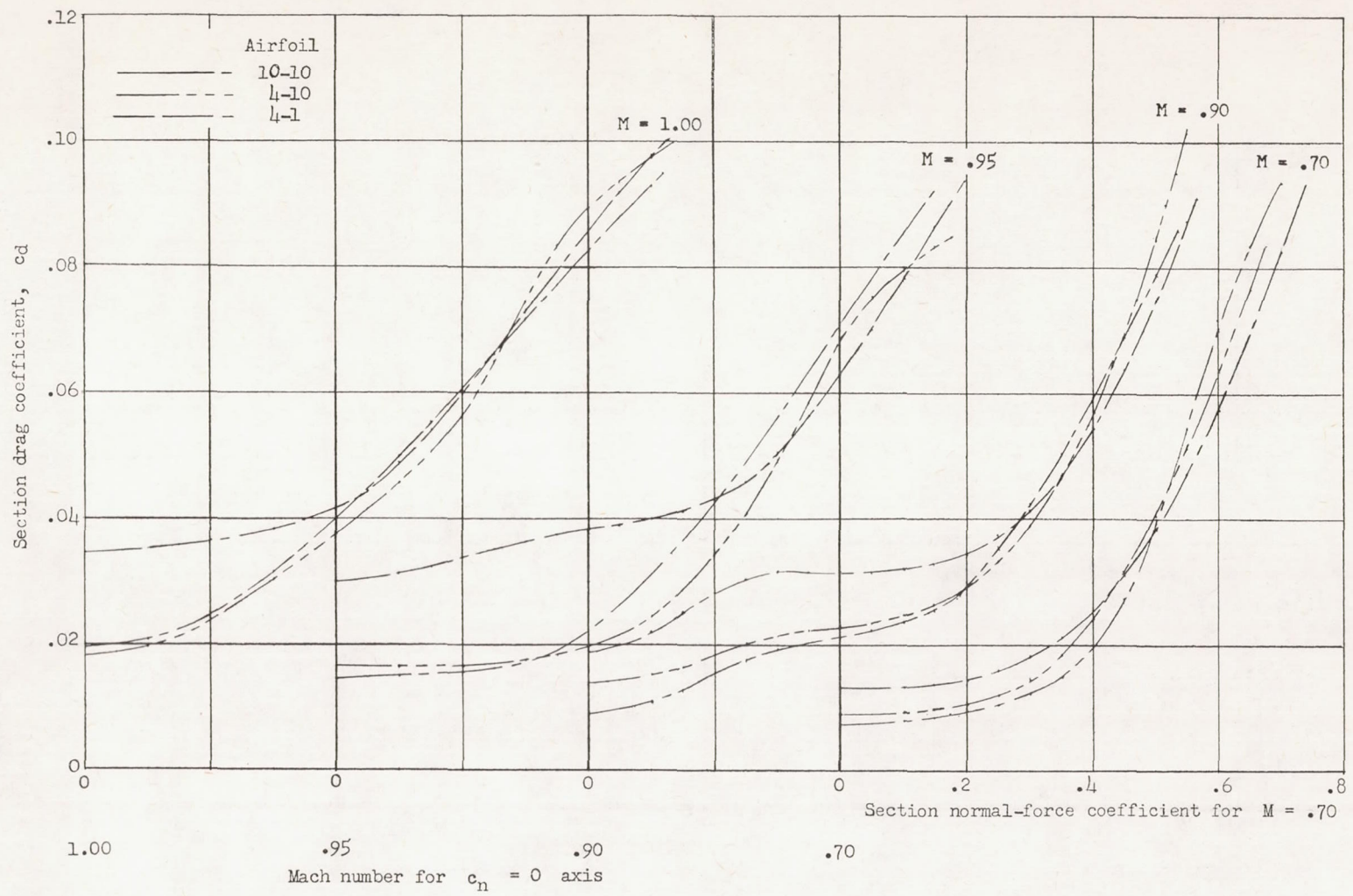
(b) Maximum trailing-edge change.

Figure 22.- Concluded.



(a) Maximum leading-edge change.

Figure 23.- Drag polars of airfoils.



(b) Maximum trailing-edge change.

Figure 23.- Concluded.

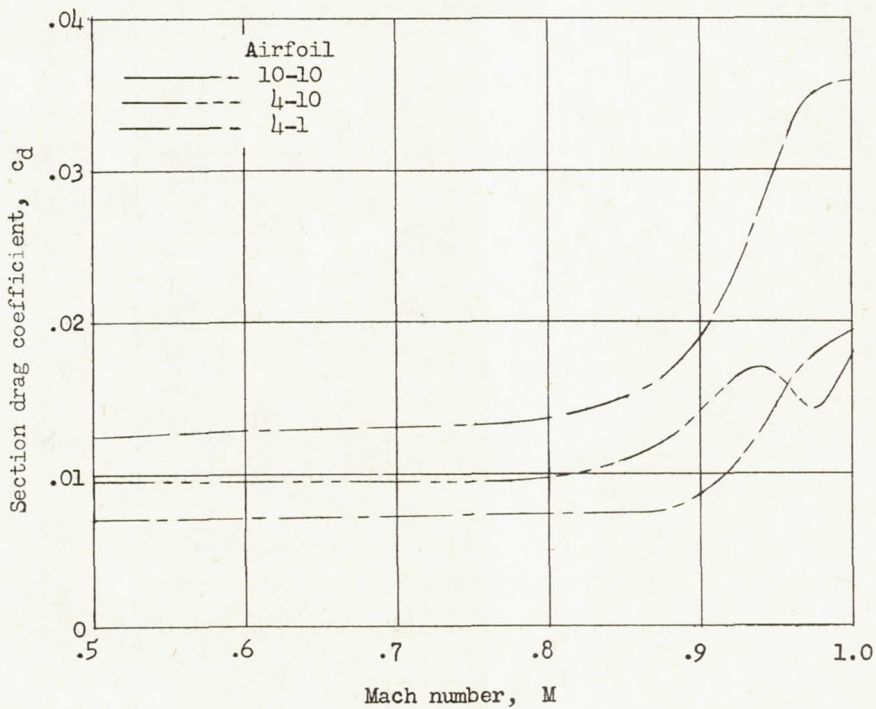
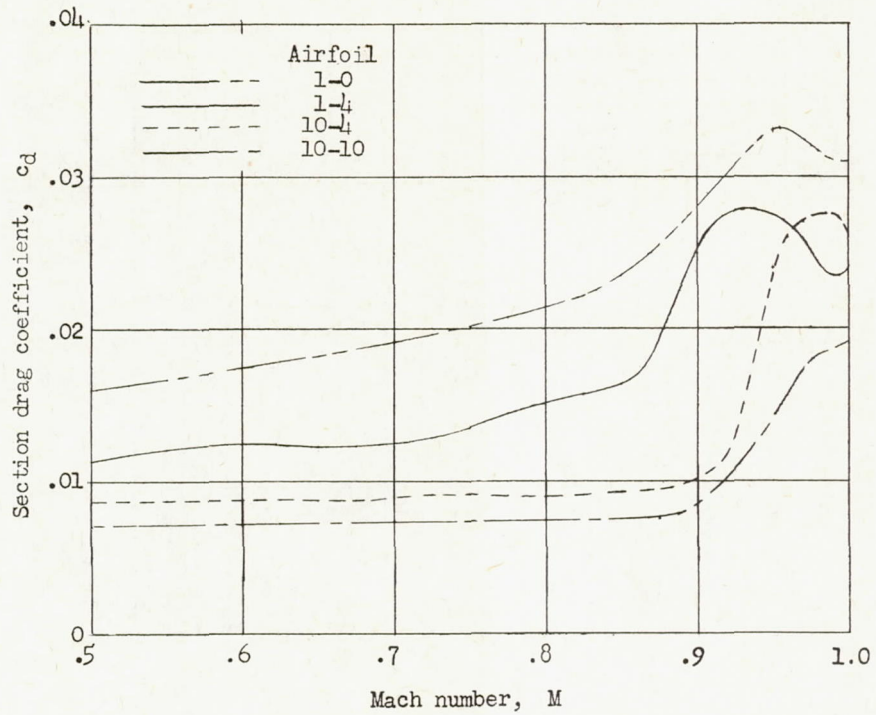
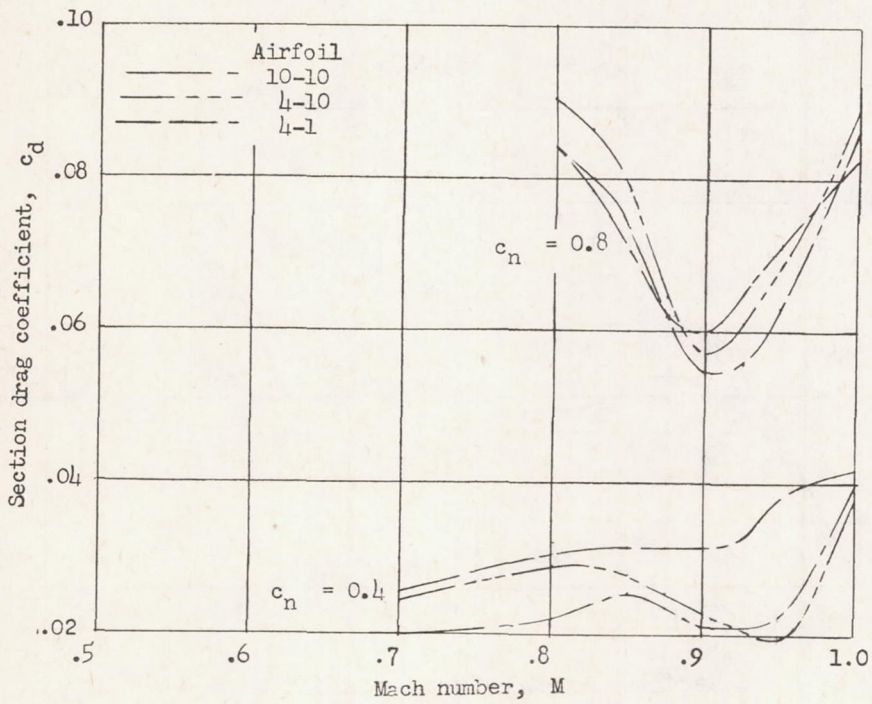
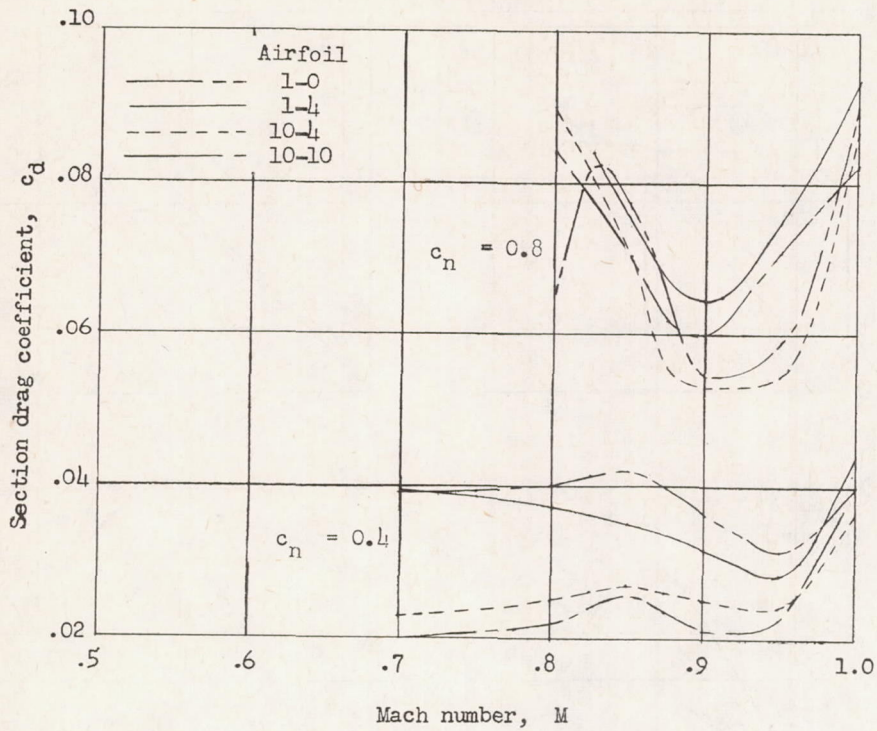
(a) $c_n = 0$.

Figure 24.- Drag coefficient variation at constant normal-force coefficient.



(b) $c_n = 0.4$ and 0.8 .

Figure 24.- Concluded.

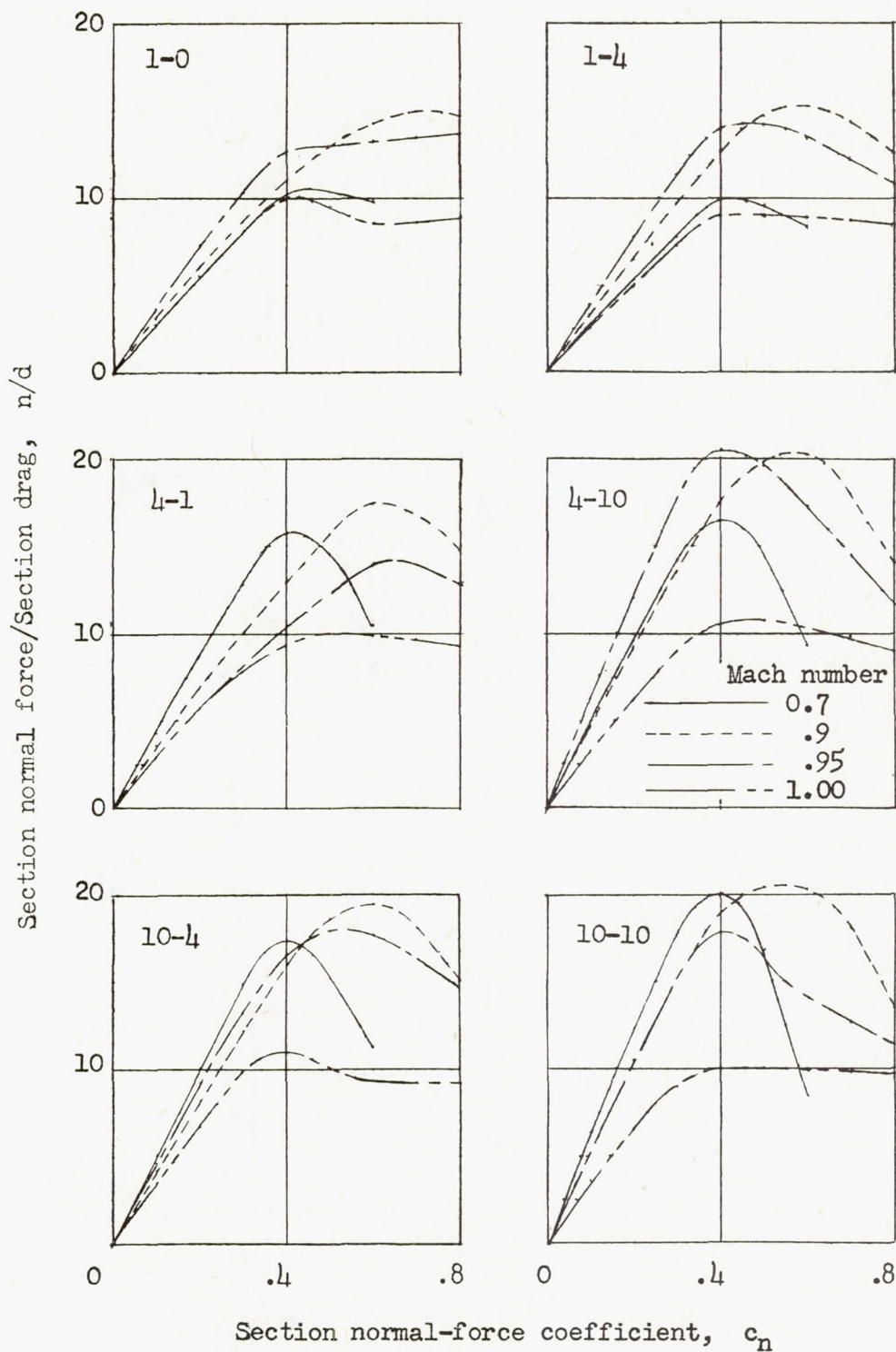


Figure 25.- Effects of Mach number on ratio of section normal force to section drag.

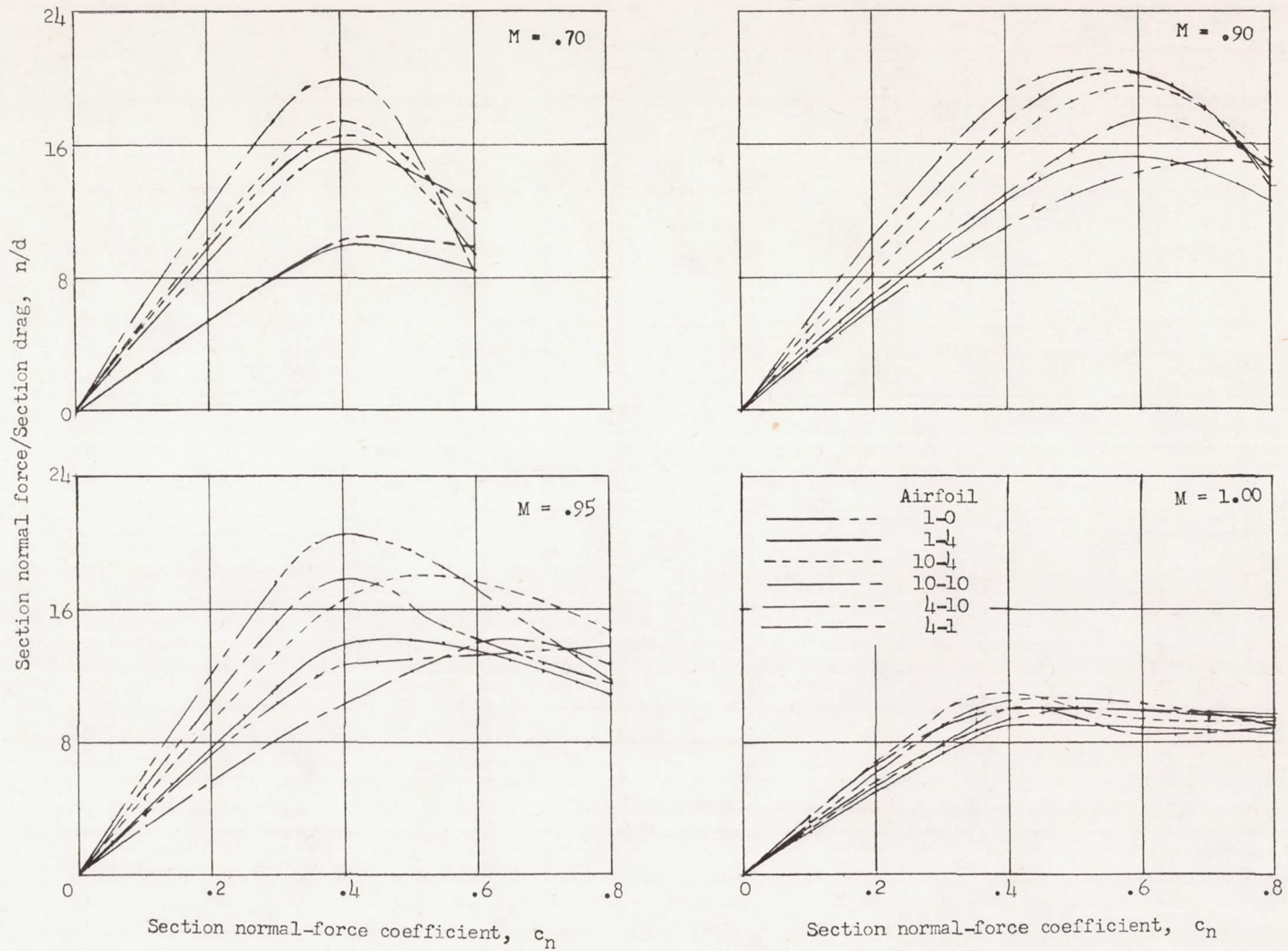
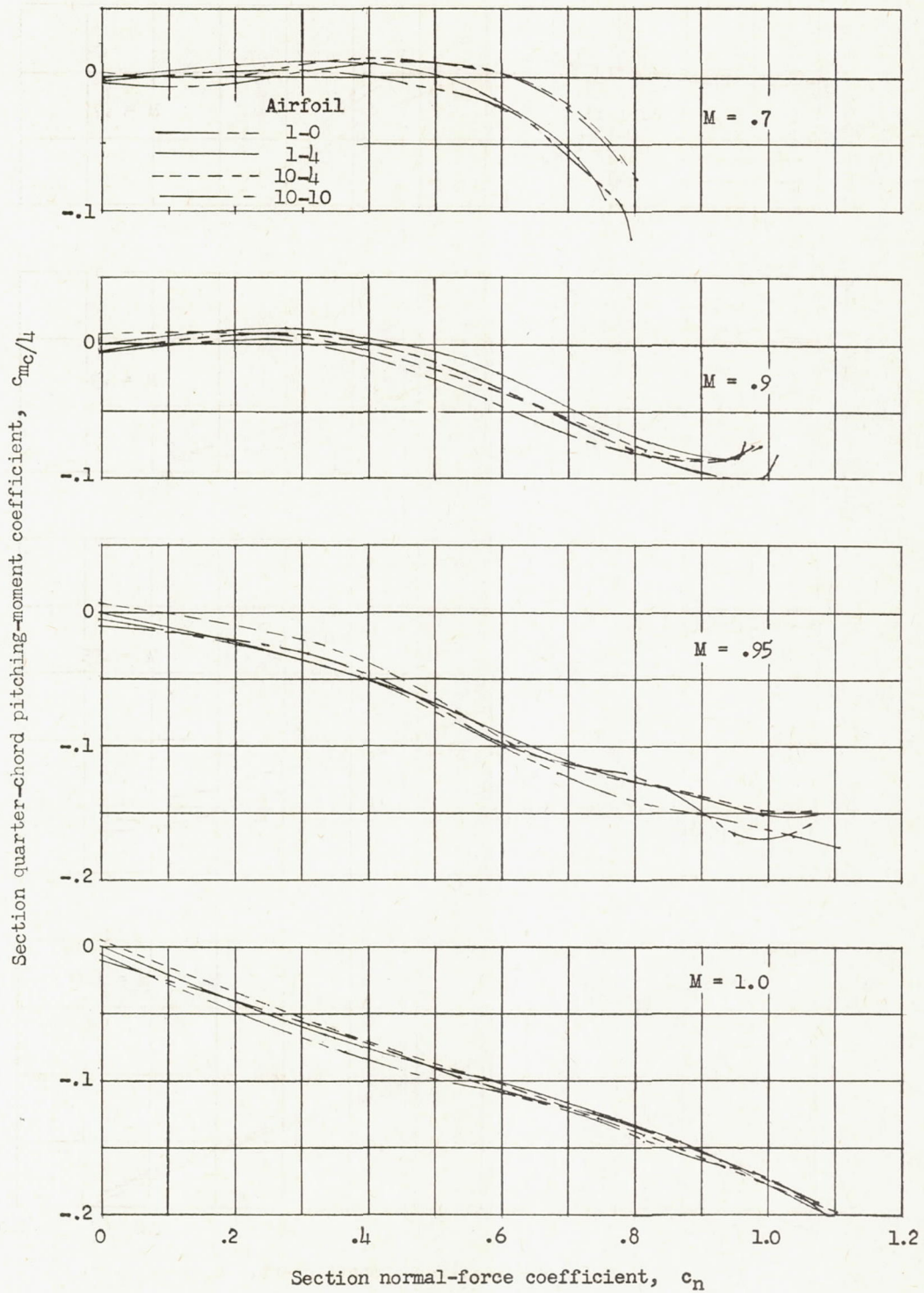
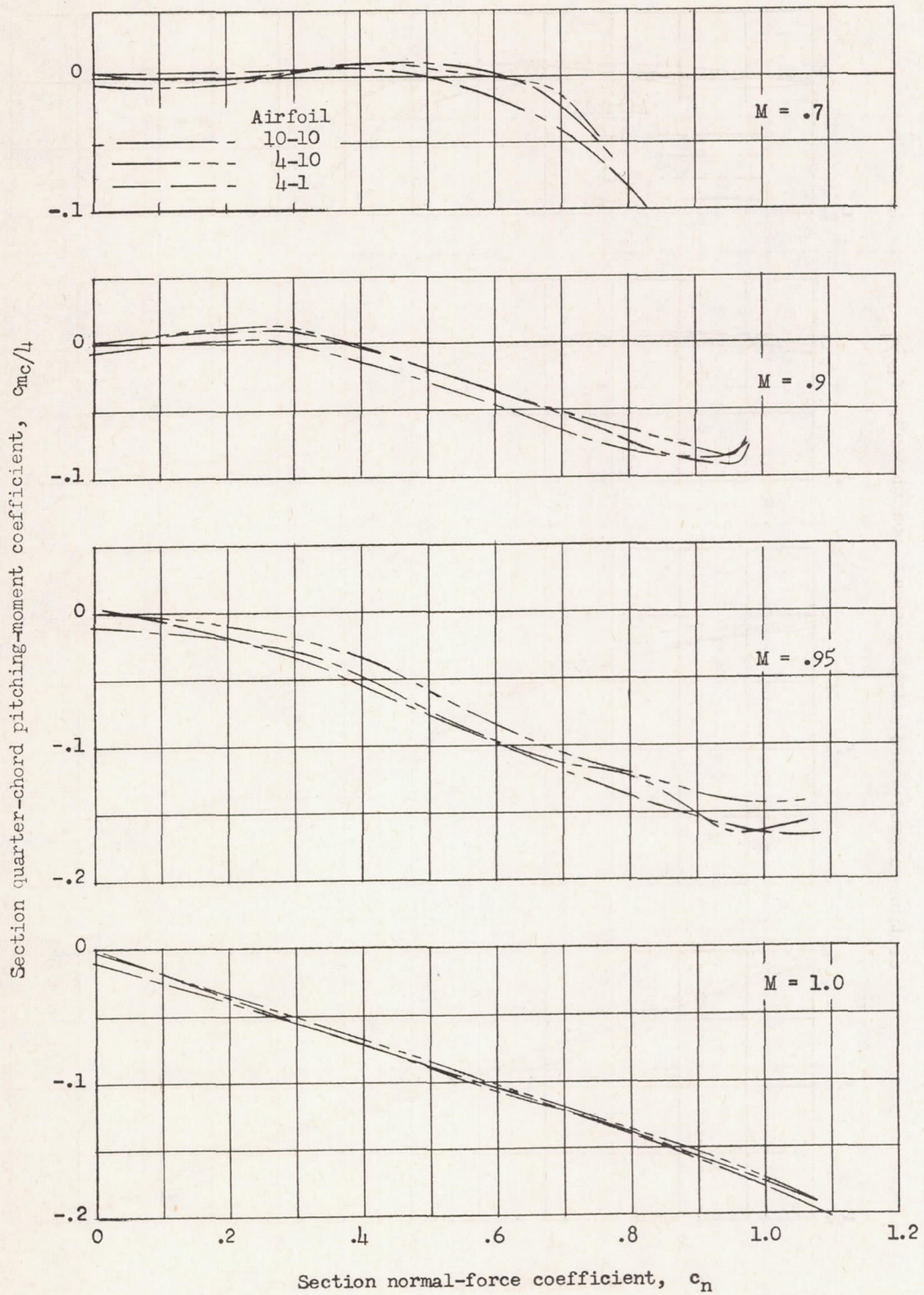


Figure 26.- Effects of profile shape on ratio of section normal force to section drag.



(a) Maximum leading-edge change.

Figure 27.- Pitching-moment characteristics of airfoils.



(b) Maximum trailing-edge change.

Figure 27.- Concluded.

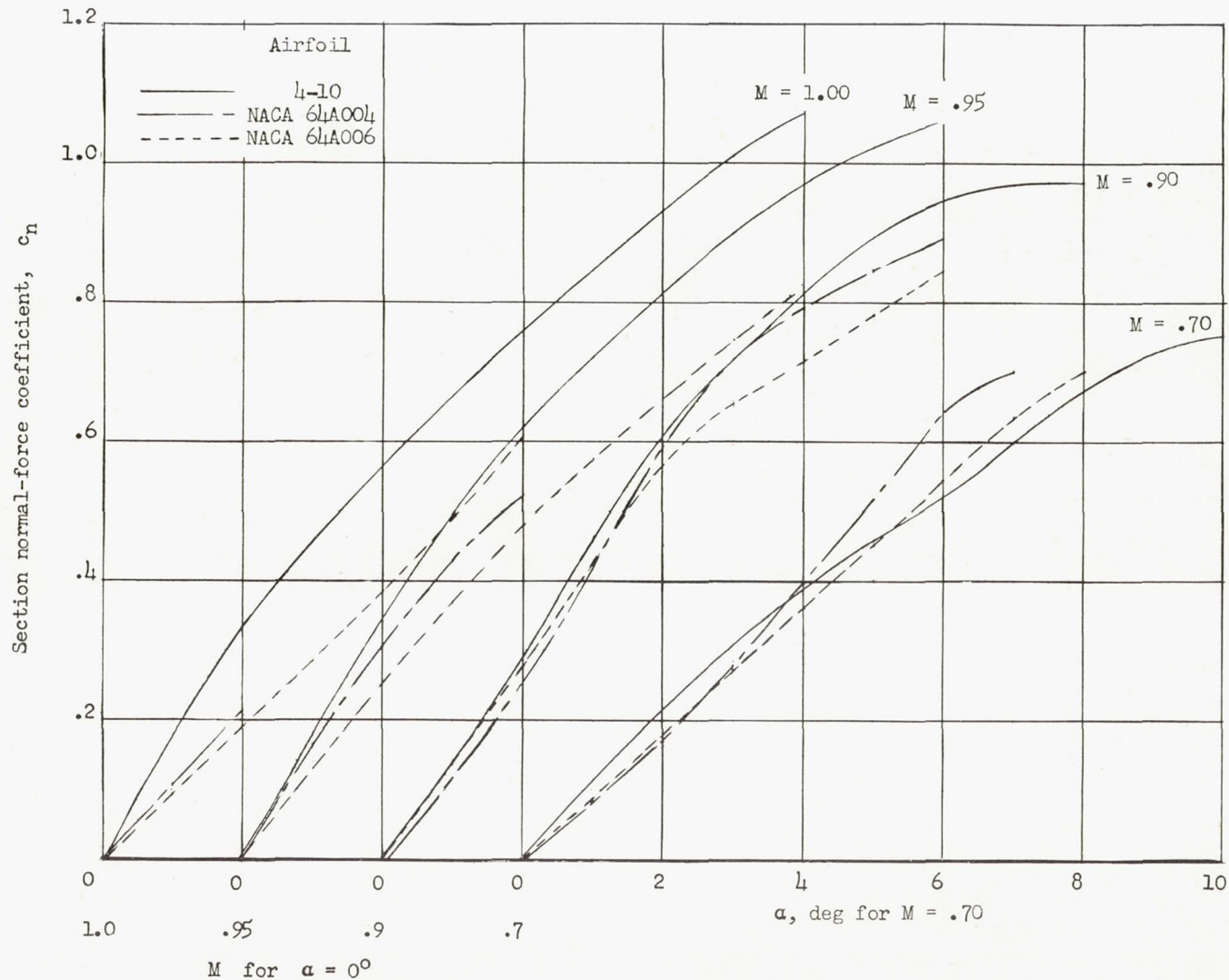


Figure 28.- Effects of thickness on normal-force coefficient.

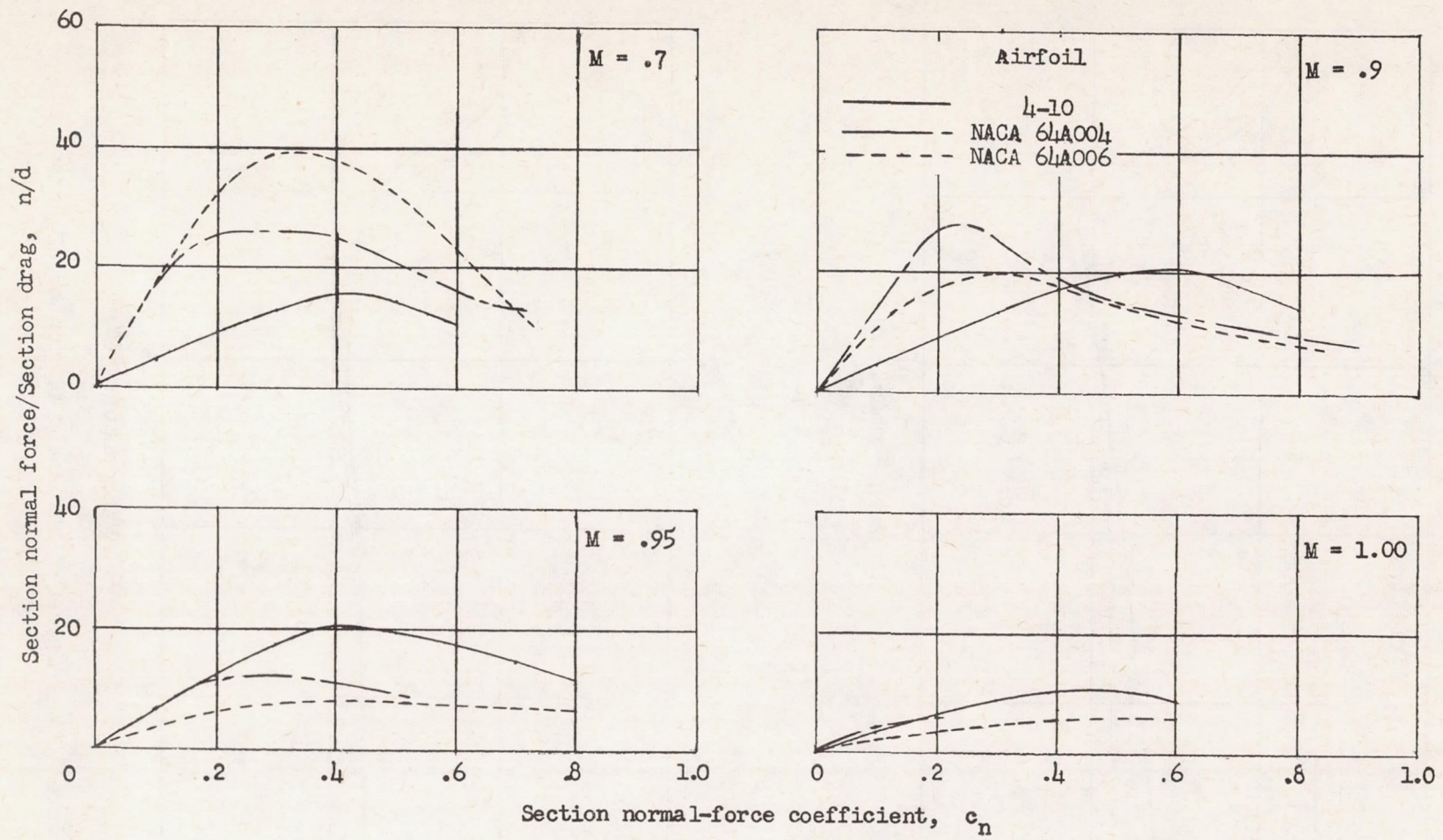


Figure 29.- Effects of thickness on ratio of section normal force to section drag.

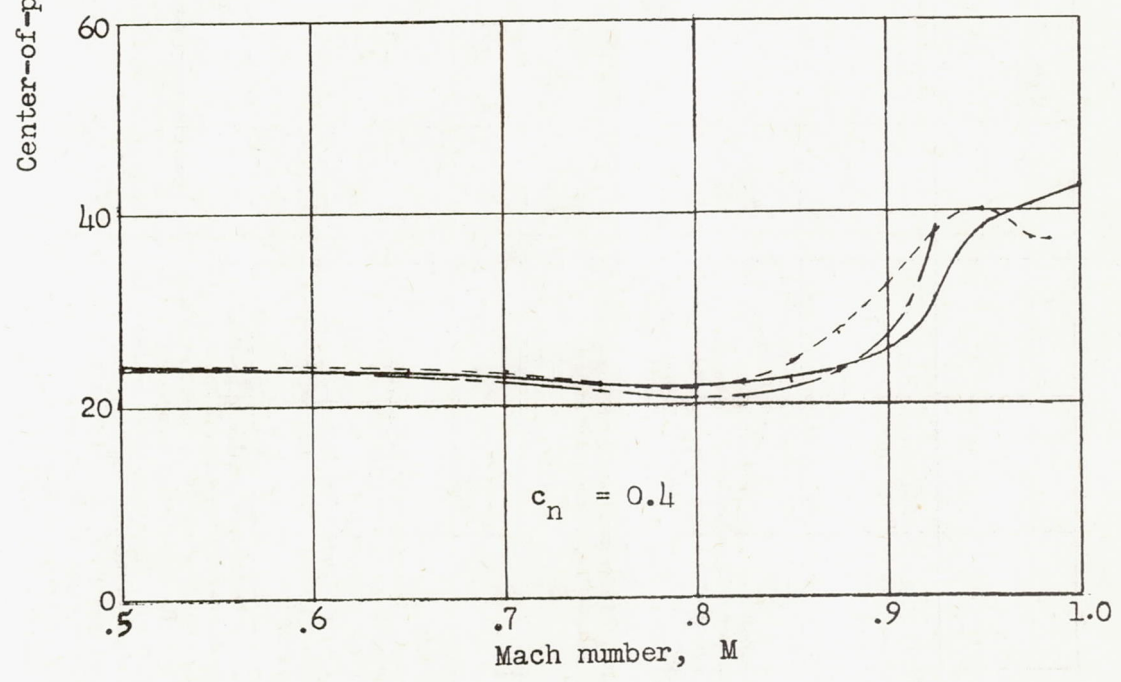
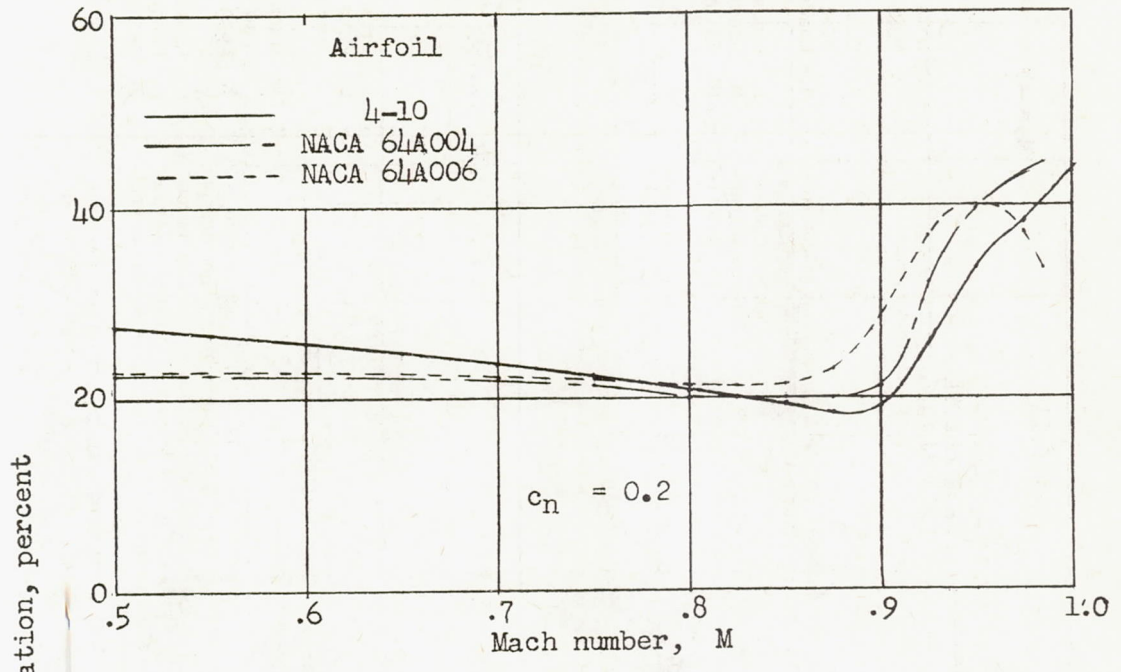


Figure 30.- Effects of thickness on center of pressure.